Journal of Power Sources 267 (2014) 831–873

Contents lists available at ScienceDirect

Journal of Power Sources

journal homepage: www.elsevier.com/locate/jpowsour

Review

# Synthesis and electrochemical properties of vanadium oxide materials and structures as Li-ion battery positive electrodes

David McNulty [a, b], D. Noel Buckley [a, b, c], Colm O'Dwyer [c, d, e, *]

[a] Department of Physics and Energy, University of Limerick, Limerick, Ireland
[b] Charles Parsons Initiative on Energy and Sustainable Environment, University of Limerick, Limerick, Ireland
[c] Materials & Surface Science Institute, University of Limerick, Limerick, Ireland
[d] Department of Chemistry, University College Cork, Cork, Ireland
[e] Micro & Nanoelectronics Centre, Tyndall National Institute, Lee Maltings, Cork, Ireland

## HIGHLIGHTS

- Full scope review of the synthesis of vanadium oxide and related phases.
- A wide ranging summary of shape and size control of vanadium oxide phases.
- Electrochemical performances of vanadium oxides as Li-ion battery electrodes.

## ARTICLE INFO

*Article history:*
Received 2 April 2014
Received in revised form
15 May 2014
Accepted 22 May 2014
Available online 20 June 2014

*Keywords:*
Li-ion batteries
Vanadium oxide
Nanomaterials
Electrochemistry
Energy storage

## ABSTRACT

The electrochemical intercalation of lithium into vanadium pentoxide was first reported in the 1970's. Over the last 40 years vanadium oxides have continued to be the subject of much research due to their desirable physical properties. Initial results with bulk $V_2O_5$ and $V_2O_5$ gels demonstrated the potential for application as a cathode material for lithium batteries. Encouraging specific capacities exceeding 250 mAh $g^{-1}$ were accompanied by severe capacity fading, which prevented widespread commercial application of $V_2O_5$-containing cathodes. Following the commercial release of the Li-ion battery, the development of layered materials that reversibly intercalated lithium, and the resurgence in nanoscale materials for Li-ion and alternative batteries, have opened new opportunities for the examination of the influence of material structure on cell performance. Recent decades have witnessed advances in the control of shape, structure and function of Li-ion battery materials. This review details the synthesis and structural properties of vanadium oxides, one of the model layered battery materials, and reviews the synthesis and structure of vanadium oxides and related polymorphs, bronzes and phases. Their electrochemical characteristics under a wide range of conditions are assessed and compared as positive electrode materials in lithium and lithium-ion batteries up to the present day.



## 1. From lithium batteries to lithium ion batteries

Lithium batteries have been investigated for decades as a means of meeting our energy storage goals. There are several reasons why lithium was initially investigated as an anode material. Lithium is the lightest and most electropositive metal (−3.04 V *vs.* standard hydrogen electrode) [1]. The combination of these two characteristics results in lithium having a particularly favourable energy content, with a theoretical specific capacity of 3860 mAh $g^{-1}$ in comparison with 820 mAh $g^{-1}$ for zinc and 260 mAh $g^{-1}$ for lead [2]. The use of lithium in primary batteries was first investigated in the 1960's and 70's [3–5] however at that time aqueous electrolytes were being used. One of the first major issues which had to be overcome was the lack of a stable electrolyte medium for use with pure lithium. The practical use of lithium cells was not realised until after the development of suitable non-aqueous electrolytes. In an effort to improve the electrochemical performance of these cells, new electrolytes were extensively studied. Initially, various insertion compounds were investigated as cathode materials for lithium batteries [6,7]. These materials host lithium ions within their crystalline structures during a state of discharge and the lithium ions are removed during a state of charge. Ideally this is a reversible

* Corresponding author. Department of Chemistry, University College Cork, Cork, Ireland. Tel.: +353 (0) 21 4902732; fax: +353 (0) 21 4274097.
*E-mail address:* c.odwyer@ucc.ie (C. O'Dwyer).

http://dx.doi.org/10.1016/j.jpowsour.2014.05.115
0378-7753/

reaction without any major phase changes to the cathode material. While these insertion compounds were being investigated as cathode materials, pure lithium was being used as the anode material. Problems associated with lithium corrosion and the formation of lithium dendrites within the cathode material were a cause for concern [8–11]. These issues resulted in poor cycling efficiency and shortened cycle life. It became clear that it was necessary to replace the lithium metal with a lithium containing compound.

Initially lithium alloys with other metals such as aluminium and tin were investigated for this purpose [12]. However, it was found that they suffer from severe morphological changes upon cycling due to large volume changes [13]. The electrochemical insertion of lithium into graphite was also investigated [14], however severe problems due to exfoliation were encountered [15]. These issues lead to the development of the "rocking chair" concept. The concept was first reported by Lazzari et al. in 1980 [16] and named by Armand [17]. It involves using two insertion compounds based on metallic oxides or sulfides as electrodes. The system described was a $Li_xWO_2/Li_yTiS_2$ cell, with an average cell voltage of 1.8 V. One of the electrodes has to have been previously lithiated (in this case $WO_2$), this electrode acts as the main source of lithium in the cell and hence solves the issues associated with using pure lithium. While this method did represent an alternative to using pure lithium, the cell had a low energy density. Thus it was not very attractive for practical use. Over the years the "rocking chair" system has been called various names including the shuttlecock [18] and swing electrode system [19]. Today these types of batteries are simply called lithium ion batteries. The real breakthrough for lithium ion batteries came in the 1980's when disordered carbon was identified as good candidate as an anode material and $Li_xCoO_2$ was identified as a suitable cathode material [20]. In 1990, Nagura announced the commercial availability of the first lithium ion battery based on a carbon (non-graphitic) anode and a $LiMnO_2$ cathode [21]. The electrochemical performance of these materials and their alternatives will now be discussed.

## 2. Cathode materials for lithium ion batteries

The capacity of lithium ion batteries is typically limited by the cathode. Therefore it is necessary to improve the capacity of the cathode in order to improve the performance of lithium ion batteries. It is for this reason that there is such a tremendous interest in developing enhanced cathode materials. As mentioned above insertion materials were quickly identified as suitable compounds for use as cathode materials. The first materials which were investigated were the chalcogenides [22]. $TiS_2$ has been extensively studied due to its stable layer structure and electronic conductivity [23,24]. In fact $TiS_2$ was used as the cathode material in the first commercial lithium battery with LiAl as the anode material [25]. The battery was a coin cell for watches. While suitable for applications such as watch batteries these cells were not practical for larger devices. Following on from the chalcogenides, a lot of attention was given to metal oxides. Initial research focused on metal oxides such as oxides of molybdenum [26,27], tungsten [28], vanadium [29], chromium [30] and manganese [31]. The possible use of $Li_xCoO_2$ and $Li_xNiO_2$ was first reported by Mizushima et al. in 1980 [32,33] and following on from improvements in non-aqueous electrolytes these compounds quickly became the most studied insertion materials for use as cathodes.

### 2.1. Lithium nickel oxide ($Li_xNiO_2$) and lithium manganese oxide ($Li_xMn_2O_4$)

The theoretical specific capacity of $Li_xNiO_2$ assuming 1 Li per $NiO_2$ may be removed is $\approx$275 mAh $g^{-1}$, however a lower capacity is obtained in actual test cells [34]. $Li_xNiO_2$ was reported to have a larger initial specific capacity than $Li_xCoO_2$, having values up to $\approx$200 mAh $g^{-1}$ compared to $\approx$150 mAh $g^{-1}$ obtained for $Li_xCoO_2$, as can be seen in Fig. 1 [25]. However, there are several reasons why this insertion compound has not received much practical use. The synthesis of $Li_xNiO_2$ is much more difficult than $Li_xCoO_2$ due to the formation of a nickel over-stoichiometric phase [35,36]. Capacity fading is a severe issue for $Li_xNiO_2$ [37,38] and also the thermal stability of $Li_xNiO_2$ is much lower than for other materials such as $Li_xCoO_2$ and $Li_xMn_2O_4$ [39,40]. It was reported that the cycle life of $Li_xNiO_2$ cells is strongly dependent on the depth of discharge [41]. When the specific capacity was restricted to $\approx$90 mAh $g^{-1}$, a cycle life of 200 cycles was reported. However, when the specific capacity was restricted to 130 and 200 mAh $g^{-1}$ cycle lives of 98 and 12 cycles respectively were reported. This poor performance for deeper discharges is due to the formation of irreversible phases due to increased concentrations of lithium in $NiO_2$ [42]. The electrochemical performance of $Li_xNiO_2$ can be improved by partial substitution of Ni with other metals such as cobalt and magnesium. Even low amounts (>10%) of these metals can significantly improve the capacity fading issues. This improvement in cycling ability is due to the suppression of phase transitions which are observed for $Li_xNiO_2$.

The performance of three dimensional spinel lithium manganese oxide has been the subject of a tremendous amount of research [43–46]. There are many advantages to using manganese over other materials such as cobalt and nickel including its lower cost and increased thermal stability [47]. However, electrochemically $Li_xMn_2O_4$ does not perform as well as the mentioned cobalt and nickel oxides. The theoretical specific capacity of $Li_xMn_2O_4$, with $x = 1$, is $\approx$148 mAh $g^{-1}$, experimentally this value is found to be closer to $\approx$120 mAh $g^{-1}$, as shown in Fig. 1 [34]. $Li_xMn_2O_4$ suffers from severe capacity fading [46,48]. It has been reported that the capacity fading issues are strongly reduced when $Li_xMn_2O_4$ is over lithiated to a $Li_{(1+\delta)}Mn_{(2-\delta)}O_4$ composition [49]. Orthorhombic $Li_xMnO_4$ has also been investigated, due to its higher theoretical specific capacity than $Li_xMn_2O_4$, however it has been reported that there is a gradual structural transformation during battery operation and after a few cycles the material behaves very much like $Li_xMn_2O_4$ [50,51].

### 2.2. Lithium cobalt oxide ($Li_xCoO_2$)

Lithium cobalt oxide is the most commonly used cathode material in lithium ion batteries today [1,2,52,53]. There are several

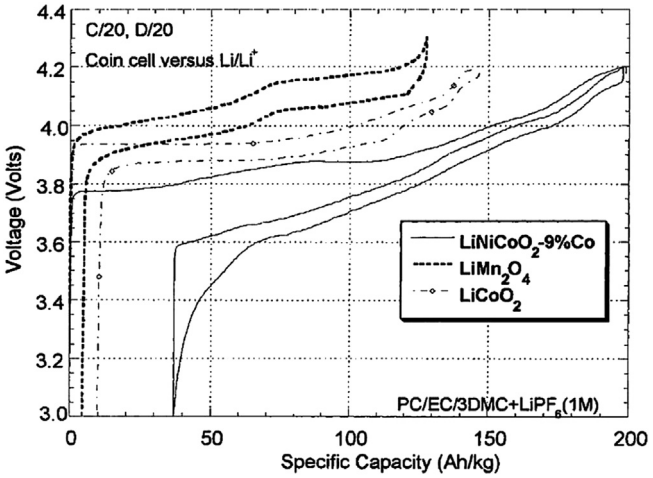


**Fig. 1.** Specific capacity for the first discharge and charge for $LiNiCoO_2$, $LiMn_2O_4$ and $LiCoO_2$ [25].

reasons why it was initially investigated. As pure lithium metal anodes were replaced with lithiated carbon, the cathode material had to have a sufficient working voltage to compensate for the voltage loss on the negative side [25]. Also, the cathode material had to be capable of hosting a large mole fraction of lithium without significant structural disorder occurring. $Li_xCoO_2$ was easy to prepare and fitted the needs and took precedence over the also suitable $Li_xNiO_2$ [54]. $Li_xNiO_2$ had a potentially higher specific capacity however it was much more difficult to prepare. The electrochemical performance of $Li_xCoO_2$ was reported to be quite good with an initial specific capacity of ≈150 mAh $g^{-1}$ being obtained after the first discharge and capacity values ranging from 140 to 145 mAh $g^{-1}$ after subsequent cycles, as shown in Fig. 2 [25]. There has been a significant amount of research on the many structural aspects of $Li_xCoO_2$, including its delithiated phases and the optimisation of its synthesis [55–60]. The cycling performance of cells comprised of a $Li_xCoO_2$ and a pure lithium anode discharged to different potentials as shown in Fig. 2. Fig. 2(a) shows a cell which was galvanostatically cycled in a potential window of 4.3 V–3.5 V [61]. Cycles 1–5, 6–10 and 11–15 were at current densities of 0.5, 1.0 and 3.0 mA $cm^{-2}$ respectively. The additional cycles (16–70) were all performed at a current density of 0.5 $cm^2$. Initially the specific capacity was ≈135 mAh $g^{-1}$, this decreased to ≈128 and ≈90 mAh $g^{-1}$ when the current density was increased to 1.0 and 3.0 mA $cm^{-2}$ respectively, showing that the specific capacity values obtained at high discharge rates are significantly lower than values obtained at lower rates. The remaining cycles show the stability of capacity retention in this potential window at 0.5 mA $cm^{-2}$. After 70 cycles the specific capacity remains to be ≈125 mAh $g^{-1}$, corresponding to a ≈8% loss in the initial capacity. If the lower limit is decreased from 3.5 to 2.75 V, capacity fading becomes a significant issue as shown in Fig. 2(b) [62]. Increasing the potential window from 4.3–3.5 V to 4.4–2.75 V has two significant effects. Firstly, there is an increase in the initial specific capacity from ≈135 to ≈174 mAh $g^{-1}$. This is due to a greater content of lithium being intercalated when discharged to a lower limit. The increase in capacity is short lived and the capacity quickly fades with increased cycling. After 50 cycles ≈51% of the initial capacity is lost. These results show that $LiCoO_2$ can be a very stable cathode material but only if an appropriate potential window is used. Hence there is a lot of interest in finding cathode materials that have stable capacity retention but for a larger potential window of operation.

While the specific capacity values obtained for $Li_xCoO_2$ are respectable, recent technological advances have highlighted that lithium ion batteries containing $Li_xCoO_2$ will not be suitable for future portable devices. For example a decade ago mobile phones could be used for a few days without the need to charge them, however today's smart phones require charging almost every day. A lot of research has been dedicated to the partial substitution of cobalt by other metals in an effort to improve the resulting specific capacity values. Metals like nickel, iron and aluminium have been investigated and have shown to increase the average discharge voltage [63–66]. There is still one major drawback for using $Li_xCoO_2$ and that is the elevated price of cobalt [52,67]. Approximately 40% of the world's share of cobalt comes from the Democratic Republic of Congo, political issues in the late 70's caused the price of cobalt to skyrocket and it has remained to be very expensive to this day. The pricing issues and perhaps more significantly today the capacity issues of $Li_xCoO_2$ have led to the need to find replacement cathode materials for enhanced lithium ion batteries. With the development of nanostructures many of the insertion materials discarded in the past have found a revitalised interest. The application of vanadium pentoxide as a cathode material to replace the currently used cobalt oxides, and the history and performance of vanadium pentoxide from bulk crystalline $V_2O_5$ to its many nanostructures, will now be discussed.

## 3. Crystalline bulk vanadium pentoxide ($V_2O_5$)

Orthorhombic crystalline $V_2O_5$ consists of layers of $VO_5$ square pyramids that share edges and corners. The crystal structure of $V_2O_5$ is illustrated in Fig. 3. The vanadium atoms form five bonds, one with the $O_1$ atoms, three with the $O_2$ atoms and one with the $O_3$ atoms. These five oxygen atoms form distorted trigonal bipyramids around the vanadium atoms. The bipyramids are linked together by sharing corners in the *x* and *z* directions. In the *y*-direction, there can only be weak van der Waals forces. These interlayer forces correspond to the longer $V–O_1$ distances of 2.81 Å. The three arrangements of oxygen atoms in the structure are shown in Fig. 3(b). The $O_1$ atoms form only one strong bond (V–O = 1.54 Å). The $O_3$ atoms form two bonds (V–O = 1.77 Å) with the angle $V–O_3–V = 125°$. The $O_2$ atoms form three bonds (mean distance V–O = 1.93 Å) with the bond angles 104°, 104° and 143°. Vanadium is desirable material due to its multiple valance states and consequently vanadium can form a variety of oxides. Vanadium pentoxide is a mixed valance material ($V^{4+}$ and $V^{5+}$) with particularly rich crystal chemistry. As a result of its multiple valence state $V_2O_5$ has versatile redox-dependent properties and finds wide applications in catalysis [68–71], electrochromism [72–75], and electrochemistry [76–79].

### 3.1. The intercalation of lithium into bulk $V_2O_5$

Vanadium oxides have been the subject of much research for over 40 years due to their desirable physical properties. Vanadium pentoxide is a typical intercalation compound as a result of its layered structure. The intercalation refers to the reversible intercalation of mobile guest species (atoms, molecules, or ions) into a

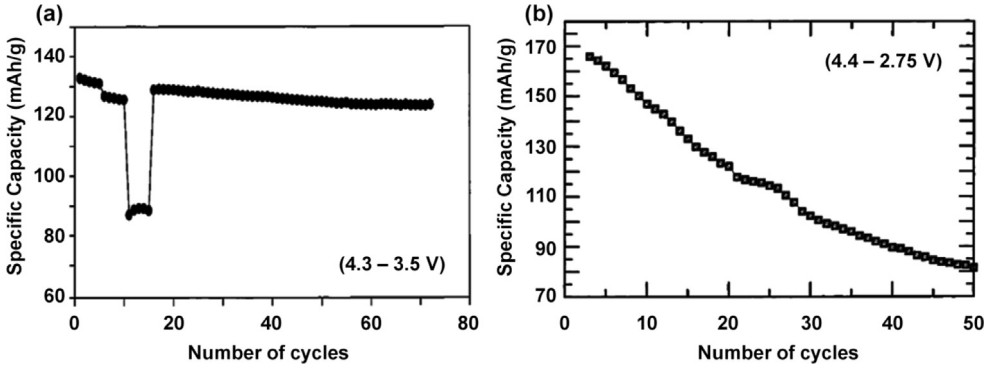


**Fig. 2.** Cycling performance of $Li_xCoO_2$ in a potential window of (a) 4.3–3.5 V and (b) 4.4–2.75 V [62].

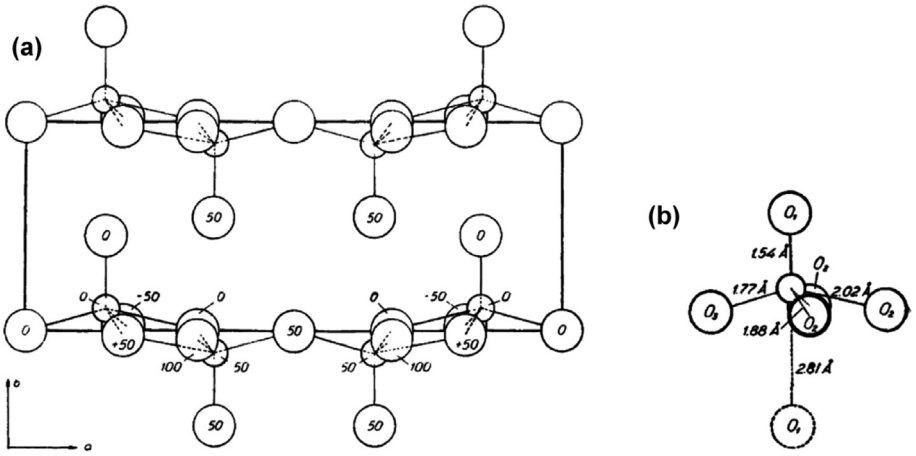


**Fig. 3.** (a) Projection of the structure of $V_2O_5$ (001). Small circles denote V-atoms, large circles O-atoms (b) the coordination around one vanadium atom [80].

crystalline host lattice that contains an interconnected system of empty lattice sites of appropriate size, while the structural integrity of the host lattice is formally conserved. Guest materials may include metal ions, organic molecules, and organometallic molecules. When guest species are incorporated into host lattices, various structural changes can take place, including change in the interlayer spacing and the formation of intermediate phases [81]. The pioneering research on the reversible intercalation of protons and alkali ions into the layers of vanadium oxide was first reported by Dickens and Whittingham [82]. The capability of these insertion reactions led to the investigation of vanadium oxides as cathode materials for lithium batteries. When electron donating cations are intercalated into vanadium oxides, the vanadium oxides become good conductors showing both ionic and electronic conductivity. Theoretically, vanadium oxides are an ideal candidate for an electrode material for electrochemical cells with the potential of high reversibility for both ions and electrons [83]. One of the first papers which investigated the potential application of vanadium oxides as a cathode material for lithium ion batteries was presented by Whittingham in 1976 [29]. Prior to this work it was believed that $V_2O_5$ reacted with lithium to give a lower vanadium oxide and a lithium oxide. However Whittingham reported that cell reactions between lithium and vanadium oxide produced ternary $Li_xV_2O_5$ phases. Cell reversibility is optimised when no chemical bonds are broken during discharge so the presence of these ternary phases made $V_2O_5$ an attractive candidate cathode material. It was observed that for small amounts of lithium ($x < 0.13$) the structure of the $V_2O_5$ crystal lattice is maintained. However as more lithium is intercalated the vanadium is reduced from $V^{+5} \rightarrow V^{+4}$, consequently bond breaking occurs resulting in structural distortion. Whittingham concluded that due to this structural distortion recharging was difficult and at that time the degree of reversibility could not be determined for certain. Initially, the intercalation of lithium into $V_2O_5$ was examined by preparing lithium vanadium pentoxide bronzes. Several methods have been reported to prepare these bronzes including chemical lithiation of $V_2O_5$ by *n*-butyl lithium in hexane [84] and the treatment of solid $V_2O_5$ with a solution of lithium iodide in acetonitrile [85–87]. The characterisation of these bronzes gave the initial understanding of the intercalation of lithium into $V_2O_5$ and lead to the formation of $Li_xV_2O_5$ compounds being prepared electrochemically by galvanostatic discharge of a $V_2O_5$ working electrode with a lithium foil counter electrode and a non-aqueous Li ion containing electrode. The various phases formed during the intercalation of lithium into $V_2O_5$ are the subject of much research and continue to maintain interest today [88–97]. Electrochemical lithium intercalation occurs together with compensating electrons leading to the formation of vanadium bronzes as follows:

$$V_2O_5 + xLi^+ + xe^- \leftrightarrows Li_xV_2O_5$$

### 3.1.1. Phases associated with lithium intercalation

The various phases of Li intercalation within vanadium oxide were further explained by Delmas et al. [98]. The electrochemical lithium intercalation into $V_2O_5$ showing the evolution of phases with degree of lithium intercalation is shown in Fig. 4. The structural behaviour of vanadium oxide with increased Li insertion is quite complex and can split into several different phases. The first α-phase ($x < 0.01$) has little effect on the $V_2O_5$ structure. This phase is followed by the ϵ-phase ($0.35 < x < 0.7$) during which the vanadium oxide layers become more puckered. The δ-phase occurs when $x = 1$ and it can be seen from Fig. 4 that at this phase there is a sudden decrease in cell potential. There are some slight structural modifications due to the intercalation of lithium ions (up to $x = 1$) such as a puckering of the layers and an increase in the interlayer spacing of the layers of vanadium oxide, the basic layered structure is maintained [99]. If more than one lithium is discharged then serious structural changes occur which lead to the formation of the γ-phase ($x = 2$). A "rock salt" structure is formed when even more lithium is intercalated. This compound is referred to as the ω-phase

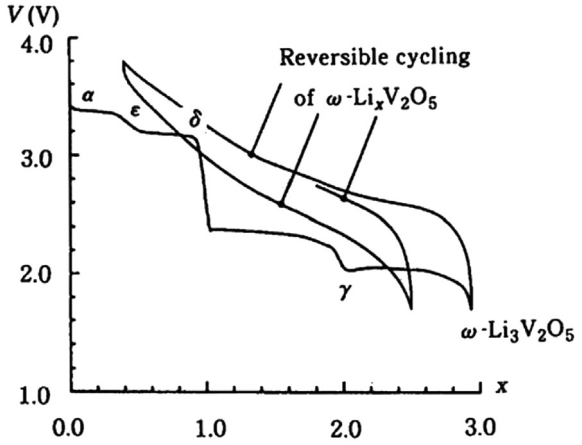


**Fig. 4.** Various phases associated with the electrochemical intercalation of lithium into $V_2O_5$ [98].

($x = 3$). The reversible cycling of this phase is also shown in Fig. 4. This shows that even for $V_2O_5$ discharged to the ω-phase, lithium ions can be successfully inserted and removed, however the lack of any discrete phase transitions in subsequent discharge curves indicate that the ω-phase is an irreversible phase and the structural changes which occur due to discharging to this level cannot be undone. It was also reported that discharging $V_2O_5$ to the ω-phase resulted in a rapid loss in capacity values with increased cycling. A rapid loss in capacity is not a desirable property for a battery cathode material. Discharging to α and ε-phases does not affect the V–O bonds and these phases are fully reversible. Intercalation of 0.5 Li per V corresponds to a specific capacity of ≈147 mAh $g^{-1}$, which is comparable to commercially used $LiCoO_2$ cathode materials. The cycling stability of $LiCoO_2$ when discharged to lower potentials is far better than that of $V_2O_5$ [52]. Several papers which focused on the intercalation of lithium at each phase all reported that α, ε and δ-phases are reversible after the first discharge [29,84–87,100].

### 3.1.2. The effect of bulk $V_2O_5$ particle size on lithium intercalation

Cocciantelli et al. investigated the effects on several different parameters on the intercalation of lithium ions into $V_2O_5$ [101]. In order to compare the effect of particle size on electrochemical performance, they compared the as received bulk $V_2O_5$ (C-$V_2O_5$) with the product of a melt quenching process using the commercial oxide (Q-$V_2O_5$). C-$V_2O_5$ had average particle sizes of 2 μm whereas Q-$V_2O_5$ had particle sizes ranging from 2 to 50 μm. It was reported that the electrochemical behaviour strongly depends on particle size. The first discharge curve for both samples up to the δ-phase ($x = 1$) is shown in Fig. 5. A Q-$V_2O_5$ electrode which was discharged to 2.8 V exhibited a much smaller specific capacity (≈70 mAh $g^{-1}$) than a C-$V_2O_5$ electrode discharged to the same potential (≈130 mAh $g^{-1}$). This significant difference is capacity values may be attributed to the size of the $V_2O_5$ particles which make up each sample. It takes more time for lithium to diffuse into larger particles. Consequently, if the $V_2O_5$ particles are on average smaller, then more lithium can be intercalated and larger specific capacity values are obtained. Cocciantelli et al. also proposed that the phase transitions associated with the intercalation of lithium ions are not as abrupt as Fig. 5 would suggest. Instead, they suggested that for various amounts of intercalated Li, a combination of phases may coexist. For example when $x = 0.55$, the α, ε and δ-phases coexist. This is because the intercalation of Li ions is diffusion based, and during discharge some particles that make up the electrode which are closer to the current collecting substrate may begin the intercalation process at a later time than particles that are closer to the electrolyte.

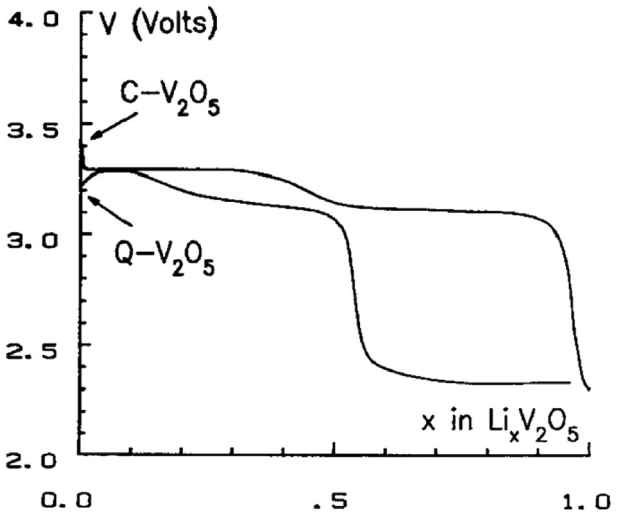


**Fig. 5.** First discharge curve for sample C-$V_2O_5$ and Q-$V_2O_5$ [101].

### 3.1.3. Intercalation to the δ-phase

The structure of the δ-phase was further investigated by Cava et al. [86]. In $V_2O_5$ the $VO_6$ "octahedra" all have one long V–O bond as the $V^{5+}$ ion is displaced toward one apex of the oxygen octahedron, making the coordination pyramidal. The result is that there are layers in the structure which are bound together only by the weak V–O bonds. It was reported that at high lithium contents ($x > 1$) the weak V–O bonds are broken and neighbouring vanadium oxide layers shift and buckle to accommodate the inserted lithium ions. Walk and Margalit proposed that δ-$Li_xV_2O_5$ should be an ideal material to provide long cycle life in lithium ion batteries [99]. They noted that the excellent high temperature stability (up to 75 °C) and high rate capability of δ-$Li_xV_2O_5$ make it a desirable candidate as a positive electrode in a lithium ion battery. The electrochemical performance of δ-$Li_xV_2O_5$ was investigated by Garcia et al. [102]. They reported a specific capacity value of ≈190 mAh $g^{-1}$ after 20 cycles in a potential window of 3.2–1.8 V. The specific capacity increased to ≈290 mAh $g^{-1}$ when discharged/charged in a potential window of 3.8–1.8 V. Both tests were performed at a charge rate of C/10.

Commercial lithium vanadium pentoxide batteries were first produced by Panasonic in the early 2000s. These button cells are intended to be used as back up batteries for devices such as video cameras, memory cards and telephones. The cells consist of a $V_2O_5$ cathode and a Li anode, separated by a porous membrane. The electrochemical performance of these cells was investigated by Moss et al. [94]. The first discharge curve is shown in Fig. 6(a). In comparison with previous results [89], a discharge to 2.0 V should correspond to a lithium content of $Li_xV_2O_5$ where $x = 2$ corresponds to formation of the γ-phase. For these commercial cells the plateau corresponding to the γ-phase is not seen when discharged to 2.0 V. The discharge and charge capacities for the first 50 cycles in a potential window of 3.4–2.1 V are shown in Fig. 6(b). The initial capacity of the battery was ≈35 mAh however after 26 cycles the capacity was reduced to less than 15% of the initial capacity. It can also be seen from Fig. 6(b) that the charge capacities were almost identical to the discharge capacities. This rapid decay in capacity values after a short number of cycles indicates that these commercial cells are useful for their intended purpose, i.e. as a back-up battery.

### 3.1.4. Intercalation to the γ-phase

The electrochemical performance of γ-$Li_xV_2O_5$ was investigated by Cocciantelli et al. [103]. The first 3 discharges and the first charge for $V_2O_5$ to the γ-phase are shown in Fig. 7. The first discharge curve exhibits plateaus at 3.4 V and 3.2 V corresponding to the α and ϵ-phases respectively. As $x \rightarrow 1$ the potential drops steeply to 2.3 V followed by a smooth curve down to 2.0 V. The recharge from $x = 1.8$ and the second and third discharges are characterised by a shortening of the plateaus at 3.4 V and 3.2 V and the formation of an additional plateau at 3.6 V. The second and subsequent discharges exhibit a less rapid drop at $x = 1$, with the formation of a smooth shoulder at =2.7 V and for $x \geq 1$, instead of a continuous variation, two quasi plateaux appear separated by a small potential decrease at $x = 1.25$. These results provide evidence of an irreversible evolution of the $Li_xV_2O_5$ system when the first discharge is carried beyond $x = 1$, i.e. to the γ-phase. Study of further cycling shows that the behaviour of the system becomes reversible again for $0 \leq x \leq 1.8$, provided the electrode potential is held above 2 V. It was reported that cycling in the 3.8–2.0 V range, corresponding to

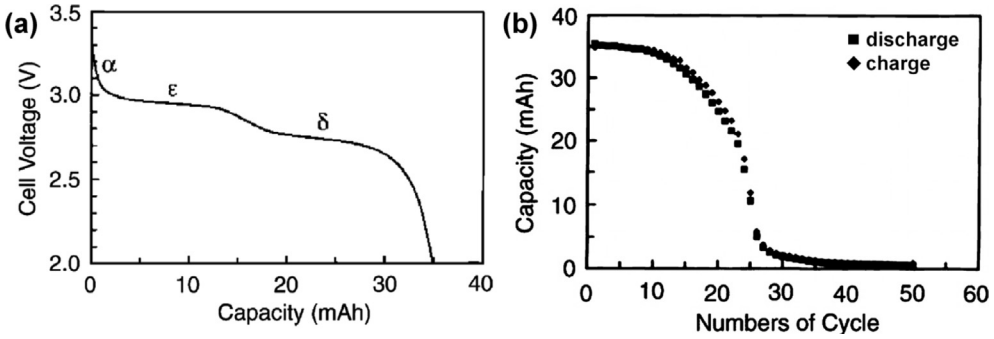


**Fig. 6.** (a) Voltage–capacity curve of the first discharge of a commercial $Li_xV_2O_5$ battery, (b) cell capacities for increased number of cycles [94].

$0 \leq x \leq 1.8$, can increase the battery capacity with an increase in reversibility over a large number of cycles with comparison to discharging to α, ε and δ-phases. Cocciantelli et al. also reported that charging γ-$Li_xV_2O_5$ above 3.5 V results in a different γ-$Li_xV_2O_5$ phase with significant changes in cell parameters [104]. It was reported that the resulting increase in a-parameter and decrease in c-parameter as a result of charging above 3.5 V improves electrochemical performance compared with cells which are not charged to a potential as high as 3.5 V.

### 3.1.5. Intercalation to the ω-phase

The electrochemical performance of ω-$LiV_2O_5$ was investigated by Delmas et al. in 1991. They reported that for the α, ε and δ-phases, in the corresponding 3.6–3.0 V range very good reversibility of the $Li_xV_2O_5$ electrode is obtained and almost 100% of the theoretical capacity is recovered at each discharge. As the amount of lithium increases ($1 < x < 2$) some structural reorganisations are observed. In this voltage domain (3.0–2.2 V) an irreversible transition occurs. This reaction is not however, complete, and even after a large number of cycles, a mixture of the various materials is recovered. This behaviour shows that all the phases involved in these reactions are metastable. When the cell had been discharged to 1.9 V a new material, ω-$Li_xV_2O_5$ was irreversibly formed. This irreversibility is emphasised by the shape of the following charge curve that does not show any of the characteristic plateaus obtained with $V_2O_5$. Nevertheless, the lithium deintercalation from this material is completely reversible. The first 20 cycles are shown in Fig. 8(a). The XRD patterns of crystalline $V_2O_5$ and ω-$Li_xV_2O_5$ are shown in Fig. 8(b). The resulting XRD pattern for ω-$Li_xV_2O_5$ characterises a very disordered structure as only a few broad diffraction lines are present. It was reported that the XRD pattern of ω-$Li_xV_2O_5$ does not significantly change with increased cycling. No significant change is observed after electrochemical deintercalation or even after a large number of cycles. This result shows, unambiguously, that the new structure that characterises ω-$Li_xV_2O_5$($Li_3V_2O_5$) is very stable as it is maintained even after removal of almost all of the intercalated lithium ($Li_{0.2}V_2O_5$). In a similar finding to this the electrochemical intercalation of lithium to high mole fractions into manganese oxide ($Li_xMn_2O_4$) was also investigated. Initially, it was found $Li_xMn_2O_4$ suffered from severe capacity fading. The over lithiation of manganese oxide significantly reduced capacity fading of subsequent cycles [49].

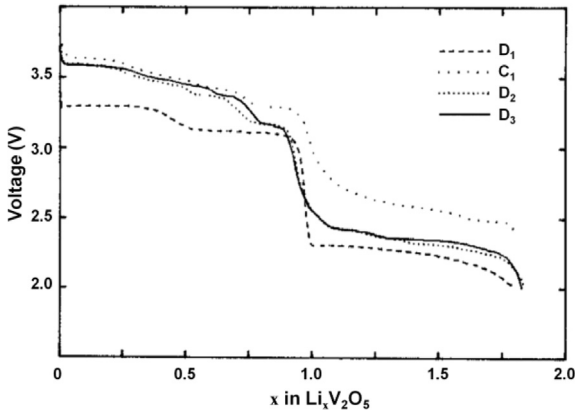


**Fig. 7.** First discharge ($D_1$); charge ($C_1$); second ($D_2$) and third ($D_3$) discharges of a $Li_xV_2O_5$ cell [103].

In order to show the practical possibilities of ω-$Li_xV_2O_5$ as an electrode material for lithium ion batteries, long cycle life tests were also performed. The specific energy values obtained for the first 100 cycles in a potential window of 3.4–1.9 V are shown in Fig. 9. Delmas et al. reported the energy density related to the electrochemical reaction to be very high. The initial value after the first cycle is ≈650 Wh $kg^{-1}$ of $V_2O_5$ and after 100 cycles the ω-$Li_xV_2O_5$ electrodes were still maintaining a value of 450 Wh $kg^{-1}$. This corresponds to a ≈30% loss in energy density after 100 cycles. In addition to this it was reported that this value can be considerably increased if the cycling domain is extended (800 Wh $kg^{-1}$ of $V_2O_5$ between 1.9 and 4.0 V). From these results and a later study also on ω-$Li_xV_2O_5$, [89] which again showed good electrochemical performance, Delmas et al. concluded that ω-$Li_xV_2O_5$ could be a suitable positive electrode material for lithium ion batteries.

The electrochemical performance of ω-$Li_xV_2O_5$ was revisited by Leger et al., in 2005 [105]. The first and second discharge curves obtained in a potential window of 3.8–1.5 V are shown in Fig. 10(a). The curves are nearly identical to those reported by Delmas et al. [100] shown in Fig. 10(a). Delmas et al. used a different potential window (3.4–1.9 V). Leger et al. noted that while the α, ε, δ and γ-phases could be seen in the first discharge, the voltage plateaus associated with these phases are not seen in the subsequent charge and discharge curves. The second discharge curve maintains the same shape as the first charge curve, indicating that the lithium intercalation reaction takes place in a new and single phase, called the ω-$Li_xV_2O_5$ phase. After the first discharge 0.4 moles of lithium are trapped in the ω-phase and the second discharge does not allow the same amount of lithium to be intercalated as for the first discharge. After the first charge, the sample has the composition of ω-$Li_{0.4}V_2O_5$ and after the second discharge the sample has the composition of ω-$Li_{2.65}V_2O_5$. This evidence that some of the lithium intercalated during the first discharge is removed during the first charge indicates that the ω-$Li_xV_2O_5$ phase is indeed irreversible. A typical cyclic voltammogram of $V_2O_5$ is shown in Fig. 10(b). The four main processes for Li insertion in the oxide are located at 3.4, 3.2, 2.35, and 1.95 V, corresponding to the two-phase regions α/ε, ε/δ, δ/γ, γ/ω respectively. One broad peak at 2.85 V appears during the anodic scanning which is in good agreement with the irreversible

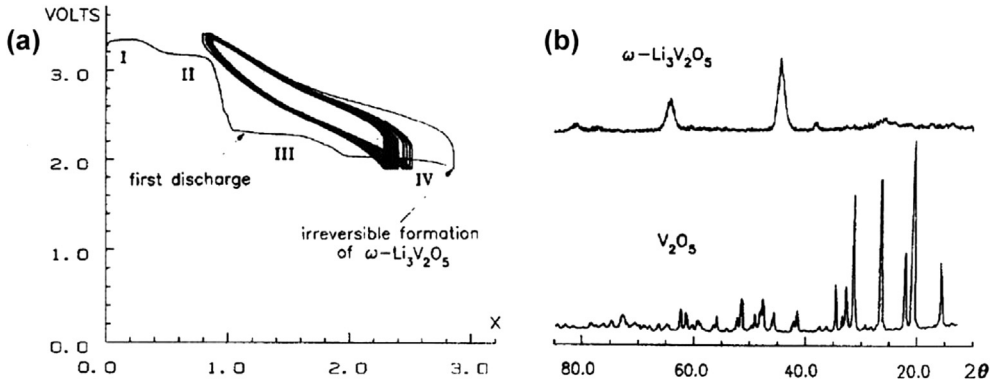


**Fig. 8.** (a) The first 20 cycles for ω-$Li_xV_2O_5$, (b) XRD pattern for crystalline $V_2O_5$ and ω-$Li_xV_2O_5$ [100].

formation of the ω-phase. The evolution of the specific discharge capacity *vs.* number of cycles for ω-$Li_xV_2O_5$ in a potential window of 3.8–1.5 V is shown in Fig. 10(c). The $V_2O_5$ electrode delivers a specific capacity of 450 mAh $g^{-1}$ for the first discharge. This is not shown in Fig. 10(c) as the first discharge is required to form the ω-$Li_xV_2O_5$ phase as discussed earlier. Each subsequent charge and discharge is for ω-$Li_xV_2O_5$, hence data from the second discharge on is reported in Fig. 10(c) and (d). For the second discharge the specific capacity drops to 335 and 300 mAh $g^{-1}$ at C/20 and C/5, respectively. The discharge capacity remains practically stable around 320 mAh $g^{-1}$ over 30 cycles at C/20. At higher rate (C/5) the capacity does not stabilise with increased cycling but slowly decreases to reach 250 mAh $g^{-1}$ after 50 cycles. This shows that faster discharge rates lead to significant capacity loss. This is due to the more severe and repeated structural changes involved in the transformation of the α-phase to the γ-phase. When the operating temperature of the cell was increased from room temperature to 55 °C and a discharge rate of C/5 was used, a more rapid decay in the specific capacity values was observed. The initial value of 370 mAh $g^{-1}$ decreased to 240 mAh $g^{-1}$ after 30 cycles. It took 50 cycles for the sample discharged at the same rate at room temperature to decay to this value, indicating that high temperatures have a detrimental effect on the electrochemical performance of ω-$Li_xV_2O_5$.

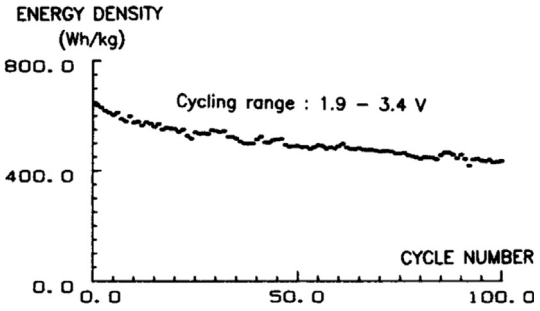


**Fig. 9.** Energy density values obtained for the first 100 cycles with ω-$Li_xV_2O_5$ [100].

The effects of varying the potential window of the specific capacity values of ω-$Li_xV_2O_5$ electrodes discharged at C/20 are shown in Fig. 10(d). The sample cycled in a potential window of 3.8–2.5 V corresponds to discharging the ω-$Li_xV_2O_5$ system in the $0 \leq x \leq 2$ range. For this sample the specific capacity decreases from an initial value of 280 mAh $g^{-1}$ to reach 230 mAh $g^{-1}$ after the 40th cycle. From Fig. 10(d) it is clear that ω-$Li_xV_2O_5$ electrodes discharged to a lower potential of 1.5 V perform better electrochemically, with stable specific capacity values of ≈320 mAh $g^{-1}$ being maintained

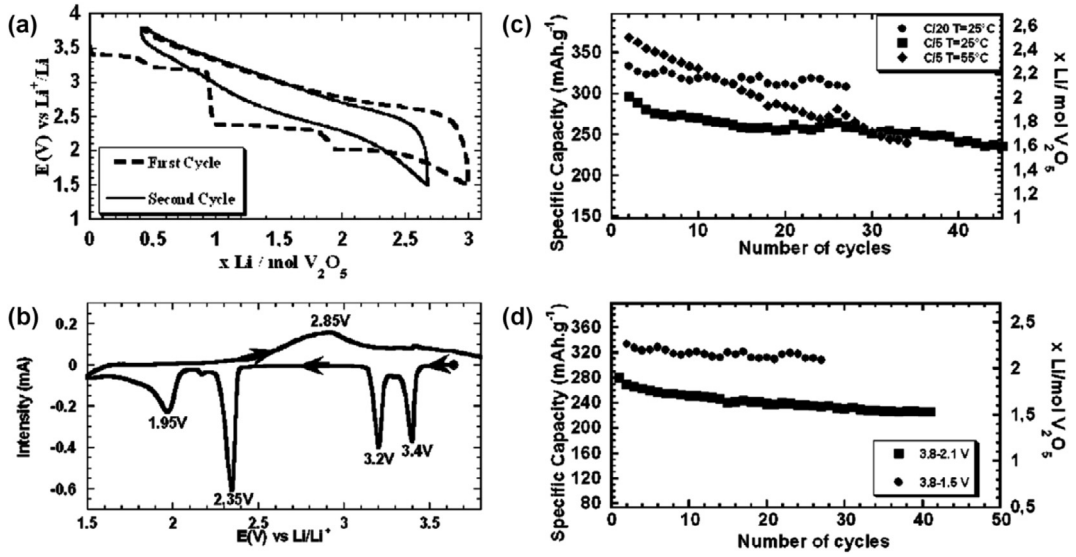


**Fig. 10.** (a) First and second discharge–charge curves of $Li_xV_2O_5$, (b) cyclic voltammetric curves of $Li_xV_2O_5$ (sweep rate 10 mV $s^{-1}$). Evolution of the specific capacity as a function of the number of cycles at (c) various temperatures and discharge charge rates and (d) various potential windows [105].

over the first 30 cycles. Leger et al. reported that the electrochemical performance of ω-$Li_xV_2O_5$ showed significant improvement over δ-$Li_xV_2O_5$ and γ-$Li_xV_2O_5$ and concluded that ω-$Li_xV_2O_5$ constitutes one of the most promising rechargeable vanadium oxide forms for Li batteries.

### 3.1.6. *Structural investigation of the ω-$Li_xV_2O_5$ system with increased cycling*

Leger et al. also investigated the structure of the ω-$Li_xV_2O_5$ system after various numbers of cycles [105]. The XRD patterns of two electrodes with compositions of ω-$Li_3V_2O_5$ and ω-$Li_{0.4}V_2O_5$ are shown in Fig. 11(a) and (b). These two compositions correspond to the ω-$Li_xV_2O_5$ sample after the first discharge and charge respectively. In the α, ε, δ and γ-phases of the $Li_xV_2O_5$ system ($x < 2$) there is little change in the structure of $V_2O_5$, as mentioned earlier. When the sample is discharged to the ω-$Li_xV_2O_5$ phase, significant structural changes occur. From the XRD pattern in Fig. 11(a), it is clear that a disordered structure is obtained with broad peaks and some peaks of very weak intensity. For the ω-$Li_3V_2O_5$ compound, the main typical diffraction lines located at 51.82° and 76.20° are broad and characterised by the interplanar distances of 2.05 and 1.45 Å and can be twice indexed as (240, 002) and (260, 242), respectively, on the basis of a tetragonal symmetry. This is also the case for a smaller peak at 69.18° which can be indexed as (350, 251). All the diffraction lines can be indexed on the basis of a tetragonal symmetry with the following unit cell parameters: $a = b = 9.20$ Å and $c = 4.09$ Å. The presence of the (020, 021, 011, 022, 122, 251) and (113) lines unambiguously demonstrates that ω-$Li_xV_2O_5$ has a tetragonal symmetry and not a cubic one. Peaks belonging to less deeply discharged phases (δ and γ-phases) still appear after the first discharge. These additional peaks are progressively suppressed from the second galvanostatic cycle and with repeated cycles. Fig. 11(b) confirms the new tetragonal structure electrochemically formed during the first discharge is retained after the first charge. Only the two main peaks at 51.94° and 76.36° are seen after the first charge and their intensities have been greatly reduced. The ω-$Li_{0.4}V_2O_5$ compound also exhibits a tetragonal structure but with slightly smaller parameters $a = b = 9.17$ Å and $c = 4.09$ Å. This reduction in cell parameters after the first charge, i.e. after the removal of lithium ions confirms that lithium ions are responsible for the ordering of the structure.

The XRD patterns ω-$Li_{2.65}V_2O_5$ after the 27th discharge and ω-$Li_{0.4}V_2O_5$ after the 20th charge at a C rate of C/5 are shown in Fig. 11(c) and (d) respectively. At the end of the 27th discharge the two major peaks (002, 240) and (260, 242) and two peaks of weak intensities (021) and (622) can be seen in the resulting XRD pattern. This clearly indicates the initial tetragonal structure is preserved after 27 cycles, having unit cell parameters $a = b = 9.21$ Å and $c = 4.11$ Å. XRD data obtained after the charge process at the 20th cycle shows that the ω-$Li_{0.4}V_2O_5$ compound has the following cell parameters, $a = b = 9.17$ Å and $c = 4.08$ Å. The unit cell parameters after 20 and 27 cycles are very close to the cell parameters measured after the first cycle. This indicates that ω-$Li_xV_2O_5$ has very stable structural properties with cycling. Leger et al. proposed that the improved electrochemical performance of ω-$Li_xV_2O_5$ over δ-$Li_xV_2O_5$ and γ-$Li_xV_2O_5$ is due to the tetragonal symmetry of ω-$Li_xV_2O_5$. This tetragonal symmetry only occurs when $Li_xV_2O_5$ is discharged to at least 1.5 V, at this point the irreversible ω-phase is formed and there is a significant improvement in electrochemical performance.

## 4. Vanadium pentoxide gels

Initial reports provided evidence that bulk $V_2O_5$ displayed poor electrochemical performance when discharged to α, ε, δ and γ-phases. $V_2O_5$ samples which were discharged to potentials corresponding to each of these phases showed rapid decay in specific

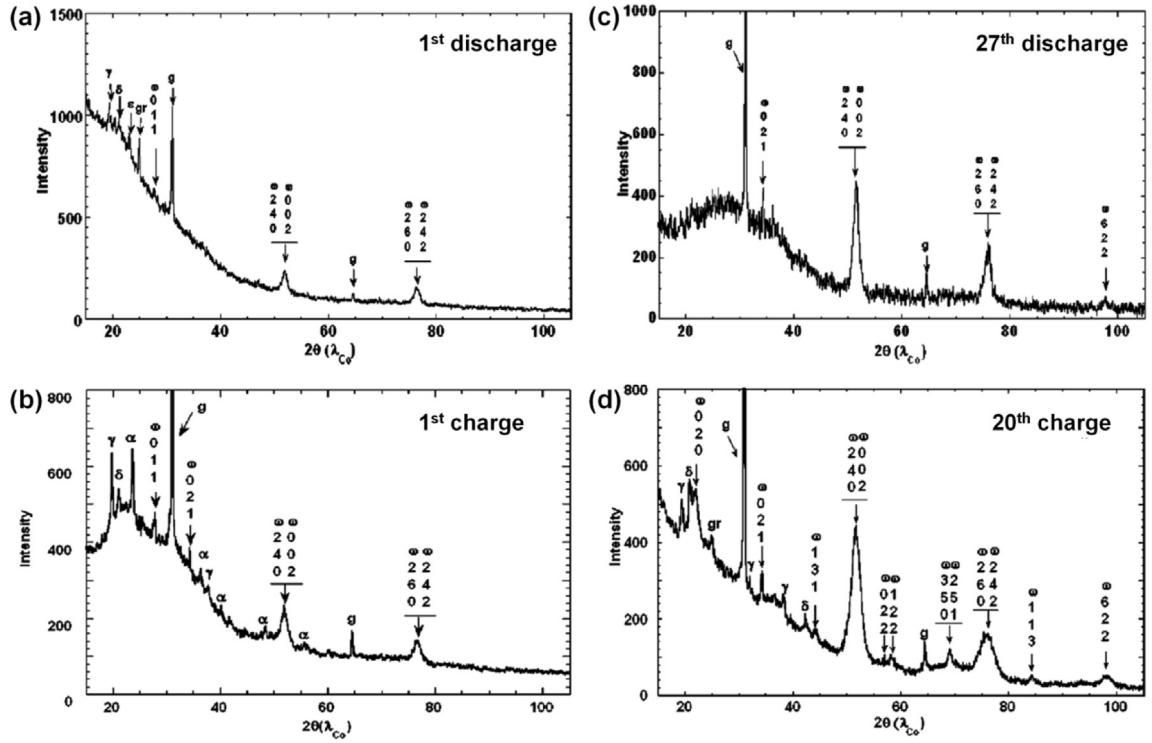


**Fig. 11.** XRD patterns of (a) ω-$Li_3V_2O_5$ at the end of the first discharge, (b) ω-$Li_{0.4}V_2O_5$ at the end of the first charge, (c) ω-$Li_{2.65}V_2O_5$ at the end of the 27th discharge and (d) ω-$Li_{0.4}V_2O_5$ at the end of the 20th charge (g: graphite, gr: grease) [105].

capacity values for increased cycling. Discharging $Li_xV_2O_5$ to the irreversible ω-phase changed the structure of the host vanadium oxide from orthorhombic to tetragonal and consequently, there was a significant improvement in electrochemical performance. In an effort to further improve the performance of $V_2O_5$ as a possible cathode material for lithium ion batteries a lot of attention was given to other forms of $V_2O_5$ such as $V_2O_5$ gels and more recently, $V_2O_5$ nanostructures. Vanadium pentoxide gels have been known for over a century and as such many synthesis techniques have been reported in the literature. The first was reported by Ditte in 1885. [106] Ditte heated ammonium vanadate in a platinum crucible and then added hot nitric acid to the resulting residue. This mixture was then poured into water and a red sol gel was formed. Following this similar experiments using hydrochloric acid were performed by Biltz in 1904 [107]. $V_2O_5$ sols have been reported as far back as 1912. Wegelin obtained the sols through the thermohydrolysis of aqueous solutions of $VOCl_3$ [108]. Initial vanadium pentoxide sol gels were obtained from treatment of chemical compounds consisting of a vanadium oxide however further research would show that vanadium pentoxide gels can also be obtained directly from the oxide. For example Müller reported that vanadium pentoxide gels can be obtained by heating crystalline $V_2O_5$ to 800 °C and pouring the molten oxide into water [109,110]. It was also shown that hydrogen peroxide reacts vigorously with crystalline $V_2O_5$ to give rise to a red gelatinous product [111]. In the last thirty years it has been shown that $V_2O_5$ gels can also be obtained through the hydration of amorphous $V_2O_5$ [112]. Amorphous $V_2O_5$ films obtained by vapour deposition [113] or $V_2O_5$ spheres as powder formed by $O_2$–$H_2$ flame fusion [114] can be ground with water to obtain vanadium oxide gels and also sols as more water is added. Research by Livage and colleagues using sol–gel chemical synthesis renewed interest in vanadium oxide gels in the 1970's and 1980's [115–117]. For electrochemical applications, the two most employed vanadium oxide gel synthesis methods are acidification of a vanadate solution using ion-exchange resin with subsequent spontaneous polymerisation of the resulting $HVO_3$ solution [118] and hydrolysis and condensation of vanadium alkoxides [119,120]. Electron microscopy shows that vanadium oxide gels they are made of ribbon like fibres as shown in Fig. 12.

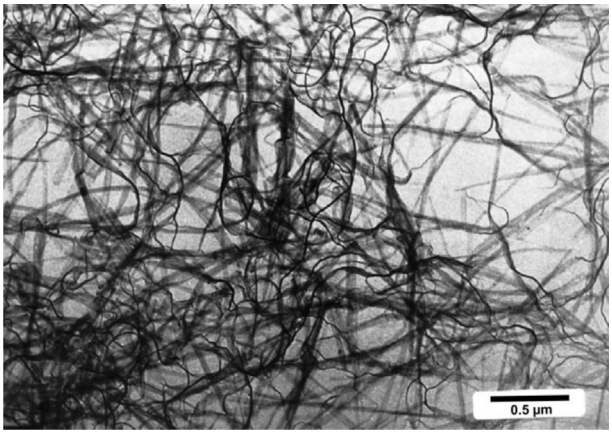


**Fig. 12.** TEM image showing the fibrous structure of vanadium pentoxide gels [118].

### 4.1. Comparison of the electrochemical performance of different vanadium oxide gels with crystalline $V_2O_5$

The initial electrochemical performance of crystalline $V_2O_5$, a layered $V_2O_5 \cdot nH_2O$ xerogel from vanadic acid and an amorphous vanadium oxide gel from alkoxides was compared by Livage [121]. The first discharge curve for each of these samples is shown in Fig. 13. It was reported that the electrochemical behaviour of vanadium pentoxide gels ($V_2O_5 \cdot nH_2O$) as a reversible cathode for lithium batteries is quite different from that of the crystalline oxide. The discharge curve of crystalline $V_2O_5$ exhibits several steps corresponding to the formation of different $Li_xV_2O_5 \cdot nH_2O$ phases as discussed earlier and also shown in Fig. 13(a). When discharged to 2.0 V the initial specific capacity for crystalline $V_2O_5$ was reported to be ≈200 mAh $g^{-1}$. The discharge curve of vanadium pentoxide gels is quite different. A single plateau is observed around 3.1 V (Fig. 13(b)). A specific capacity close to 250 mAh $g^{-1}$ was obtained at 2.0 V corresponding to the reduction of all $V^{5+}$ ions into $V^{4+}$. Through cyclic voltammetry and XPS analysis, Özer also reported that $V^{5+}$ is reduced to a lower valence state, $V^{4+}$ by lithiation, and can be returned to the original valency through delithiation [122]. Livage reported that the $V_2O_5$ xerogels from vanadic acid show good reversibility and with ≈70% of the initial capacity being recovered after 30 cycles (at a current density, $j = 0.05$ mA $cm^{-2}$). It was proposed that the improved behaviour of gels could be due to the weak interactions between $V_2O_5$ layers allowing the insertion of $Li^+$ ions between the ribbons which make up the xerogel, rather than in the layers of vanadium oxide as for crystalline $V_2O_5$. It was also reported that for increased cycling the layered structure is lost and the material becomes amorphous. This process of $V_2O_5 \cdot nH_2O$ xerogels from vanadic acid becoming completely amorphous with increased cycling was also reported by Anaissi et al. [123]. Initially, the xerogel films consist of heterogeneous regions and as Li ions are intercalated, a gradual reorganisation takes place and the several non-equivalent redox sites collapse into a uniform band-type structure. The electrochemical behaviour of amorphous thin films deposited from vanadium alkoxides is quite different from that of layered $V_2O_5 \cdot nH_2O$ gels synthesised from vanadic acid. A continuous decrease of the discharge curve rather than a large plateau is observed (Fig. 13(c)). In fact there is an almost completely linear discharge for gels prepared from alkoxides. The open circuit voltage and the capacity are slightly smaller than those of polyvanadic acid, at least during the first discharge. This might be due to the greater extent of reduction of $V^{5+}$ to $V^{4+}$ during the synthesis.

### 4.2. Varying water content in vanadium oxide gels

For electrochemical testing purposes vanadium oxide gels are deposited on current collecting substrates and as such can be treated as thin films. Initial electrochemical testing of these films

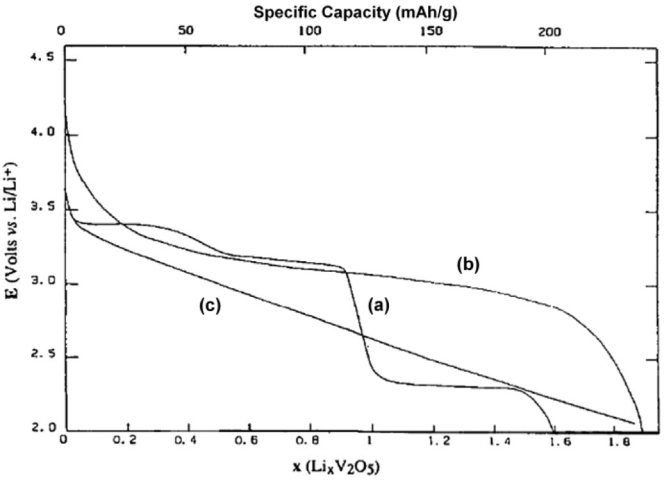


**Fig. 13.** Discharge curve of vanadium oxides in $Li/LiClO_4$-propylene carbonate/$V_2O_5$ cells; (a) crystalline $V_2O_5$, (b) layered $V_2O_5 \cdot nH_2O$ xerogel from vanadic acid and (c) vanadium oxide gel from alkoxides [121].

was performed in a $LiClO_4$-propylene carbonate electrolyte [124,125]. One of the main issues when comparing electrochemical results of vanadium oxide gels which were prepared using different methods is that they can contain varying amounts of water. It was reported that the initial high water content of the $V_2O_5 \cdot nH_2O$ gels ($n = 1.6–2.05$) is partially exchanged with the propylene carbonate in the electrolyte. Also any additional residual water might still limit the recharge ability of the cells. The ability to intercalate lithium ions into vanadium pentoxide gels as given by the composition parameter $x$ in $Li_xV_2O_5 \cdot nH_2O$, has been reported to vary from 0.8 to 1.8 for discharge to 2.0 V (*vs.* Li) [124,125]. This variation in the amount of lithium being intercalated is most likely related to differences in hydration [118] and to solvent exchange, but also to differences in the preparation and post treatment of the gel. Different procedures may lead to variations in the degree of polymerisation and in the average oxidation state of vanadium in the oxide [126]. TGA analysis of vanadium oxide xerogels gave a greater understanding of the water content present in the gels. As mentioned vanadium oxide gels typically consist of layers of ribbon-like units and this structure is stabilised by physisorbed and chemically bound water. According to DTA and TGA measurements three types of water are present in a dried $V_2O_5 \cdot nH_2O$ gel [115]. Initially at ambient conditions $n$ can vary from 1 to 1.6, when the gel is dried under vacuum or by heating to 100–120 °C, $n$ is reduced to approximately 0.5–0.6. Below $n = 0.5$, the dehydration becomes more difficult. Most of the remaining water can be gradually removed by further heating. However a small amount is chemically bound to vanadium (about $0.1H_2O$ per $V_2O_5$) and is only liberated by heat treatment at temperatures above approximately 320 °C where the xerogel is converted to orthorhombic vanadium pentoxide. In order to comply with the strict anhydrous conditions in a lithium battery, the physisorbed water should be removed from xerogel electrode films before use [126]. This is typically done by heating the films to 100 °C in a vacuum oven overnight.

### 4.3. Effect of temperature on electrochemical performance

West et al. investigated the effects of heating vanadium oxide xerogels (from vanadic acid) to different temperatures on their electrochemical performance [126,127]. It was reported that the resulting cycling curves are smooth without any discrete phases in contrast to the multiphase curves which are obtained with crystalline $V_2O_5$. Orthorhombic $V_2O_5$ has a crystalline structure; typically $V_2O_5$ gels have an amorphous structure [127,128]. Hence there is no evidence of structural rearrangements induced by the insertion and removal of lithium ions. West et al. heated vanadium oxide xerogel electrodes to 100 °C in a vacuum oven and to 300 °C in air. These samples were then discharged to different potentials; the upper limit in each case was 3.8 V. The number of moles of lithium being intercalated into these samples with increasing number of cycles is shown in Fig. 14(a). It was reported that for xerogel samples heated to 100 °C, the capacity retention is not very good as can be seen in Fig. 14(a). For samples discharged to 1.5 V, only ≈50% of maximum capacity is retained after 20 cycles. There is a significant improvement in the cycling efficiency when the samples are discharged to 2.0 V. After 50 cycles ≈70% of the maximum capacity is retained. As mentioned above the xerogel samples which were heated to 300 °C are more crystalline than samples heated to 100 °C. The samples heated to 100 °C were able to intercalate ≈1.4 mol of lithium whereas samples heated to 300 °C intercalated ≈1.8 mol of lithium, as seen in Fig. 14(b). The increased crystallinity and reduced amount of water in the sample heated to 300 °C results in these samples having greater capacities and performing better electrochemically when compared with samples heated to

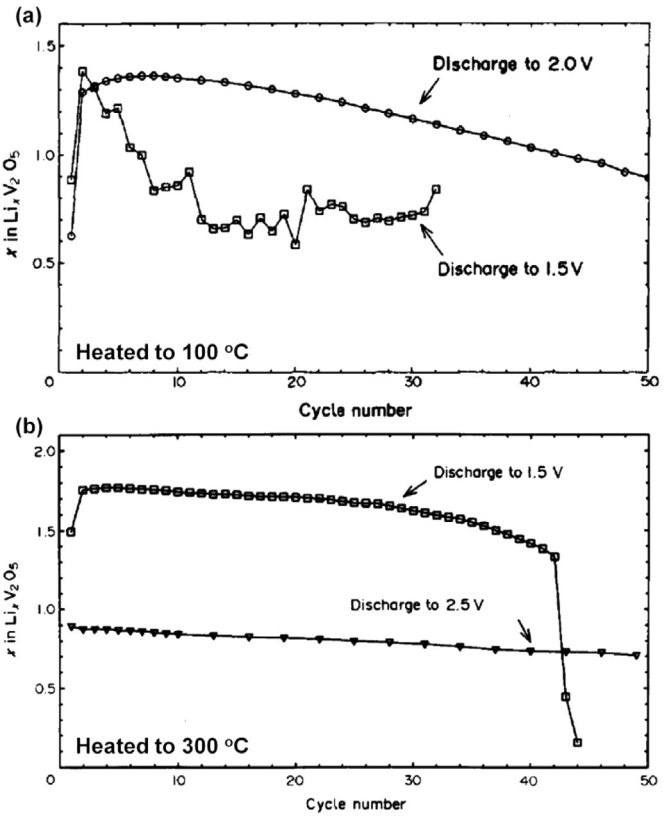


**Fig. 14.** Cycling performance for $V_2O_5 \cdot nH_20$ samples heated to (a) 100 °C and (b) 300 °C [126].

100 °C. It was reported that as the vanadium oxide ribbons comprising the xerogel are identical in all of these materials, the conductivity along the length of the ribbons decreases with lithium intercalation in all cases, but that inter-ribbon conduction is facilitated in the material dried at 300 °C. In such cases, the ribbons are in much better layer-on-layer registry, and the amount of material inserted between the ribbons is smaller.

Park et al. also investigated the electrochemical performance of $V_2O_5$ xerogels from vanadic acid heated to 300 °C and reported initial specific capacity values of ≈470 and ≈565 mAh $g^{-1}$ for samples discharged to the point where the composition of Li in $Li_xV_2O_5 \cdot nH_2O$ was $x = 3.3$ and $x = 4.0$ respectively [128]. These initial values are significantly larger that values obtained with $LiCoO_2$ (≈170 mAh $g^{-1}$) [52] which is currently used in the majority of lithium ion batteries, however unlike $LiCoO_2$, $V_2O_5 \cdot nH_2O$ electrodes suffer from rapid capacity loss [126,127,129,130]. The rapid decay in specific capacity was also reported by Tipton et al. [131]. They reported that for coin cells with $V_2O_5$ xerogel working electrodes, cycled in a potential window of 3.75–1.5 V, ~73% of the initial capacity is retained after the 2nd discharge and ~44% is retained after the 16th discharge. The specific capacity of $V_2O_5$ xerogel electrodes can be lowered if lithium ions are retained in regions of the active material that become isolated during cycling. This would most likely happen as a result of the swelling and contracting associated with the insertion and removal of Li ions.

## 5. Vanadium oxide aerogels

Vanadium oxide aerogels are prepared by supercritical drying of vanadium oxide gels. First reported by Hirashima and Sudoh in

1992, initial vanadium oxide aerogels were prepared from alkoxides by hydrolysis and then supercritical drying with an autoclave at 255 °C and 210 atm for 1 h [132,133]. Upon supercritical drying a shrinking of the vanadium oxide gel occurs. The resulting aerogels have a fibrous structure, and they consist of micro-fibrils <10 nm in diameter. It was also reported that the porosity of the $V_2O_5$ aerogels was more than 90%. Aerogels have also been prepared at low temperatures using liquid $CO_2$ [120,134–137] and ambient pressure methods [138]. For each method, the resulting materials possess the low densities and high surface areas typical of aerogels [139]. It has been shown that vanadium oxide aerogels represent a different host material than vanadium oxide xerogels [136,140,141]. The first discharge curve showing discharge to a composition of $Li_4V_2O_5$ for xerogel (from vanadic acid) and aerogel (supercritically cooled with liquid $CO_2$), as reported by Le et al. is shown in Fig. 15 [134,135]. Initial electrochemical experiments showed that for vanadium oxide aerogel, ~4 Li per $V_2O_5$ could be reversibly cycled. $V_2O_5$ xerogels are also able to intercalate 4 Li per $V_2O_5$ however the xerogel samples have to be discharged to far lower potential to incorporate this amount of lithium. An aerogel sample must be discharged to a potential of ≈2.75 V to reach a composition of $Li_4V_2O_5$, whereas a xerogel sample must be discharged to ≈1.80 V. It was proposed that the processing of the precursor xerogel to the aerogel causes the intercalation sites to be altered significantly. It has also been reported that through chemical lithiation with *n*-butyl lithium aerogels with compositions of $Li_xV_2O_5$ having values of $x = 5.8$ are possible [142]. The equilibrium voltage composition curves shown in Fig. 15 suggest that xerogels and aerogels have different mechanisms for lithium intercalation. The ability of aerogels to intercalate larger amounts of lithium at higher potentials may be due to their extremely high surface area, large interlayer spacing and the nearly amorphous structure [83].

The cycling performance of $V_2O_5$ aerogel was investigated by Sudant et al. [143]. Samples were cycled in different potential windows with a discharge/charge rate of C and the resulting specific capacities for increasing number of cycles is shown in Fig. 16. Although $V_2O_5$ aerogels do perform well electrochemically initially, like xerogels they also suffer from significant capacity fading issues [144–146]. Sudant reported capacity fading for different cut-off voltages. The greatest loss in capacity occurs in a potential window of 4.0–1.5 V. The specific capacity decreases from 300 to

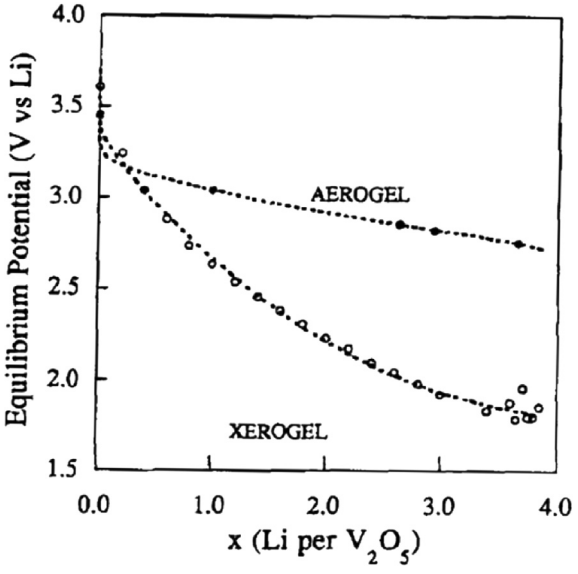


**Fig. 15.** Equilibrium potential as a function of lithium composition for $V_2O_5$ aerogel and xerogel [134].

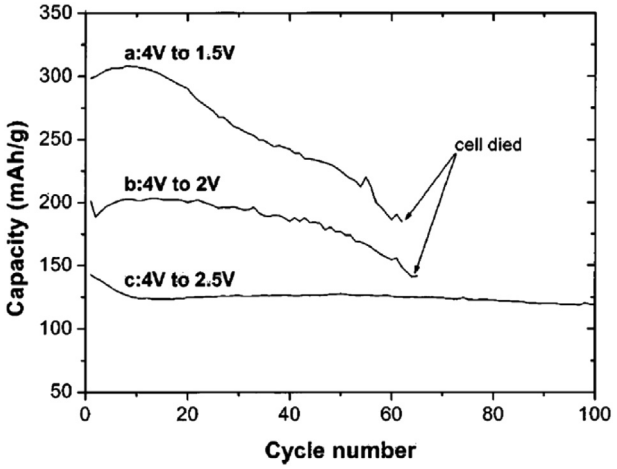


**Fig. 16.** Cycling behaviour for $V_2O_5$ aerogel at 1C rate for different cut-off voltages (a) 1.5 V, (b) 2.0 V, and (c) 2.5 V [143].

200 mAh $g^{-1}$ after 60 cycles for a rate of 1C. When the lower limit is increased to 2 V the capacity fading is not as severe and there is even better stability for discharge to 2.5 V. The specific capacity value of ≈125 mAh $g^{-1}$ obtained in the latter case is small. Mansour et al. reported an almost 30% loss in the initial specific capacity after 16 cycles for a $V_2O_5$ aerogel electrode discharged/charged at a C/5 rate in a potential window of 4.0–1.5 V [147]. Mansour et al. also examined the evolution of the oxidation state and atomic structure of V in $V_2O_5$ aerogel cathodes as a function of state of charge and cycling in a non-aqueous cell. It was reported that during discharge, the average oxidation state of V is consistent with the amount of Li inserted in the cathode (i.e. $x$ in $Li_xV_2O_5$). Initially, $V^{5+}$ is reduced to $V^{4+}$ in the intercalation range $0 < x < 2$ and then $V^{4+}$ is reduced to $V^{3+}$ with additional intercalation of Li. Upon charging, $V^{3+}$ is re-oxidised to $V^{4+}$ and then to $V^{5+}$ upon removal of Li. Mansour proposed that these results suggest that the origin of capacity fade is due to the formation of electrochemically irreversible phases such as $LiVO_3$ and $Li_3VO_4$. The reasons for the deterioration of the electrochemical activity of the composite electrodes are quite straightforward: reduced surface due to the particle agglomeration and collapse of the porous morphology [83].

## 6. Specific capacity fading

This review of the electrochemical performance of crystalline bulk $V_2O_5$, vanadium oxide sol–gels, xerogels and aerogels has shown that in each case capacity fading is a significant issue which hampers the application of $V_2O_5$ as a cathode material for commercial lithium ion batteries. The capacity fading upon long term cycle life tests is a phenomenon frequently observed in intercalation materials. Usually there are two main reasons why this occurs [146]. The first is related to the nature of the intercalation compound and the intercalation process. Irreversible reactions may take place in the electrode during cycling. Every form of $V_2O_5$ discussed so far undergoes some irreversible reaction upon intercalation of lithium ions. The structure of the intercalation compound may change with increased cycling. This may be a consequence of the formation of irreversible phases or over time the active material may be soluble in the electrolyte. The second common reason why capacity fading may occur can be considered as a mechanical cause and is associated with the loss of electrical contact within the composite electrode. The volumetric changes associated with the insertion and removal of lithium ions can cause cracking in thin film electrodes (for sol–gels, xerogels and aerogels) and the

pulverisation of larger particles (for crystalline $V_2O_5$). This can lead to the isolation of regions of the electrode which will no longer be contributing to the electrochemical performance of the electrode being tested. It is for this reason that in many cases a conductive additive is added to the active material when preparing electrodes. Another issue is that over time the portions of active material may lose electrical contact with the current collecting substrate. This may happen again due to volume changes of the host material during cycling. It is an issue for all samples but it can have quite a significant effect on thin film electrode samples for sol–gels, xerogels and aerogels. As mentioned earlier these $V_2O_5 \cdot nH_2O$ gels can contain large amounts of water ($n \approx 2$). The gels are either drop-casted or spin coated onto a current collecting substrate and then they must be heated to remove physisorbed water before they can be electrochemically tested. As a result of the dried coated films are very brittle, and delaminate easily from the substrate during handling and electrochemical testing [126]. In an attempt to improve the mechanical properties of these films without impairing their electrochemical properties, binders such as (poly)ethylene oxide are mixed with the vanadium oxide gels before drying on the substrate. Typically these films are more flexible than the pure gel films, and can be easily handled and incorporated into test cells without delamination. In order to improve the electrochemical performance of $V_2O_5$ novel approaches to the electrode architecture were required. Smaller particle sizes would overcome many of the issues associated with volume changes during cycling and would offer more diffusion sites for Li ions, potentially increasing capacity values. Interest in this would eventually lead to the investigation of vanadium oxide nanostructures as cathode materials for improved lithium ion batteries.

## 7. Introduction to nanostructured materials

The properties of solid state materials mainly depend on their structure and morphology [148]. Nanostructured materials continue to be a thriving subject of scientific interest due to an outstanding range of properties that vary from their bulk counterparts, such as optical, electrical, magnetic, catalytic, chemical, structural, and electrochemical properties [81,83,149]. Consequently nanostructures find applications in many fields such as nano-electronics, batteries, sensing devices and nano-medicine [150–163]. Today there is a wide range of chemical synthesis techniques to produce nanostructured materials of various shapes. Chemical reactivity as well as the physical properties of materials are dependent on the size of the structures; hence there is a lot of research comparing the properties of different nanostructures of the same materials. Nanostructures can take many different forms such as wires [164–166], rods [167–169], tubes [170–173], belts [174–176], platelets [177–179], spheres [180–182], urchins [183–185]; the form which is produced has a huge impact on the properties of the material.

## 8. Nanomaterials for lithium ion batteries

The ongoing exponential increase in computer processing power has led to remarkable improvements in many devices such as mobile phones, laptop computers and more recently tablet computers. One of the major issues over the last few decades is that batteries are not keeping up with other technological advances. Furthermore, the emerging energy resource crisis and ecological concerns unambiguously show that energy storage is one of the great challenges in the current century. Now more than ever there is a very serious demand for improved batteries for portable consumer electronics, electrical vehicles and for the storage of renewable energy. Nanomaterials are being investigated as electrode materials in order to achieve the increase in energy and power densities required to meet growing demands. There are many advantages and disadvantages associated with the use of nanomaterials in lithium ion batteries as detailed by Bruce et al. [186]. The advantages include (i) the ability to enable electrode reactions to occur that cannot take place for materials composed of micrometre sized particles, (ii) the reduced dimensions lead to shorted Li diffusion paths which significantly increases the rate of lithium insertion/removal, (iii) the larger surface area allows a larger contact area with the electrolyte and hence permits a high Li ion flux across the interface. The disadvantages include (i) nanostructures may be difficult to synthesise and their dimensions may be difficult to control, (ii) the high contact areas between the electrolyte and electrodes may lead to more significant side reactions with the electrolyte.

### 8.1. $LiCoO_2$, $LiMn_2O_4$ and $LiNiCoO_2$ nanotubes as a cathode material for lithium ion batteries

By far, the most common cathode active materials that are being researched and commercially used in lithium ion batteries are the lithiated transition metal oxides such as $LiCoO_2$, $LiNiO_2$, $LiMn_2O_4$, and their doped counterparts [1,52,187–189]. The performance of bulk particles of each of these compounds was previously discussed in Section 2. Following the development of carbon nanotubes [170] there was an immediate interest in revisiting traditionally used cathode materials to determine if their nanostructure counterparts would offer improved performance. The electrochemical performance of nanotubes of $LiCoO_2$, $LiNi_{0.8}Co_{0.2}O_2$ and $LiMn_2O_4$ and were compared by Li et al. [190]. The second discharge curves for all three of these compounds are shown in Fig. 17(a). These samples were discharged to 3.0 V using a current density of 10 mA $g^{-1}$. The specific capacities of all three nanotube samples are higher than the initial capacities obtained with their bulk counterparts. The initial capacities for bulk $LiCoO_2$, $LiNiCoO_2$ and $LiMn_2O_4$ were ≈150, 200 and 120 mAh $g^{-1}$ respectively. The specific capacities for the nanotube variants of these samples increased to ≈180, 210 and 140 mAh $g^{-1}$ respectively.

The cycling performance of the three nanotube samples for the first 100 cycles in a potential window of 4.3–3.0 V, at a current density of 10 mAh $g^{-1}$, is shown in Fig. 17(b). Starting from the first cycle the discharge capacity decreased for each subsequent cycle. After 100 cycles the specific capacity value obtained for the nanotubes of $LiCoO_2$, $LiNi_{0.8}Co_{0.2}O_2$ and $LiMn_2O_4$ corresponded to a loss in initial capacity of 11%, 29% and 31% respectively. It is clear that the $LiCoO_2$ nanotubes performed the best out of these three samples. After 50 cycles the specific capacity of the $LiCoO_2$ nanotubes has decreased by 10% of its initial value but after that almost no further capacity was lost. The cycling performance of nanotubes of $LiCoO_2$, $LiNiCoO_2$ and $LiMn_2O_4$ is a significant improvement over their bulk counterparts. While $LiCoO_2$ has shown stable capacity retention with increased cycling both $LiNiCoO_2$ and $LiMn_2O_4$ have been shown to suffer from significant capacity fading issues. $LiCoO_2$ in particular exhibits stable capacity values with increased cycling; however, there is an ever growing need for enhanced cathode materials to meet increasing energy storage demands [1]. Hence alternative materials are being investigated. Vanadium oxides thin films and xerogels were extensively studied as a cathode material for lithium batteries. Following the development of the lithium ion battery [21] and carbon nanotubes [170] a lot of research was devoted to the fabrication of vanadium oxide nanostructures.

## 9. Introduction to vanadium oxide nanostructures

Among the many nanostructures which have been developed over the last few decades, nanostructured vanadium oxides have

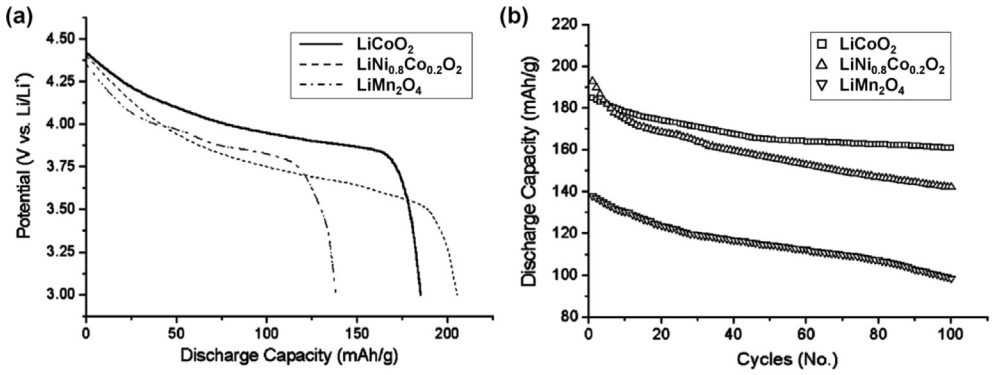


**Fig. 17.** The electrochemical performance of nanotubes of $LiCoO_2$, $LiNi_{0.8}Co_{0.2}O_2$ and $LiMn_2O_4$ (a) second discharge curves, (b) cycling performance [190].

been extensively studied [52,148,191–198]. Vanadium oxides in general attract a lot of attention due to their interesting catalytic properties, their structural flexibility and electrochemical properties [29,199–205]. Vanadium oxide nanotubes (VONTs) were first reported by Spahr et al. [206] in 1998 and since then there has been a tremendous amount of interest in their application across a wide variety of devices, most noticeably as a cathode material for lithium ion batteries [207–211]. Other nanostructured vanadium oxides with various morphologies have also been reported including: nanobelts [212,213], nanowires [214,215], nanorods [216,217], nanourchins [218,219], nanocogs [220] and flower like nano shapes [221,222]. Typically vanadium oxide nanostructures are synthesised via the hydrothermal treatment of aqueous solutions of vanadium (V) precursors [148]. The pH of the precursor mixture and temperature of the thermal treatment appear to be the main parameters to control the resulting morphology of $V_2O_5$ based nanomaterials [218,223–226]. Vanadium oxide nanostructures have been employed in a wide range of applications including FETs [227,228], sensors [212,229], spintronic devices [230] and nanolithography templates [231,232]. As mentioned over the last 20 years there has been a tremendous amount of research into the nanostructures of the most commonly used cathode materials with the hope of improving electrochemical performance. For the same reasons there has also been renewed interest in vanadium oxide nanostructures for enhanced lithium intercalation, most notably for nanotubes. Nanotubes are particularly attractive as an electrode material for lithium ion batteries since they provide several access regions for intercalates such as lithium ions [233–235]. The synthesis and electrochemical performance of vanadium oxide nanotubes shall now be discussed.

## 10. Synthesis and discovery of vanadium oxide nanotubes (VONTs)

Spahr et al. first synthesised VONTs by a hydrothermal treatment of a vanadium oxide precursor mixed with a primary amine [206]. Vanadium triisopropoxide and hexadecylamine were mixed together, hydrolysed and allowed to age. This resulted in a yellow lamellar-structured composite of hydrolysed vanadium oxide and amine surfactant as shown below in Fig. 18(a). The contrasting light and dark layers seen in Fig. 18(a) are the expected layers of vanadium oxide however a layer thickness of approximately 3 nm was reported. This is a wider spacing than vanadium oxide on its own and it implies that there is a widening of the layers due to hydrolysis and the intercalation of amine molecules between the vanadium oxide layers.

Thermal treatment resulted in a black powdered material consisting of clumps of VONTs as shown in Fig. 18(b). Therefore a colour change from yellow to black is observed before and after thermal treatment respectively. The resulting VONTs were reported to be paramagnetic with a semi metallic conductivity presumably due to mixed valency vanadium centres. Such nanotubes also exhibited good conductivity, even when intercalated with a considerable volume fraction of organic species [236]. Fig. 18(b) shows the hollow core of the nanotubes as well as their open ends. The lengths of the VONTs were measured to be 2000 nm with outer diameters

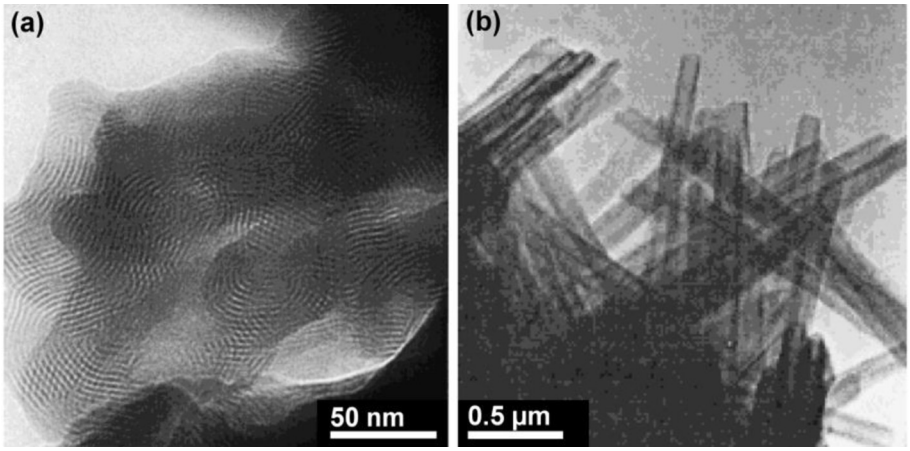


**Fig. 18.** (a) TEM image of the resulting structure, after ageing of hydrolysed mixture of vanadium triisopropoxide and hexadecylamine, (b) TEM image of VONTs after thermal treatment [206].

ranging from 15 to 100 nm. Through TEM analysis it was observed that the walls of the VONTs consist of several concentric shells however a model for the formation of the VONTs during hydrothermal treatment was not yet presented.

Spahr et al. developed on their initial study of VONT synthesis in 1999 [237]. VONTs were prepared by stirring a solution of vanadium triisopropoxide and hexadecylamine in a molar ratio of 2:1 respectively in ethanol under an inert gas for 1 h. After this time the mixture was hydrolysed, stirred vigorously and then allowed to age for 2 days. Heating this mixture at 180 °C for one week at a pressure <10 bar resulted in the formation of VONTs. According to their chemical analysis the as synthesised VONTs had a nominal chemical composition of $VO_{2.45}(C_{16}H_{33}NH_2)_{0.34}$ indicating that a relatively large amount of hexadecylamine had been intercalated between the layers of vanadium oxide during the hydrothermal treatment. Details of the various vanadium oxidation states present in the synthesised VONTs were obtained through magnetic susceptibility measurements. These measurements revealed that the VONTs contained ~5% vanadium (IV) and ~95% (V) in the material. This indicates a slight reduction of vanadium (V) during the thermal reaction and accounts for the colour change before and after synthesis. Prior to being put in the oven the mixture is a yellow colour consisting of $V_2O_5$ with vanadium (V), after 7 days in the oven the synthesised VONTs are black containing $V_y^{4+}V_z^{5+}O_x$ as well as the intercalated amine molecules. In general mixed-valence vanadium (IV, V) oxides are black.

Measurements from TEM images indicated an interlayer spacing of approximately 3 nm and this was confirmed by X-ray diffraction (XRD) analysis. The *d*-spacing of the first peak in the XRD pattern scanned in the {00*l*} region, i.e. $2\theta < 20°$, corresponds to the interlayer spacing of the VONTs. Spahr et al. reported an interlayer spacing of ≈3.27 nm for VONTs synthesised with hexadecylamine as shown in Fig. 19 below.

## 11. Structural characterisation of VONTs

In 1999 Krumeich et al. carried out the first in-depth structural investigation of VONTs [238]. They suggested that the synthesis of VONTs is extremely sensitive to the applied experimental conditions during hydrothermal treatment, including temperature, pH and the duration of time spent in the oven. The experimental procedure for synthesising VONTs was the same as used by Spahr et al. detailed above. Previously VONTs had only reportedly been synthesised using a hexadecylamine surfactant however Krumeich et al. investigated the synthesis of VONTs with primary amines in the range of ($C_nH_{2n+1}NH_2$ with $4 \leq n \leq 22$) and with α,ω-diamines in the range of ($H_2N[CH_2]_nNH_2$ with $14 \leq n \leq 20$). It was proposed that the amines act as templates which direct the formation of the vanadium oxide structure towards a desired target arrangement. They report the successful synthesis of VONTs with primary amines within a large size range, varying between 4 and 22 $CH_2$ groups. It was suggested that the variety in chain lengths is somewhat more limited for diamine templates extending only between 14 and 20 $CH_2$ groups, with shorter chain lengths leading to the formation of vanadium oxide fibres ($n = 12$) and shorter chain lengths resulting in the formation of lamellar structured composites with irregular shapes ($n = 4$).

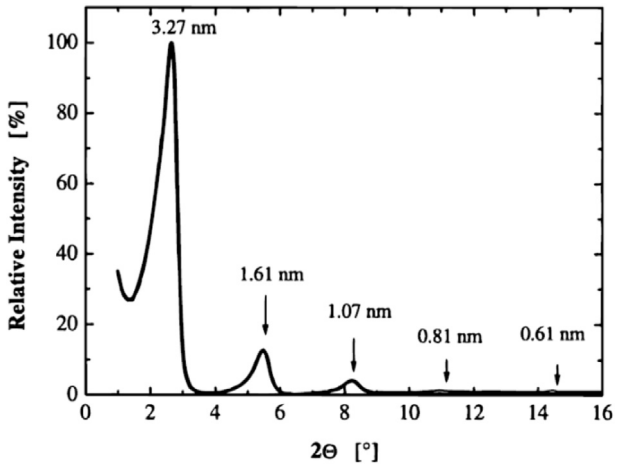


**Fig. 19.** Powder XRD pattern of VONTs synthesised with hexadecylamine [237].

Various molar ratios of vanadium oxide precursor to primary amine were investigated. The molar ratios of vanadium oxide to primary amine used were 2:1, 3:1 and 4:1 respectively with the amounts of ethanol and water which are added to the mixture prior to ageing kept constant in all cases. They reported that VONTs were successfully synthesised with molar ratios of 2:1 and 3:1, however, a molar ratio of 4:1 with the vanadium oxide precursor in excess led to the formation of lamellar structured products which were not nanotubes. The effects of varying the ageing time as well as the duration of hydrothermal treatment were also investigated. It was found that VONTs were obtained at a temperature of 180 °C within 2–7 days. By extending the ageing time prior to putting the mixture in the oven from 2 days to for example 4 days it is possible to shorten the reaction time in the oven at 180 °C to 2 days. It was also found that lower synthesis temperatures (140–160 °C) did not produce VONTs, instead lamellar structured composites were obtained. A temperature of at least 180 °C is required for the formation of VONTs.

The interlayer spacing for VONTs synthesised with primary amines of various molecular lengths were measured from XRD patterns. Once again the layer distances were determined from the *d* values of the {00*l*} reflections in the XRD patterns. The results of these measurements are shown below in Table 1. It is immediately clear that the resulting interlayer spacing increases with increasing amine chain length. Krumeich et al. suggest that when the primary amines are intercalated between the layers of vanadium oxide, it is the $NH_2$ end of the amine which is directed towards the vanadium oxide layers. From XPS analysis it is shown that the $NH_2$ group has become protonated and hence is electrostatically bound to reduced oxygen within the layers of vanadium oxide. It is in this manner that primary amine molecules are intercalated within the layers of vanadium oxide. Hence by measuring the resulting interlayer spacing of VONTs synthesised with primary amines of various chain lengths it is possible to get an idea of the arrangement of the amines within the vanadium oxide layers.

The resulting interlayer spacings measured from XRD patterns are compared with 2 times the corresponding amine length in Fig. 20 below. VONTs synthesised with primary amines in the range

**Table 1**
Interlayer spacings of VONTs synthesised with a range of different primary amines (data from Ref. [238]).

| Primary amine | Layer spacing (nm) |
|---|---|
| Butylamine | 1.66 |
| Hexylamine | 2.00 |
| Octylamine | 2.24 |
| Decylamine | 2.50 |
| Undecylamine | 2.62 |
| Dodecylamine | 2.77 |
| Tetradecylamine | 3.02 |
| Hexadecylamine | 3.35 |
| Octadecylamine | 3.48 |
| Eiscosylamine | 3.67 |
| Docosylamine | 3.80 |

of $4 \leq n \leq 22$ can be split into two groups. The first group is VONTs synthesised with primary amines in the range of $4 \leq n \leq 11$ the resulting interlayer spacing as measured from XRD is larger than twice the length of each corresponding amine molecule. This implies that the ends of the aliphatic chains must only touch or slightly overlap. The second group is VONTs synthesised with primary amines in the range of $12 \leq n \leq 22$. The measured interlayer spacings for VONTs prepared with amines in this range were all less than 2 times the corresponding amine chain length. This implies that a significant overlap of the aliphatic tails and/or large tilt angles must be occurring between the host vanadium oxide layers. If the amine molecules are orientated perpendicular to the vanadium oxide layers then the tilt angle is said to be 0°, for the layer spacings of group 2 to occur, it is believed that tilt angles greater than 50° would be required.

The tubular structure of the VONTs is evident from TEM images, as shown in Fig. 21. The walls of the VONT on either side of the hollow core appear as alternating fringes of light and dark contrast. Regions which appear darker in TEM images indicate a material with a high electron scattering potential, hence the darker regions in Fig. 21(a) and (c) are vanadium oxide layers whereas the brighter layers contain the intercalated amine molecules. Fig. 21(b) explains what is seen when VONTs are imaged in transmission mode. The concentric walls of the VONTs are only visible at the sides with a hollow core visible in the centre. Fig. 21(c) shows layers of vanadium oxide visible within the hollow core of the VONT. Fig. 21(e) is a dark field image of the cross section shown in Fig. 21(a). The bright contrast indicates vanadium in the same location as in the bright field images. Furthermore the carbon map in Fig. 21(f) shows the carbon atom, presents in the amine molecules, is found between the layers of vanadium oxide. The cross sectional TEM images in Fig. 21(d)–(f) offer further information on the structure of the VONTs. From these images it appears as though the nanotubes are scrolled rather than being made up of concentric layers of vanadium oxide.

## 12. Different vanadium oxide precursors for synthesising VONTs

### 12.1. Vanadium triisopropoxide

Over the past decade several different methods for synthesising VONTs have been reported. This section highlights the most commonly used methods which have repeatedly been reported to successfully lead to the formation of VONTs. In general a vanadium oxide precursor is mixed with either primary or secondary amines, this mixture is hydrolysed and then subject to hydrothermal treatment for an extended period of time (from 24 h to upwards of 7 days). The biggest difference in the experimental methods used however, is the variety of vanadium oxide precursors that are used.

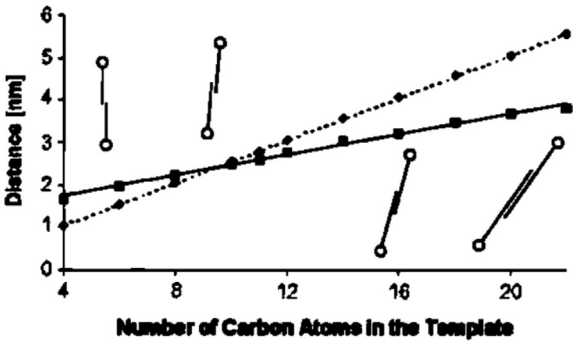


**Fig. 20.** Comparison between measured interlayer spacings and twice the amine chain length (dotted line) [238].

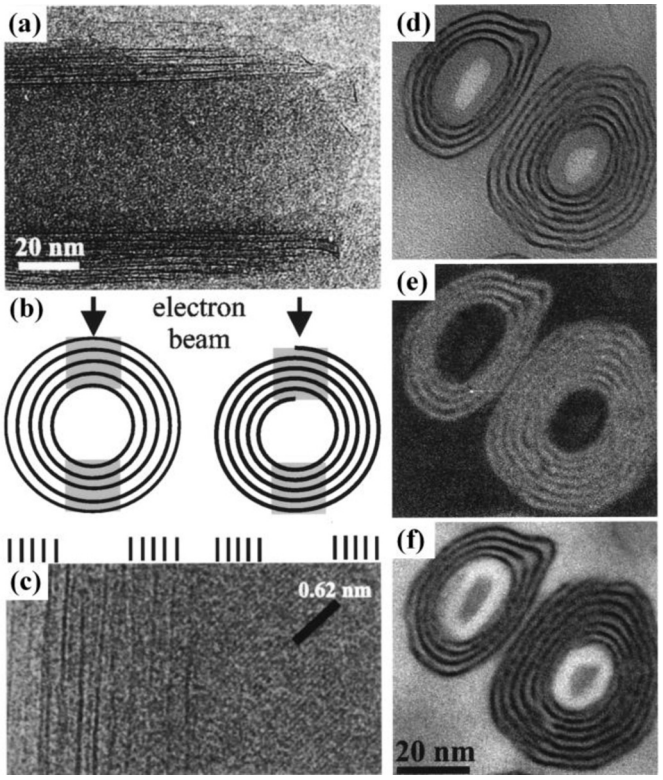


**Fig. 21.** (a) TEM of a typical VONT synthesised with dodecylamine, (b) schematic representation of how a concentric tube (left) and a scrolled tube (right) appear when imaged on TEM, (c) HRTEM image of the hollow core of a VONT, (d) cross section image of VONTs synthesised with hexadecylamine, elemental distribution images of (e) vanadium and (f) carbon [238].

As mentioned above the first reported VONTs were synthesised with a vanadium triisopropoxide precursor [206,238,239]. Vanadium triisopropoxide was mixed with a primary amine or diamines in a molar ratio of 2:1 in absolute ethanol and stirred for 1 h. This resulted in an alkoxide-amine adduct which was then hydrolysed with water and stirred prior to hydrothermal treatment. Other vanadium containing precursors as well as purpose synthesised vanadium oxide sol gels and xerogels have been shown to also lead to the formation of VONTs.

### 12.2. Vanadium oxytrichloride and vanadium pentoxide

In 2000 Niederberger et al. reported the synthesis of VONTs via two non-alkoxide routes using both vanadium (V) oxytrichloride ($VOCl_3$) and vanadium (V) pentoxide ($V_2O_5$) as vanadium sources and primary amines as templates or intercalates, respectively [240]. Both $VOCl_3$ and $V_2O_5$ are interesting precursors because of their individual properties. $VOCl_3$is said to readily form compounds with nitrogen donors, such as primary amines, and it also condenses to form a hydrated oxide when mixed with water in the formation of a sol–gel. The layered structure of $V_2O_5$ makes it ideal for the intercalation of various ions [118,241,242]. The method used to synthesise VONTs from vanadium oxytrichloride was as follows. $VOCl_3$ was mixed with a primary amine, water and an acetate buffer. The resulting precipitate was then allowed to age for 24 h before being washed with ethanol. The dried powder was then added to 2-propanol and thermally treated at 180 °C for 7 days. VONTs made from crystalline bulk $V_2O_5$ were prepared as follows. Bulk $V_2O_5$ powder was mixed with a primary amine and ethanol and allowed to stir for 2 h. After this time water was added and the mixture was stirred for a further 48 h before hydrothermal treatment again at

180 °C for 7 days. It was found that both $VOCl_3$ and $V_2O_5$ can be used as vanadium sources for the synthesis of VONTs. These were the first precursor alternatives to the initially used vanadium triisopropoxide.

Niederberger et al. noted that VONT synthesis from the $V_2O_5$ precursor could easily be scaled up for potential industrial purposes. By using a larger Teflon lined autoclave (750 mL) and increasing the hydrothermal reaction time from 7 to 14 days they report that several tens of grams can be produced in a single synthesis. Shorter synthesis times lead to an increase in the amount of unreacted material and lamellar by product. Some general trends in the synthesis of VONTs which were independent of the vanadium oxide precursor used were noticed. At the time the precursors examined were vanadium alkoxides (from vanadium triisopropoxide), crystalline $V_2O_5$ and $VOCl_3$. Their observations were as follows: (i) highest quality VONTs were formed when the molar ratio of vanadium to amine is 2:1, (ii) primary amines of different lengths vary the resulting interlayer spacings in the walls of the VONTs and have no effect on the resulting vanadium oxide phase obtained and (iii) the addition of alcohol prior to hydrothermal treatment is not essential in the formation of VONTs.

Initially the most common method of synthesising VONTs involved effectively making a vanadium alkoxide gel. After hydrolysing and ageing and prior to hydrothermal treatment the vanadium triisopropoxide/amine mixture has a gel consistency. This is not the only gel route which leads to the formation of VONTs. Over the last decade there has been a renewed interest in vanadium oxide sol gels and xerogels for application as a precursor for VONT formation. So far several different gels have been reported to successfully produce VONTs. The details of these gels shall now be discussed.

### 12.3. Crystalline $V_2O_5$ and hydrogen peroxide

Chandrappa et al. prepared $V_2O_5 \cdot nH_2O$ gels with crystalline $V_2O_5$ and hydrogen peroxide [243]. Crystalline $V_2O_5$ (1 g) was dissolved in a solution of hydrogen peroxide (50 mL, 30%). The resulting exothermic reaction leads to the partial decomposition of hydrogen peroxide which in turn leads to the release of both oxygen gas and the formation of vanadium (V) peroxo complexes [242]. After ≈10 min a clear orange solution is formed which after ageing for 24 h becomes a red gel. This gel corresponds with $V_2O_5 \cdot nH_2O$ with $n \approx 300$. Following this preparation the sol gel was mixed with hexadecylamine in a molar ratio of vanadium to amine of 2:1 and this mixture was hydrothermally treated using the same method as VONTs synthesised with alkoxides. It was concluded that the formation of VONTs was a three step process (i) preparation of the $V_2O_5 \cdot nH_2O$ gel (ii) the room temperature ageing of the gel/amine mixture and (iii) the hydrothermal treatment of this mixture. In other work, Chandrappa et al. investigated the consequences of not adhering to these steps and altering their experimental method [244]. Instead of preparing the gel first, hexadecylamine was added initially to crystalline $V_2O_5$ and then hydrogen peroxide was added to this mixture. It was suggested that both the gelation process and the intercalation of hexadecylamine between the vanadium oxide layers occur simultaneously. This method results in a macroporous vanadium oxide, the pores of which are arranged in an irregular honeycomb-like morphology.

#### 12.3.1. Comparison of VONTs from crystalline $V_2O_5$ and VONTs from crystalline $V_2O_5$ mixed with hydrogen peroxide

While VONTs which are synthesised using different vanadium oxide precursors may appear very similar when viewed on the TEM and SEM, their subtle differences become clear when they are statistically characterised. For example Kweon et al. compared VONTs synthesised with the "powder" method (PVNT) with VONTs synthesised by the sol gel method (SVNT) [245]. PVNTs were synthesised through the addition of dodecylamine to crystalline $V_2O_5$ powder whereas SVNTs were synthesised by adding dodecylamine to a $V_2O_5 \cdot nH_2O$ gel prepared by adding hydrogen peroxide to crystalline $V_2O_5$. In both cases the molar ratio of vanadium to amine was 2:1. From XRD analysis the resulting interlayer spacings were measured to be 2.78 nm for PVNTs and 3.04 nm for SVNTs. Their measured value for PVNTs was similar to values previously reported (2.74 nm) for VONTs synthesised via that route [238].

Further work on this suggests that the greater interlayer spacing can be attributed to water molecules being intercalated between the layers of vanadium oxide, in addition to the amine molecules [243], which is not the case for PVNTs. Furthermore it has been reported that the {*hk*0} reflections for SVNTs are dissonant, implying a slight distortion of the vanadium oxide layers in the nanotubes due to the presence of the intercalated water molecules [245,246]. The resulting XRD patterns for PVNTs and SVNTs showing both {00*l*} and {*hk*0} reflections are shown in Fig. 22(a). The differences between PVNTs and SVNTs are also evident in their resulting FTIR spectra, shown in Fig. 22(b) The vibrations of various V—O type bonds are well known for FTIR spectra, in comparing PVNTs and SNVTs the bonds of interest are the bonds associated with $V^{4+}$═O bonds, which occur at 971 and 999 $cm^{-1}$. In their comparison Kweon et al. reported that the vibrations associated with these bonds appear stronger for SVNTs than for PVNTs. This implies that the intercalation of water molecules between the layers of vanadium may increase the concentration of $V^{4+}$ present in the resulting VONTs. Also they found that the absorbing intensity of the H—O—H stretching vibration is much stronger for SVNTs than for PVNTs, which again is indicative of water intercalation in the SVNTs.

### 12.4. Melt quenching method to prepare $V_2O_5$ sol gels

As mentioned earlier several sol gel methods have been reported in the literature as being appropriate vanadium oxide sources for VONT synthesis. Many of the older techniques which were initially used to prepare sol gels were revisited to determine if these sol gels were suitable for VONT formation. Chen et al. used a melt quenching method to prepare $V_2O_5$ sols [247]. Crystalline $V_2O_5$ powder was heated at 800 °C in a ceramic crucible for 20 min to form a molten liquid. This molten liquid was then quickly poured into distilled water and stirred, resulting in a brownish solution. The solution was heated to its boiling point and then allowed to cool naturally. Once cooled the solution was filtered and allowed to age for 7 days, after this time brown $V_2O_5$ sols were obtained. These prepared sol gels were then hydrothermally treated with amine molecules using the usual methods. Also in 2004 Chen et al. reported the use of $NH_4VO_3$ a vanadium oxide containing precursor [248]. $NH_4VO_3$ was mixed with a selection of primary amines and diamines in a molar ratio of 2:1 under stirring with water; ethanol was not added to the mixture. TEM images were shown to verify that $NH_4VO_3$ can be used as precursor to form VONTs. It was also noted that the starting materials were for the most part translated into the final materials, claiming an 80% yield of VONTs observed from repeated syntheses.

### 12.5. Preparation of a $V_2O_5$ xerogel through reflux and distillation

Another successful gel route for the formation of VONTs was reported by Lavayen et al. [249]. Orthorhombic $V_2O_5$ was mixed with *t*-butyl alcohol at reflux for 6 h to form a xerogel. After this time the mixture was allowed to cool and water was added to the resulting dark yellow solid. The remaining *t*-butyl alcohol and the

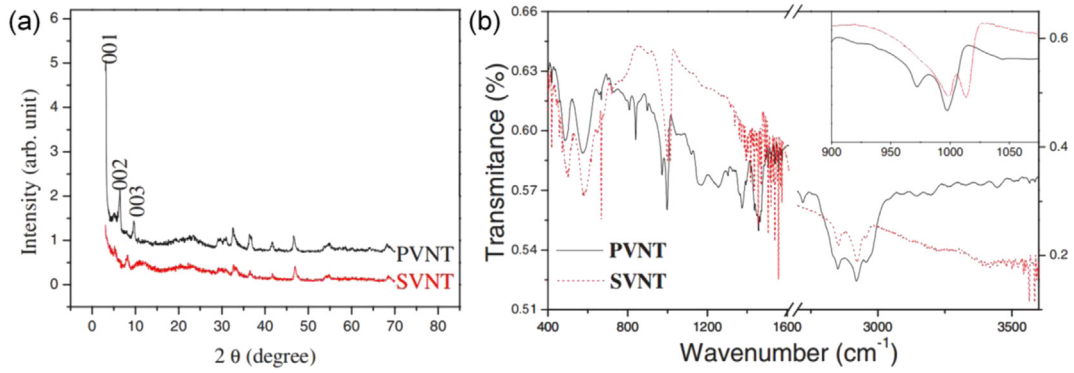


**Fig. 22.** (a) XRD pattern for VONTs synthesised via different routes, (b) FTIR spectra for PVNT and SNVT [245].

additional water were removed through distillation. As the mixture was being heated, a red-brown colloidal $V_2O_5$ suspension formed which after ageing at room temperature could be used as a precursor to form VONTs.

### *12.6. Vanadyl (IV) acetate, ($VO(Ac)_2$) precursor route*

In each of the precursors mentioned above, initially vanadium is found in the fully oxidised $V^{5+}$ state. During hydrothermal treatment there is a partial reduction of vanadium from $V^{5+}$ to $V^{4+}$. Wörle et al. suggested that this reduction might be the driving force for the scrolling of the layers of vanadium oxide to eventually form the nanotubes [250]. VONTs have also been successfully synthesised from a precursor that starts from the reduced $V^{4+}$ oxidation state by using vanadyl (IV) acetate $VO(Ac)_2$ as the vanadium source and dodecylamine as template. Vera-Robles et al. have shown that with $VO(Ac)_2$ the inverse path, i.e. a partial oxidation of $V^{4+}$ to $V^{5+}$ in the presence of oxygen takes place, producing a mixed valence system which can then be used in the formation of VONTs [251]. The sol–gel used by Vera-Robles et al. was first prepared by Choudary et al. [252]. Vanadyl (IV) acetate was prepared by refluxing vanadium (V) oxide in excess acetic anhydride for 1 h. The resulting solid product was then filtered, washed with $CHCl_3$ and dried under vacuum at room temperature for 1 h. Dodecylamine was added to the resulting sol gel and the mixture was then hydrothermally treated with the typical volumes of ethanol and water being added. One difference however was the temperature at which the mixture was treated. Typically the hydrothermal treatment lasts for 7 days at 180 °C; however Vera-Robles et al. treated their samples for 7 days at 140 °C. This work proposed that it is mandatory to obtain a layered composite in order to obtain nanotubes. Initially the formation of a layered structure between $VO(Ac)_2$ and dodecylamine was investigated. When ethanol was added to this mixture an olive green suspension was obtained. After the addition of water to this mixture, hydrolysis–condensation reactions start and, during ageing, the formation of a V–O network is accomplished while, simultaneously, the amine molecules are interwoven between the layers of the developing network. In order to verify this, FTIR analysis of the layered composite and before and after hydrothermal treatment was performed as shown in Fig. 23.

The intercalation of amines is verified by the presence of bands at 2919 and 2850 $cm^{-1}$ (C–H bond stretching) and the band at 1595 $cm^{-1}$ (assigned to amine protonation, $N–H^{3+}$ bond bending). The formation of the V–O network can be seen from the bands which appear in the 1000–400 $cm^{-1}$ region. The vanadyl $V^{4+}$ group stretching mode is evident at 904 $cm^{-1}$, thus signalling the vanadium (IV) oxidation state [253,254]. In the FTIR spectrum before hydrothermal treatment (Fig. 23(a)) only peaks associated with the $V^{4+}$ state were observed but after hydrothermal treatment (Fig. 23(b)) peaks associated with both the $V^{4+}$ and $V^{5+}$states were observed. This is evidence that prior to hydrothermal treatment the vanadium in the $VO(Ac)_2$/dodecylamine mixture is exclusively in the $V^{4+}$ state. During hydrothermal treatment part of the $V^{4+}$ forming the totality of the sample is partially oxidised to $V^{5+}$. Hence the final crystalline arrangement of the VONTs is independent of the oxidation state of the vanadium source from which the reaction started.

### *12.7. Physical properties of VONTs synthesised with different precursors*

The structural characteristics of VONTs synthesised with the most commonly used precursors are listed in Table 2. In general it can be seen that there is little variance in the physical properties of the VONTs, the most obvious outlier being VONTs synthesised with vanadium triisopropoxide ($VO(OPr^i)_3$). VONTs prepared with this precursor have the smallest inner and outer diameters and have the fewest number of layers present in the walls of the nanotubes. However these characteristics are not significantly different to VONTs prepared with the other precursors so it appears as though these physical properties are essentially independent of the vanadium source used in the synthesis of these VONTs.

## 13. Different amines used for VONT synthesis

While there has been a lot of interest into finding appropriate vanadium oxide precursors there has also been some attention

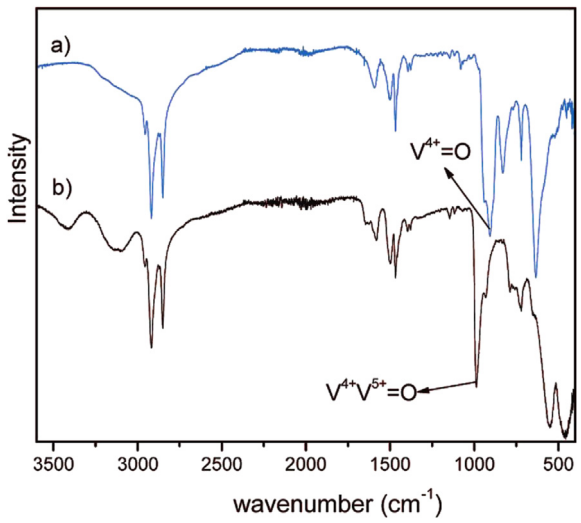


**Fig. 23.** FT-IR spectra of (a) $V^{4+}–O_x$ layered composite, (b) VONTs [251].

**Table 2**
Structural characteristics of VONTs prepared with different precursors [255].

| Precursor | Outer diameter (nm) | Inner diameter (nm) | No. of layers | Length (μm) |
|---|---|---|---|---|
| $V_2O_5 \cdot nH_2O$ gels | 50–130 | 30–40 | 5–25 | 1–10 |
| $VO(OPr^i)_3$ | 15–150 | 5–50 | 2–30 | 1–15 |
| $VOCl_3$ | 80–100 | 20–35 | 11–14 | 0.8–1.5 |
| $V_2O_5$ | 70–100 | 20–45 | 6–11 | 1–2 |

given to the various amines which can be added to a vanadium oxide source to form VONTs. Initially, VONTs were synthesised with primary monoamines ($C_nH_{2n+1}NH_2$ with $11 \leq n \leq 16$) [238,256]. It was subsequently demonstrated that α,ω diamines ($H_2N[CH_2]_nNH_2$ with $12 \leq n \leq 20$) could also be used as structure-maintaining templates for VONT formation [257]. It is now generally accepted from this work that aliphatic amines in these ranges are appropriate for VONT formation, and in 2001 Bieri et al. reported that aromatic amines can also be used to synthesise VONTs [258]. They reported successfully synthesising VONTs with 3-phenylpropylamine. Vanadium triisopropoxide was mixed with 3-phenylpropylamine in a molar ratio of 2:1 in absolute ethanol (3 mL $g^{-1}$ of vanadium precursor) and stirred for 1 h. The resulting alkoxide-amine adduct was hydrolysed with water (5 mL $g^{-1}$ of vanadium precursor), stirred and allowed to age for 12 h. The mixture was then hydrothermally treated in an autoclave for 6 days at 180 °C. Hence the experimental method was similar to that used with aliphatic amines with the differences being a shorter ageing time and a shorter hydrothermal treatment. The resulting VONTs were quite similar to VONTs obtained through more traditional routes with comparable physical properties being reported.

The same synthesis method was repeated using different aromatic amines and they found that in those cases VONTs were not formed. The other aromatic amines used were methylnaphthylamine or xylylenediamine. Bieri suggested that it is likely that the C chain of the aliphatic propyl group is necessary for the reaction to occur. From XPS results it can be seen that the N-atoms of the atoms are protonated in the VONTs synthesised with aliphatic amines. This implies that the high basicity of the $NH_2$ group is required for the eventual formation of the tubes. 3-Phenylpropylamine has a similar basicity to the more commonly used aliphatic amine and hence is appropriate for tube formation. To test this, other amines with reduced basicity were also hydrothermally treated with vanadium triisopropoxide as detailed above. These included the amino acids alanine, glycine and cysteine. It was reported that they also failed to support VONT formation suggesting that steric effects may limit the range of suitable amine templates.

As previously mentioned in the case of aliphatic amines the possibility of synthesising VONTs using aromatic amines by non-alkoxide routes has also been investigated. Sediri et al. successfully synthesised VONTs by a hydrothermal treatment of crystalline $V_2O_5$ mixed with 3-phenylpropylamine [241], showing once more the flexibility available in the choice of vanadium sources for VONT formation.

## 14. The effects of varying synthesis parameters

### 14.1. Molar ratio

The typical conditions for synthesising VONTs include mixing a vanadium oxide precursor with amines in a molar ratio of 2:1 respectively, this mixture is then hydrolysed and allowed to age for 2 days prior to hydrothermal treatment in a Teflon lined autoclave for 7 days at 180 °C. These conditions have been refined and are now known to reliably produce VONTs. There has been much work done in getting to this point. Several research groups have investigated the effects of varying each of these parameters. The vanadium oxide/amine molar ratio is a crucial parameter for the large scale synthesis of VONTs [238,240,245,248,259,260]. In one of the first papers published on VONTs, Krumeich et al. used various molar ratios of vanadium oxide precursor to primary amine while attempting to synthesis VONTs [238]. The molar ratios of vanadium oxide to primary amine used were 2:1, 3:1 and 4:1 respectively with the amounts of ethanol and water which are added to the mixture prior to ageing kept constant in all cases. They report that VONTs were successfully synthesised with molar ratios of 2:1 and 3:1, however a molar ratio of 4:1 with the vanadium oxide precursor in excess led to the formation of lamellar structured products which were not nanotubes. Consistently, the most well defined VONTs were obtained when the molar ratio of vanadium oxide to amine was 2:1. They proposed that for cases when the molar ratio was 3:1, the lower template content increased the amounts of amorphous by-products. These findings were confirmed by Niederberger et al. who after also varying the molar ratio concluded that nanotubes of highest quality are typically formed if the molar ratio of metal to surfactant is 2:1 [240].

### 14.2. Ageing time prior to hydrothermal treatment

Krumeich et al. initially investigated the effects of varying the ageing time as well as the duration of hydrothermal treatment [238]. It was found that VONTs were obtained at a temperature of 180 °C within 2–7 days. By extending the ageing time prior to putting the mixture in the oven from 2 days to for example 4 days it is possible to shorten the reaction time in the oven at 180 °C to 2 days. It was also found that lower synthesis temperatures (140–160 °C) did not produce VONTs, with the precursor which was used (vanadium triisopropoxide). Instead lamellar structured composites were obtained instead. A temperature of at least 180 °C is required for the formation of VONTs to occur.

### 14.3. Duration of hydrothermal treatment

This work was continued by Chandrappa et al. who performed various experiments to investigate the effect of modifications to the hydrothermal treatment on the morphology of the final product [255]. Four samples were prepared (NT1–NT4) at different temperatures and for different durations of hydrothermal treatment as listed in Table 3. Each of these VONT samples were synthesised with $V_2O_5 \cdot nH_2O$ gels prepared by mixing crystalline $V_2O_5$ with hydrogen peroxide, as detailed above. As a comparison VONTs were also prepared using crystalline $V_2O_5$ as the precursor as reported by Niederberger et al. [240], these VONTs are labelled as c-$V_2O_5$-NT in Table 3. Each VONT sample was characterised by powder X-ray diffraction as shown in Fig. 24.

The X-ray diffraction pattern of NT1 (Fig. 24(a)) was typical of a layered compound. Two series of reflections can be observed (i) a {00*l*} set of reflections with high intensity corresponding to the stacking of the vanadium oxide layers within the VONTs and (ii) a {*hk*0} set of reflections with lower intensity corresponding to the two-dimensional structure of the layers, which also gives an indication of the quality of the VONTs. The interlayer spacing of the VONTs can be determined from the *d*-spacing of the 001 peak observed in the 00*l* series (e.g. $d_{001} = 3.7$ nm for NT1). It was proposed that the intercalated hexadecylamine molecules lay perpendicular to the oxide planes and the basal distance should be close to the length of the amine chain ($d_{calc}(C_{16}H_{33}NH_2) = 3.3$ nm)

**Table 3**
Synthesis conditions and interlayer spacings for the resulting VONTs [255].

| Samples | Hydrothermal process | | $d_{001}$ (nm) |
|---|---|---|---|
| | $T$ (°C) | Times (days) | |
| NT1 | 150 | 2 | 3.7 |
| NT2 | 180 | 2 | 3.7; 3.2 |
| NT3 | 180 | 4 | 3.2 |
| NT4 | 180 | 7 | 3.2; 3.0 |
| c-$V_2O_5$-NT | 180 | 7 | 3.2 |

[261]. The resulting interlayer spacing observed for NT1 VONTs was slightly larger than the length of the amine molecule and also larger than the interlayer spacing reported for c-$V_2O_5$-NT (3.2 nm) [240]. As the VONTs for samples NT1–NT4 were synthesised with $V_2O_5 \cdot nH_2O$ gels with water present in the crystal structure of the vanadium oxide source, Chandrappa et al. suggested that the larger interlayer spacing was due to the presence of water in the product synthesised from aqueous gels. Water molecules could be intercalated together with the protonated amines within the layers of vanadium oxide thereby increasing the interlayer spacing. The {*hk*0} set of reflections for NT1 did not correspond to that of the c-$V_2O_5$-NT sample; therefore there is a difference in the structure of the vanadium oxide layers for the two products. When the sample was heated at 180 °C for 4 days as was the case for sample NT3, the double set of {00*l*} reflections were no longer observed. Instead, just one set of reflections was observed which correspond with the c-$V_2O_5$-NT sample. However, once again the {*hk*0} reflections were different than for the c-$V_2O_5$-NT sample. From sample NT1 it was clear that 150 °C is too low a temperature to result in a *d*-spacing for the {001} peak similar to the c-$V_2O_5$-NT sample, but until the temperature is increased to 180 °C for 2 days, the corresponding *d*-spacing is not observed. Even after 4 days at 180 °C the resulting {*hk*0} reflections are still not consistent with the c-$V_2O_5$-NT sample. This implies that after 2 and 4 days of hydrothermal treatment at 180 °C the VONT formation process has begun to occur, small quantities of VONTs can be observed on TEM but the majority of the products is a lamellar structure which has not yet formed VONTs. The reaction in the autoclave had to be performed for at least 7 days at 180 °C in order to obtain nanotubes NT4 (Fig. 24(d)) giving the same X-ray pattern as c-$V_2O_5$-NT (Fig. 24(e)). The {00*l*} and {*hk*0} series of reflections for NT4 corresponded with the reflections for the c-$V_2O_5$-NT sample. TEM and SEM images confirmed that the majority of the sample heated at 180 °C for 7 days were VONTs. Chandrappa et al. concluded that the hydrothermal treatment has to be performed at 180 °C for at least 7 days to obtain solely VONTs. At lower temperatures and for shorter hydrothermal treatment times, some lamellar vanadium oxides incorporating amines are obtained that may act as intermediates during the formation of the VONTs.

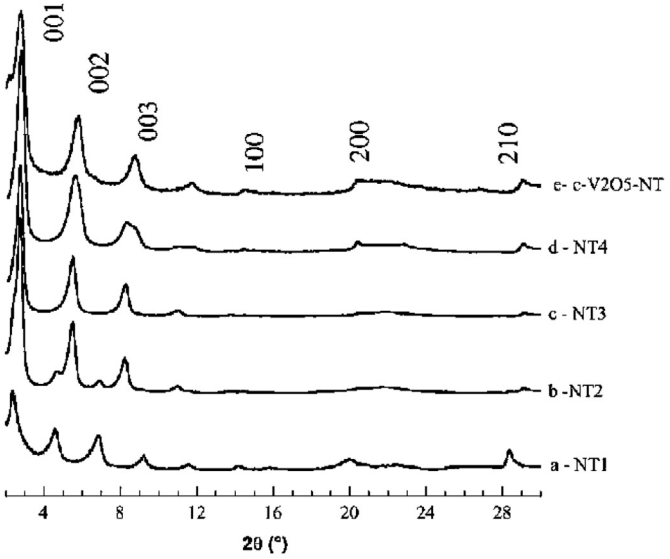


**Fig. 24.** X-ray diffraction patterns for each sample obtained under different conditions [255].

## 15. VONT growth mechanism

### 15.1. Rolling method

The discovery of carbon nanotubes in 1991 sparked a tremendous amount of interest in tubular structures [170,199,262–277]. Over the last twenty years various kinds of nanotubes have been reported. Nanotubes such as tungsten sulfide nanotubes [278–281], molybdenum disulfide nanotubes [282–285], boron nitride nanotubes [286–289], titanium oxide nanotubes [290–293], and tin sulfide nanotubes [294–296] with various synthesis techniques and different growth mechanisms have been reported. After Spahr et al. [206] first reported the synthesis of VONTs through the hydrothermal treatment of a vanadium oxide precursor mixed with primary amines there was a tremendous amount of interest in their growth mechanism. Understanding the formation mechanism for VONTs would be a significant breakthrough for all nanotube synthetic methods and could open even more fascinating possibilities for experimental and theoretical explorations for nanostructures in general.

One of the first growth mechanisms for VONTs was proposed by Chen et al. [248] following on from work their group had previously developed with $WS_2$ nanotubes. When discussing the formation of $WS_2$ nanotubes Li et al. proposed that, for a layered compound, if the interaction between neighbouring layers could be reduced from the edges of the layer, while keeping the interactions of in-layer atoms or molecules, tubular structures (or nanotubes) might also form through the rolling of these lamellar structures [279]. It should be noted that Chen et al. synthesised their VONTs using $NH_4VO_3$ as a vanadium source however the same growth mechanism is likely to occur for VONTs prepared with each of the precursors detailed above. In each case the precursor is mixed with amines and water, this mixture is then allowed to age for a period of time, usually 2 days, before thermal treatment in a Teflon lined autoclave. Vanadium oxide is a layered structure and during the 2 days of ageing the amine molecules are intercalated between the vanadium oxide layers. It was proposed that if, under certain conditions, the interlayer interaction between the layers of vanadium oxide could be diminished from the edges then the rolling of the layers of vanadium oxide into nanotubes should take place. They suggested that the hydrothermal treatment is the driving force for rolling of the lamellar sheets. Heidenreich et al. reporting that severe bending of graphite sheets occurs at high temperatures [297] as well as Ugarte reporting curling graphite networks under electron beam irradiation [298] provided some evidence of lamellar structures beginning to roll when heated. Chen et al. named their proposed scheme for VONT formation the "rolling method" and explained that it could be divided into three main steps. (i) The surfactant molecules condensed into aggregations with $VO_3^-$ to form lamellar structures. (ii) When treated under hydrothermal conditions, the condensation process continued and brought out more ordered lamellar assemblies. (iii) These lamellar sheets became loose at the edges and then rolled into themselves to finally

form vanadium oxide nanotubes. This process is illustrated schematically in Fig. 25.

In an attempt to confirm the rolling mechanism, the mixtures of $NH_4VO_3$ and amines were hydrothermally treated at 180 °C for various durations of time. These samples were then imaged on TEM to determine if the intermediate structures appeared to be following the rolling mechanism. The resulting images are shown in Fig. 26. For samples which were not heated for the full 7 days, a mixture of VONTs and unrolled lamellar structures were observed. The proposed VONT forming process can be seen in TEM images as shown in Fig. 26. The initial lamellar structure of the precursor/amine mixture prior to hydrothermal treatment is shown in Fig. 26(a). After 1.5 days of hydrothermal treatment, the amorphous precursor became a crystallised ordered layered structure as shown in Fig. 26(b). After 2.5 days of hydrothermal treatment large vanadium oxide plates could be seen and most significantly some plates were found curling at their edges as shown in Fig. 26(c). Finally, after 4.5 days of hydrothermal treatment, VONTs were formed as can be seen in Fig. 26(d) and (e). The most direct evidence for the rolling mechanism was the presence of the intermediate plate like structures which begin to curl along their edges.

### 15.2. Comparison with $BaV_7O_{16}{\cdot}nH_2O$ structure

In 2002 Wörle et al. proposed a theory on the structure of the walls of synthesised VONTs. Inspired by previous work on $BaV_7O_{16}{\cdot}nH_2O$ bronzes [299] and initial characterisation of VONT XRD patterns. Initial analysis of the structure of the $VO_x$ layers through XRD characterisation by Krumeich et al. [238] pointed to a structure consisting of $VO_4$ tetrahedra and $VO_5$ square pyramids simultaneously. This theory was supported by later work by Dobley et al. [300] The resulting VONT XRD pattern could be indexed with a tetragonal basal plane with $a = 6.144$ Å and an interlayer spacing of $c = 26.6$ Å. Dobley et al. noted that the $a$ parameter is similar to that, $a = 6.160$ Å and $c = 21.522$ Å, of $BaV_7O_{16}{\cdot}nH_2O$ [299], synthesised hydrothermally, where six of the vanadium atoms are in octahedral coordination and the seventh is in a tetrahedrally coordinated site. Following on from this work Wörle et al. proposed that flexible $V_7O_{16}$ layers are the common structural element of VONTs [250]. VONTs were prepared using the alkoxide route with primary and secondary amines. A model for the structure in the tube walls was constructed on the basis of a previous study, from this a theoretical XRD pattern was determined and this was compared with the XRD pattern obtained from VONTs synthesised with dodecylamine. The proposed VONT wall structure is composed of $V_7O_{16}$ layers between which amine molecules are embedded, as illustrated in Fig. 27(a). The layers of $V_7O_{16}$ comprise

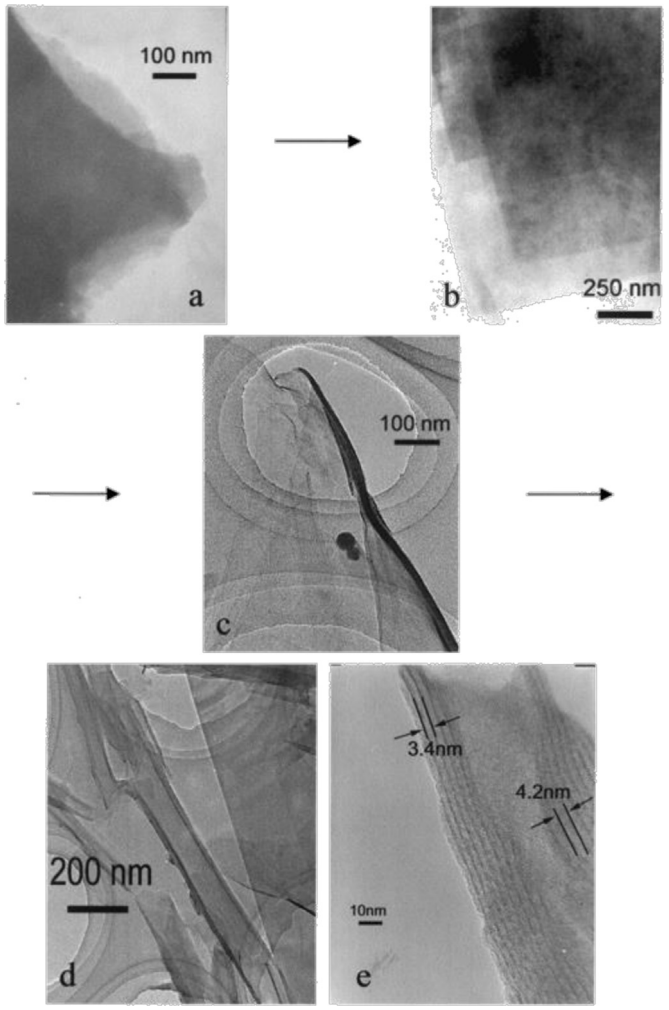


**Fig. 26.** A suggested formation process for VONTs: (a) TEM image of the lamellar-structured, periodic assembly of surfactant and $VO_3^-$ of the precursor obtained by co-precipitation. This precursor was amorphous. (b) TEM image of the ordered layered structure after hydrothermal treatment for 1.5 days. (c) HRTEM image of the beginning stage of the rolling process obtained after hydrothermal treatment for 2.5 days (d) and (e) HRTEM image of the formed nanotube after hydrothermal treatment for 4.5 days [248].

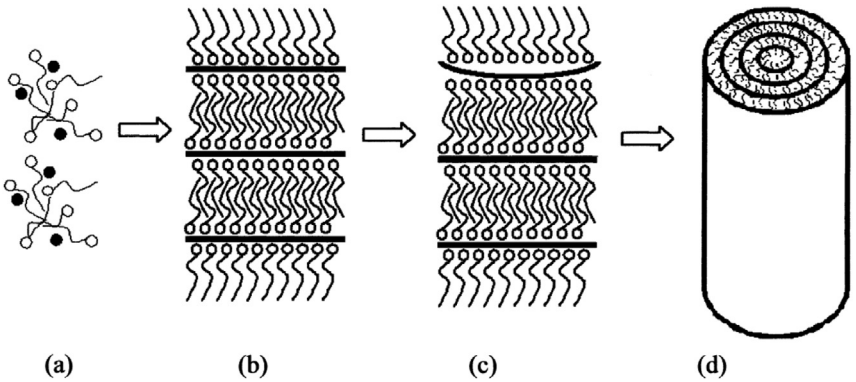


**Fig. 25.** Schematic presentation of the whole rolling mechanism for the formation of the vanadium oxide nanotubes: (a) the mixture of the $NH_4VO_3$ and the template molecules, (b) layered structures formed through the hydrothermal treatment, (c) the beginning stage of the rolling process, and (d) the formed nanotubes [248].

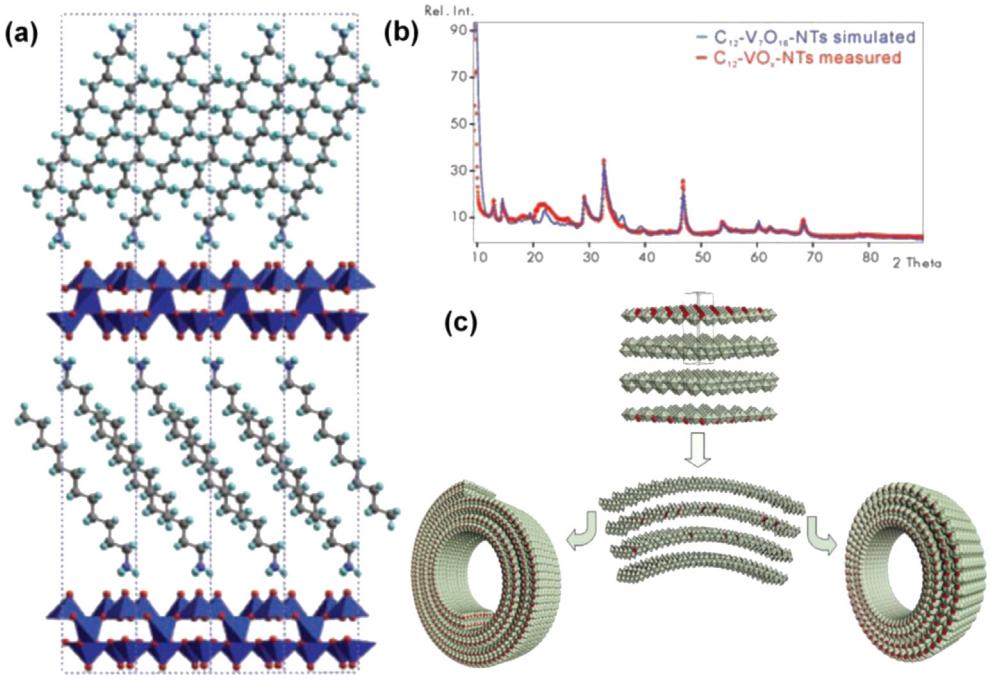


**Fig. 27.** (a) Structural model for the layer structure in the tube walls of $C_{12}$-$VO_x$-NTs. (b) Experimentally measured and simulated XRD pattern of $C_{12}$-$VO_x$-NT [250]. (c) Growth mechanism for VONTs with a flexible $V_7O_{16}$ layer [301].

of two sheets of square $VO_5$ pyramids and $VO_4$ tetrahedra that connect these sheets. All of the apices of the square pyramids point out of the layers. The amine molecules are connected to the vanadate layers via their protonated amino group. The arrangement of the dodecylamine molecules within the vanadium oxide layers cannot be unambiguously determined from the experimental data and thus only one possibility is shown.

From previous findings it was proposed that the alkyl chains of the amines do overlap to some extent [238]. Wörle et al. found that their simulated XRD pattern of VONTs, calculated with a structural model based on the $VO_x$ layers present in $V_7O_{16}$, fit very well with the observed pattern. The two XRD patterns are compared in Fig. 27(b). It can be seen that there is indeed a close correlation between the simulated and experimental patterns. Through their analysis Wörle et al. suggested that $V_7O_{16}$ layers serve as the framework of the structure while amine molecules are embedded in-between. For diamine templates they suggest that it is the length of the alkyl chain that directs the structure towards either a nanotubular or a crystalline phase. It was concluded that, in comparison to other nanotubes, like those of carbon or of $WS_2$, the structure of the VONTs is much more complex. There are not only the rather complicated vanadate layers in the inorganic part of this composite but also organic layers of amine molecules filling up space between the vanadium oxide layers.

Petkov et al. presented a model for the structure of vanadium oxide layers with in VONTs. VONTs were synthesised through the hydrothermal treatment of a solution of vanadium (V) triisopropoxide and primary amines as detailed above. The as synthesised VONTs were then characterised through the atomic pair distribution technique (PDF). Different vanadium oxide structural models were created and the resulting simulated data was compared with experimental data to determine the best fit. Initially a model based on the 14-atom unit cell of crystalline $V_2O_5$ was used, as shown in Fig. 28(a). The experimental PDF data obtained from as synthesised VONTs is shown as circles and the simulation data is shown as a solid line. The crystalline $V_2O_5$ model did not reproduce the experimental data well, especially in the region beyond the first PDF peak. Petkov proposed that VONTs may not be considered as built of single layers of square pyramidal V—$O_5$ units that occur in crystalline $V_2O_5$. Since the nanotubes were obtained via a sol—gel route, this work also used a model based on the structure of $V_2O_5 \cdot nH_2O$ gel in the analysis. This model also failed to reproduce the experimental data as can be seen in Fig. 28(b). The unsuccessful outcome of this simulation led Petkov to believe VONTs are not built of double layers of square pyramidal/octahedral V—$O_5$ units that occur in $V_2O_5 \cdot nH_2O$ gel. Following on from these unsuccessful simulations, models which allowed two different types of vanadium—oxygen coordination: tetrahedral V—$O_4$ and square pyramidal V—$O_5$, were used.

The investigation of these coordinations in the VONTs was prompted by previously proposed theories [238,250,300]. This combination of vanadium—oxygen coordinations is present in $BaV_7O_{16} \cdot nH_2O$ and as such this structure was the basis of another simulation model. $BaV_7O_{16} \cdot nH_2O$ can be viewed as an ordered assembly of double layers of pyramidal/octahedral vanadium—oxygen units with a small number of V—$O_4$ tetrahedra embedded into the layers. The stacking of the layers in $BaV_7O_{16} \cdot nH_2O$ occurs in two modifications triclinic and tetragonal. It was noted that from the two modifications only the triclinic one showed good promise in the PDF fitting process. Hence a model based on that modification was used and only vanadium and oxygen atoms were considered in the model calculations. The simulated data from this model was in good agreement with the experimental data as shown in Fig. 28(c). Through this comparison of simulated and experimental data, the layers of vanadium oxide in VONTs were suggested to arrange in a pattern very similar to that observed with $BaV_7O_{16} \cdot nH_2O$, i.e. double layers of pyramidal/octahedral vanadium—oxygen units with a small number of V—$O_4$ tetrahedra embedded into the layers.

The flexible layers of $V_7O_{16}$ which are reported to make up the layers of vanadium oxide within VONT walls were further described by Hellmann et al. [302]. Hellmann described the VO-layer as consisting of two sheets of edge sharing $VO_6$ octahedra which are

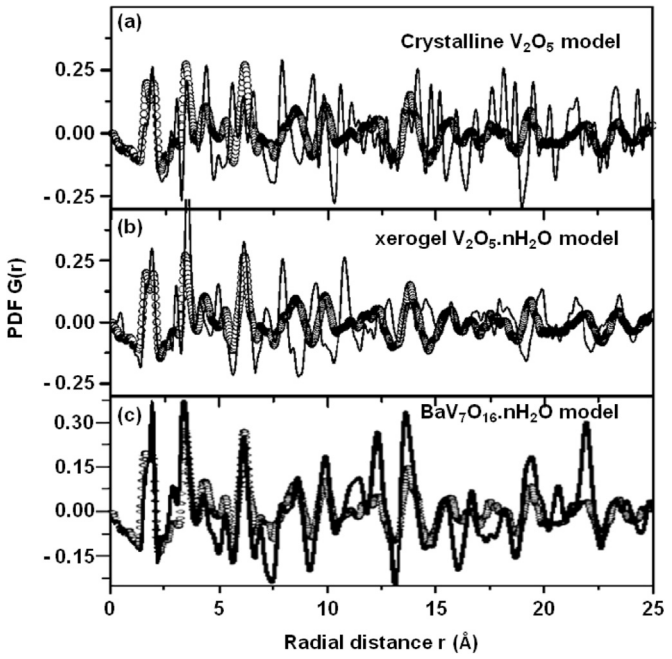


**Fig. 28.** Comparison between the experimental PDF for $V_2O_5$ nanotubes (circles) and model PDFs (solid line) for (a) crystalline $V_2O_5$, (b) $V_2O_5 \cdot nH_2O$ gel and (c) $BaV_7O_{16} \cdot nH_2O$ [301].

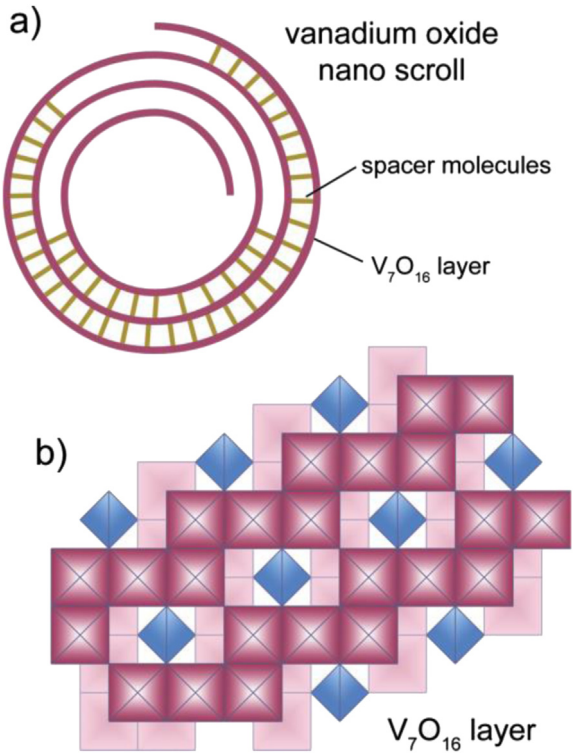


**Fig. 29.** (a) Cross section schematic representation of a VONT showing amine molecules between curved VO layers. (b) Scheme of the VO double layer which consists of two sheets of zig-zag chains of edge sharing square pyramids (red) linked by tetrahedrally coordinated vanadium sites (blue) [302] (For interpretation of the references to colour in this figure legend, the reader is referred to the web version of this article.).

coupled in zig-zag chains. The octahedra are slightly distorted and elongated basically taking the shape of square pyramids with their apices pointing in opposite directions in the two sheets. In addition, rather isolated V-ions in tetrahedral coordination are located between neighbouring chains as illustrated in Fig. 29(b). As suggested by Wörle et al. [250], Hellmann assumes that the planar unit cell is $V_7O_{16}$. The organic molecules serve as structure directing template and are sandwiched between the VO-planes in order to stabilise the tubular structure, as illustrated in Fig. 29(a). Hellmann et al. suggest that scrolled VONT walls as illustrated in Fig. 29(a) may consist of one or two curved vanadium oxide layers.

Recent direct investigation of curvature accommodation in layered nanofibers of vanadium oxide demonstrated how the role of the amine organic bilayered template intercalated in the van der Waals gap between the vanadium oxide lamina, helped to accommodate flexure and curvature [303] (see Fig. 30).

Molecular dynamics simulations for optimised thiol-functionalised layered vanadium oxide nanofibers show how substrate-induced surfactant packing effects may provide a tolerance for bending and curvature accommodation in the stacked hybrid films. The most useful insight from the point of view of future experiments is that the intercalated film can tolerate the observed moderate ~20° substrate curvature, preserving a stable layered configuration without delamination. Compared to the analysis provided in Fig. 29, curvature-induced changes in film stability are very small and much lower in magnitude than the electronic strain inherent in bending crystalline $V_2O_5$ (010), estimated to be least 25 kcal $mol^{-1}$ per $V_2O_5$ unit cell or >31 kcal $mol^{-1}$ per alkyl chain in Ref. [304]. Structural models allow two types of vanadium–oxygen coordination. Tetrahedral $V–O_4$ and square pyramidal $V–O_5$ replicate the structure within vanadium oxide nanotubes, but does not account for the organic intercalants influence on the overall net charge. Stacked bilayers comprising $V–O_5$ octahedra perfectly described non-curved vanadium oxide structure. This organic 'velcro' however, is a requirement for the accommodation of curvature in thiol-$V_2O_5$ nanofibers.

### *15.3. The effect of the $V^{4+}/V^{5+}$ ratio within the vanadium oxide layers*

Bulk crystalline $V_2O_5$ can successfully be used as a precursor for the formation of VONTs both used as received and through the use of various gels derived from the bulk material. From studying the colour change from the starting material to the synthesised VONTs, the FT-IR spectrum and the TGA curve of VONTs, it could be concluded that the oxidation states of vanadium in VONTs could not all be the same as that in crystalline vanadium pentoxide [247]. The VONTs in this study were synthesised via a melt quenching method detailed above using a crystalline $V_2O_5$ precursor. Crystalline $V_2O_5$ has a high content of $V^{5+}$ so Chen et al. performed XPS analysis of VONTs in order to obtain some information about the oxidation state of the vanadium element after hydrothermal treatment. It was found that for the as-synthesised VONTs, the maximum of the V $2p_{3/2}$ peak is located at 156.70 eV (Fig. 31), which is quite similar to that of $V^{4+}$. Chen et al. concluded that this confirms that a great proportion of vanadium existed in the VONTs in lower oxidation states.

This initial confirmation of the partial reduction of $V^{5+}$ to $V^{4+}$ during the formation of VONTs sparked much interest in the importance of the $(V^{4+}/V^{5+})$ ratio on the VONT growth mechanism. Sun et al. suggested that the difference in the $(V^{4+}/V^{5+})$ ratio plays an important role in the formation of the nanoscale structure of the VONTs and in determining the local crystal structure of the VONT walls [305]. The VONT walls are composed of vanadium oxo-anions and thus carry a neutral or negative charge. Sun et al. propose that $V^{5+}$ effectively neutralises this charge whereas $V^{4+}$ does not and as a result the total anionic charge density on the

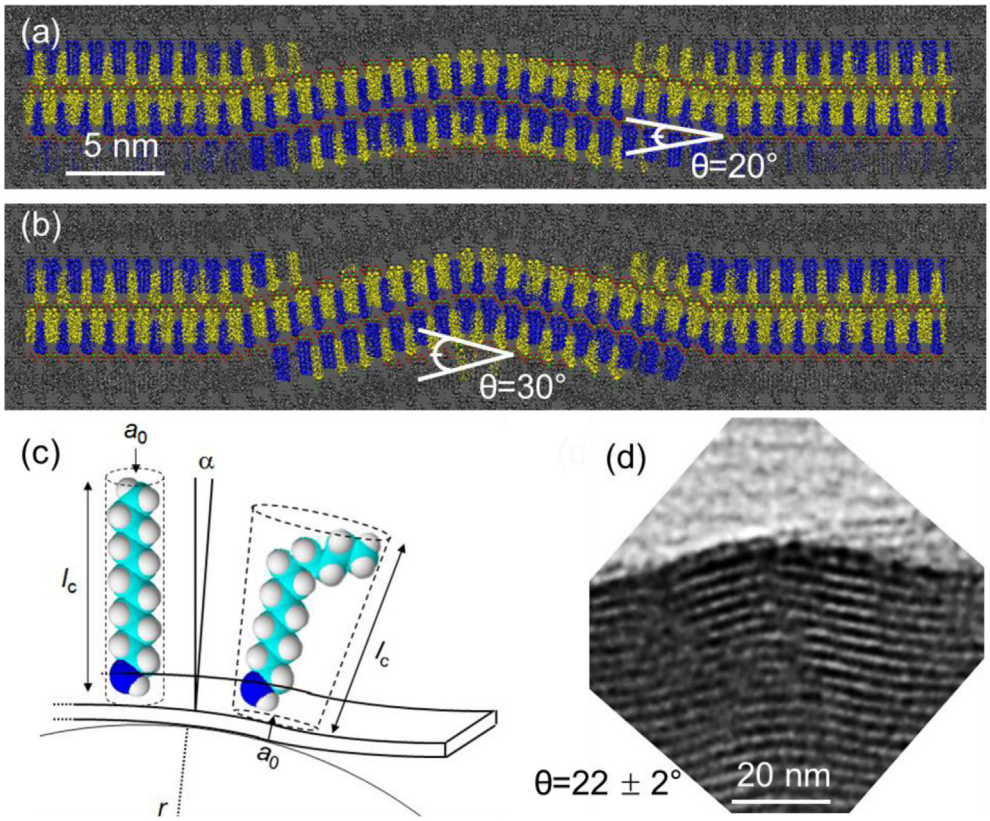


**Fig. 30.** Panels (a) and (b) show representative curved nanofiber structures, computed with bending angles of (a) 20° and (b) 30°. Surfactant molecules are coloured blue and yellow to distinguish between molecules bound on opposite substrate faces. The alkyl chains of the molecules are shown as bonds with a terminal sulphur sphere while the $V_2O_5$ (010) substrate is shown as green vanadium and red oxygen spheres. Surrounding periodic image cells are coloured grey. Panel (c) shows a schematic representation of the analytical model for a curved nanofiber, with parameters described in the text. Panel (d) shows the experimental HRTEM image with measured bending angle of 22 ± 2° (For interpretation of the references to colour in this figure legend, the reader is referred to the web version of this article.).

vanadium oxide layer is a direct function of the $V^{4+}$ content. The higher the anionic charge on the VONT wall, the larger the amount of cationic amine molecules that can be attracted to the VONT wall. Sun et al. suggest that the electrostatic interaction between the anionic $V^{4+}$sites and the cationic ammonium surfactants (from the intercalated amine molecules) is much stronger than the dative bonding between neutral $V^{5+}$sites and the neutral amine head group.

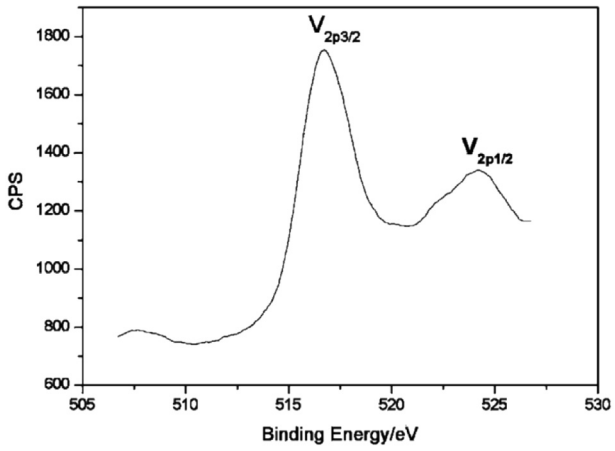


**Fig. 31.** V 2p core-level XPS spectrum of VONTs showing peaks associated with the $V^{4+}$ oxidation state [247].

Yu et al. performed XPS analysis on VONTs which were synthesised directly from crystalline $V_2O_5$, [306] the results of this analysis are shown in Fig. 32(a) and the fitted-curves about V $2p_{3/2}$ and V $2p_{1/2}$ are illustrated in Fig. 32(b). It was observed that no peaks from elements other than C, O, N and V are observed on the survey spectrum and the core level binding energies of V $2p_{3/2}$ and V $2p_{1/2}$ spectra are located at 516.2 eV and 524.0 eV, respectively. The V $2p_{3/2}$ peak of the sample is divided into two peaks at the binding energies of 517.4 eV and 516.1 eV, assigned to $V^{5+}$ and $V^{4+}$, and the V $2p_{1/2}$ peak of the sample is divided into two peaks at the binding energies of 524.2 eV and 522.3 eV, assigned to $V^{5+}$ and $V^{4+}$, respectively [307–309]. This XPS analysis supported the initial finding by Chen et al. [247] and confirmed that during the formation of VONTs there is a partial reduction of $V^{5+}$ to $V^{4+}$.

### *15.3.1. Bottom up and top down chemical approaches to synthesising VONTs*

As mentioned above Vera-Robles et al. synthesised VONTs from a $VO(AC)_2$ precursor [251]. They presented this synthesis as a "bottom up" process through the oxidation of $V^{4+} \rightarrow V^{5+}$ as opposed to the more commonly used "top down" process through the reduction of $V^{5+} \rightarrow V^{4+}$. From XRD analysis it was proposed that the nanotube walls are identical no matter what the oxidation state of the precursor is. It was suggested that, depending on the precursor used, the reduction of $V^{5+}$ or the oxidation of $V^{4+}$ is not precisely the crucial step in the formation of the VONTs; instead it is the achieving of an appropriate ($V^{4+}/V^{5+}$) ratio which causes the scrolling of the vanadium oxide layers to occur. Once again following the theory proposed by Wörle et al., Vera-Robles et al.

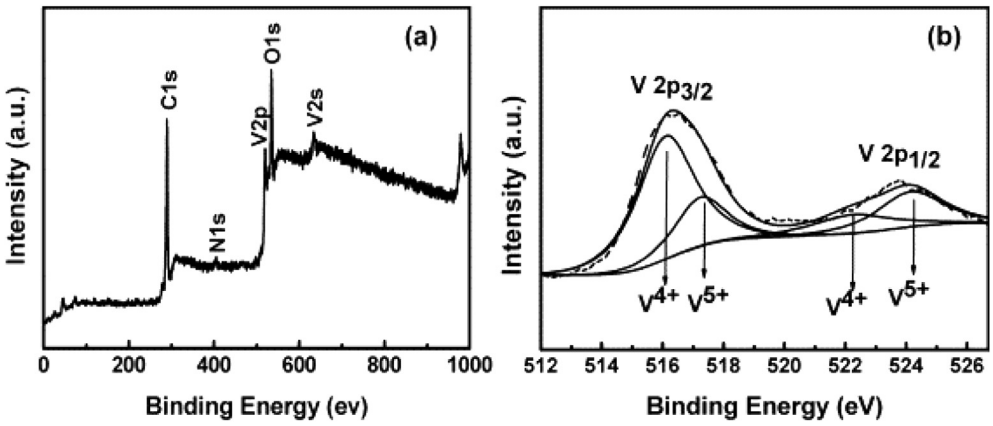


**Fig. 32.** VONT XPS spectrum (a) full survey spectrum (b) core-level spectrum of V 2p [306].

assumed that the tube walls are formed by $V_7O_{16}$ layers consisting of two sheets of $VO_5$ square pyramids with apexes pointing toward opposite directions and joined by $VO_4$ tetrahedra with the protonated $C_{12}{-}NH_3^+$ species bound to the $V_7O_{16}$ layers by means of the $-NH^{3+}$ group. A formation mechanism was proposed for their "bottom up" method for synthesising VONTs as follows, and as can be seen in Fig. 33. (i) A lamellar composite is first obtained by the reaction between the V–O framework and dodecylamine during ageing, (ii) during hydrothermal treatment of the $V(^{4+})$–O species a layered composite is partially oxidised to $V^{5+}$ by the oxygen dissolved in the reaction medium, thus decreasing the $(V^{4+}/V^{5+})$ ratio, as long as the pH is kept in between 3.0 and 3.5. As the $(V^{4+}/V^{5+})$ ratio diminishes, the layers begin their deformation. When the ratio is about 1.0 a complete scrolling is triggered allowing nanotubes to form. Simultaneously, a substantial expulsion of the amine from ≈72% to ≈36% out of the interlayer region is found.

For the "top down" approach it was proposed that it is the intercalation of the amine molecules within the vanadium oxide layers that causes the partial reduction of $V^{5+} \rightarrow V^{4+}$. In the "top down" method the amine has two functions: to act as a structure maintaining template and to act as the reducing agent that generates $V^{4+}$ species. By adjusting the $(V^{4+}/V^{5+})$ ratio through the partial reduction of $V^{5+} \rightarrow V^{4+}$ to a ratio of approximately 1.0 the scrolling of the vanadium oxide layers occur and VONTs are formed. It was concluded that regardless of which vanadium oxide precursor is used, obtaining a $(V^{4+}/V^{5+})$ ratio of approximately 1.0 is the key parameter in the formation of VONTs. This $(V^{4+}/V^{5+})$ can be adjusted through an appropriate control of the mixtures pH prior to hydrothermal treatment as well as through the use of the optimum vanadium/amine ratio for the precursor mixture. It has been shown that when the $(V^{4+}/V^{5+})$ ratio is not suitably balanced nanotubes are not produced [304]. Instead 2 dimensional nanobelt like structures are formed.

Lastly, vanadium oxide layered materials grown by previously mentioned methods can utilise their scrolling characteristics to create nanotubes, but also use methods of self-assembly during this process to create nano-urchin structures. The first report of urchin-like nanostructures by O'Dwyer et al. demonstrated how a high-density spherical nanotube radial arrays of vanadium oxide nanocomposite can be successfully synthesised by a simple chemical route using an ethanolic solution of vanadium triisopropoxide and alkylamine hexadecylamine for 7 days at 180 °C [183,218]. The growth process of the nano-urchin occurs in stages, starting with a radial self-organised arrangement of lamina followed by the rolling of the lamina into (Fig. 34). The tube walls comprise layers of vanadium oxide with the organic surfactant intercalated between atomic layers.

Compared with hollow structures and other morphologies designed to increase overall surface area, the urchin-like architecture provides an option to incorporate higher surface area nanomaterials in a defined volume with some degree of nanostructure density control. Typically, the formation of urchin-like structures is

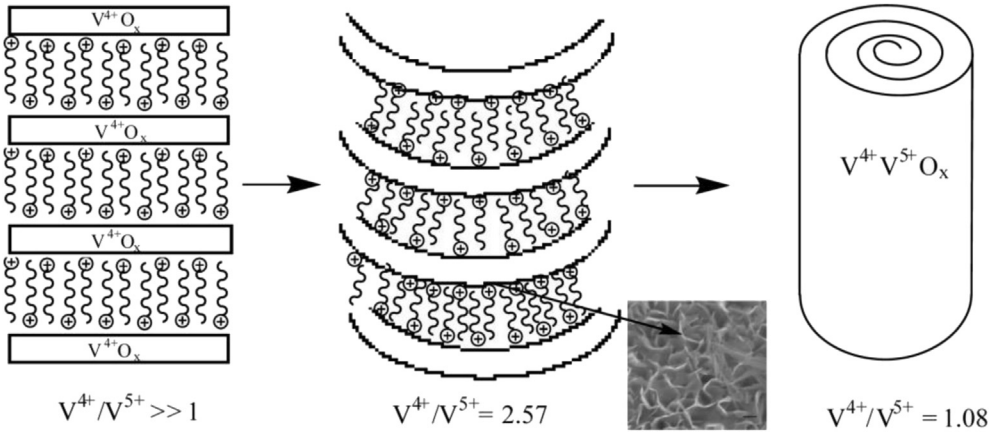


**Fig. 33.** Schematic representation of VONT formation for the "bottom up" synthesis approach. The $(V^{4+}/V^{5+})$ ratio is adjusted through the partial oxidation of $V^{4+} \rightarrow V^{5+}$. Thus decreasing the content in $V^{4+}$ and increasing the $V^{5+}$ until the $(V^{4+}/V^{5+})$ ratio is ≈1 [251].

driven by the minimisation of interfacial energy so that a balanced arrangement of constituent nanostructures forms an energy-minimised arrangement. In the vanadium oxide nano-urchin, for example, anisotropic laminar structures were first formed and self-assembled into spherical aggregates in a radially manner under the influence of amine-based structural templates. Subsequent rolling of the lamina in a manner similar to that found for individual vanadium oxide nanotubes produce the resulting nano-urchin structure. There are now many examples of urchin based superstructures made from multivalent transition metal oxides.

## 16. Electrochemical characterisation of VONTs as a cathode material for lithium ion batteries

### 16.1. Initial electrochemical characterisation

The initial electrochemical characterisation of VONTs was performed by Spahr et al. in 1999 [237]. The VONTs used were synthesised by hydrothermal treatment of a mixture of vanadium triisopropoxide and hexadecylamine. In order to ensure the VONTs were in good electrical contact with the current collecting substrate a slurry was made with the VONTs, a binder (polytetrafluoroethylene) and a conductive additive (carbon black). When calculating the specific current and the specific charge only the mass of the active material on the working electrode, i.e. the VONTs, was taken into account. Spahr et al. also performed the same cyclic voltammetry tests on VONTs which had the amine molecules removed from the layers of vanadium oxide. The VONTs were refluxed in a saturated solution of NaCl in ethanol for 24 h in order to remove the hexadecylamine template. During discharge, lithium ions are intercalated between the layers of vanadium oxide present within the VONT walls. However, this is also where the amine molecules are located hence Spahr et al. compared the electrochemical performance of VONTs with and without intercalated amines present.

Cyclic voltammograms of VONTs with and without the structure maintaining amine template in the potential range between 1.2 and 4.0 V *vs.* $Li/Li^+$ are shown in Fig. 35(a). The cathodic current observed for VONTs with amine template at potentials lower than 2 V *vs.* $Li/Li^+$ corresponds to the electrochemical insertion of lithium into the nanostructured material as follows:

$$xLi^+ + xe^- + V_2O_5 \rightleftarrows Li_xV_2O_5$$

The corresponding oxidation process for VONTs with amines begins at about 3 V *vs.* $Li/Li^+$, indicating a kinetically hindered reoxidation of the material. Spahr et al. reported that the shape of the cyclic voltammogram changed drastically when the template was removed from the nanotubes. The electrochemical intercalation of Li ions occurred at potentials more negative than 3 V *vs.* $Li/Li^+$. In addition to this two other reduction processes could be seen in the cyclic voltammogram, as shown in the solid line in Fig. 35(a). It was observed that $Li^+$ insertion was fairly reversible, as can be seen from the corresponding broad oxidation peak with a maximum at about 2.7 V *vs.* $Li/Li^+$. The first three voltammetric cycles of the template-free VONTs are shown in Fig. 35(b). A significant change in shape of the voltammogram with cycle number was observed and it was proposed that this is an indication of a change of the material during cycling and consequently the material has lost electroactivity to some extent. The most likely reason for this is the amorphisation and/or other structural changes of the material upon cycling. Further evidence for an irreversible change occurring with the nanotubes is the irreversible oxidation peak appearing in the first voltammetric cycle at a potential of about 3.8

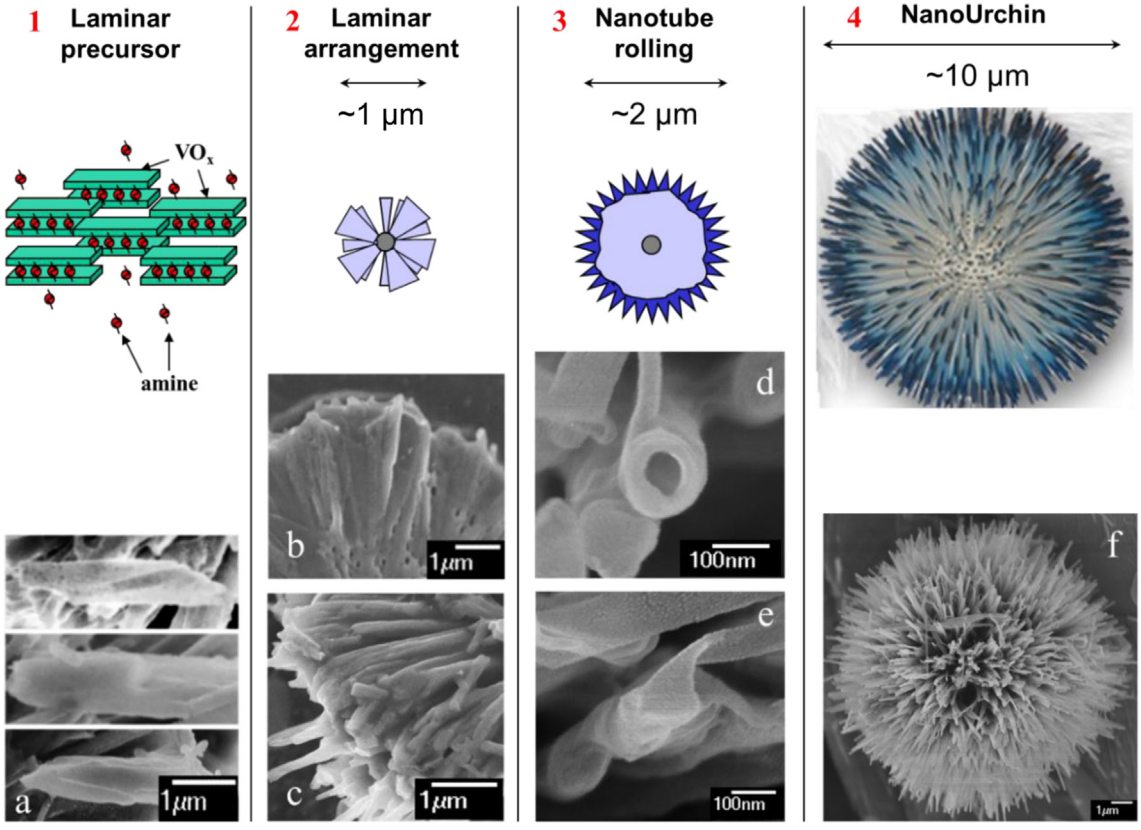


**Fig. 34.** Schematic illustration of the morphology evolution and the growth mechanism of vanadium oxide nanourchin. (a–f): SEM images of the as-synthesised nanostructures at different growth stages.

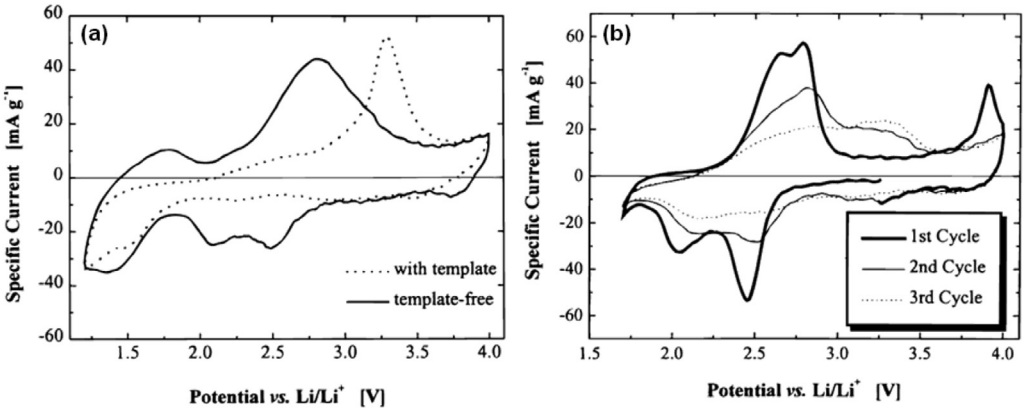


**Fig. 35.** (a) Cyclic voltammograms of VONTs with and without amine template. (b) The first three voltammetric cycles of the template-free VONTs [237].

*vs.* $Li/Li^+$, which only occurs for the first cycle. It was concluded that the significant difference in specific charge as well as in the shape of the voltammograms for VONTs with and without templates indicates that the organic amine molecules are involved in the electrochemical cycling of the former, or at least contribute to a partial passivation of the nanotubes.

The specific charge of the VONTs for increasing number of cycles was investigated through potentiodynamic measurements at 50 $\mu V\ s^{-1}$ in a potential window of 1.5–4.0 V *vs.* $Li/Li^+$. It was noted that for VONTs with amines for the first five cycles, a rather stable specific charge of about 120 mAh $g^{-1}$ was obtained. After ten cycles the specific charge had gradually decreased number to less than 100 mAh $g^{-1}$. From potentiodynamic measurements of VONTs without amine template a specific charge of ≈170 mAh $g^{-1}$ was obtained for the first cycle. After 10 cycles this value had dropped significantly to ≈100 mAh $g^{-1}$, as shown in Fig. 36. From these results it can be concluded that initial electrochemical testing of VONTs showed poor performance with rapidly decreasing capacities.

### 16.2. The effects of thermal treatment on electrochemical performance

The electrochemical performance of as-synthesised VONTs heated to different temperatures was investigated by Li et al. [207]. Spahr et al. had previously shown that as-synthesised VONTs suffered from rapidly decreasing specific capacities so Li et al. investigated the effects of annealing the VONTs to different temperatures with an aim of improving their electrochemical performance. The VONTs were synthesised using a method proposed by Niederberger et al. [240], using crystalline $V_2O_5$ as the precursor. The as-synthesised VONTs were washed with ethanol and then dried at 80 °C (sample #0). A series of VONT samples were annealed to different temperatures under static air or flowing argon and the resulting influence of the temperature on the structure and cycling performance of the nanotubes was also investigated. The annealing conditions for the 6 samples used in this study are detailed in Table 4. Working electrodes were fabricated by preparing a mixture of VONTs, acetylene black, acting as a conductive additive and PTFE, acting as a binder. Galvanostatic tests were performed with a current density of 80 mA $g^{-1}$ in a series of different potential windows.

It was found that VONTs heated to 200 and 400 °C in air collapse and lose their nanotube structure. This is most likely due to the removal of amine molecules which act as a structure maintaining template. VONTs heated to the same temperatures in Ar gas maintained their nanotube morphology. The specific capacities for the heat treated VONTs, cycled in a potential window of 1.5–4.0 V, are shown in Fig. 37. Variations in heating conditions affected the capacity values of the cathodes, with the thermally treated VONTs showing better performance than the as-synthesised material. The poor performance of the as-synthesised sample can be clearly seen by the rapidly decreasing specific capacity values. The initial specific capacity of the as-synthesised VONTs was ≈175 mAh $g^{-1}$ after just 10 cycles this value had dropped to ≈37 mAh $g^{-1}$, corresponding to a ≈79% loss in the initial specific capacity. After 30 cycles the loss was ≈86%. Samples #1 and #2, which were heated to 200 and 400 °C in static air both exhibited a dramatic improvement in cycling performance. After 30 cycles their specific capacities corresponded to a ≈48% and 33% loss in their initial capacity respectively. Fig. 37(b) shows the specific capacity values obtained for samples #0, #3 and #4, which were annealed to 80 °C under static air and to 200 and 400 °C under flowing argon gas respectively. Samples #3 and #4 exhibited rapid capacity fading having lost 89% and 75% of their initial capacity after 30 cycles. The improved performance of the thermally treated VONTs is due to a partial removal of amine molecules from within the VONT structure. The intercalated amines impede the intercalation of Li ions, resulting in poor electrochemical performance. By heating the VONTs and partially removing some of the amine molecules the specific capacity of the VONT samples is significantly improved.

Li et al. also investigated the effects of annealing time on the electrochemical performance of the VONTs. As mentioned,

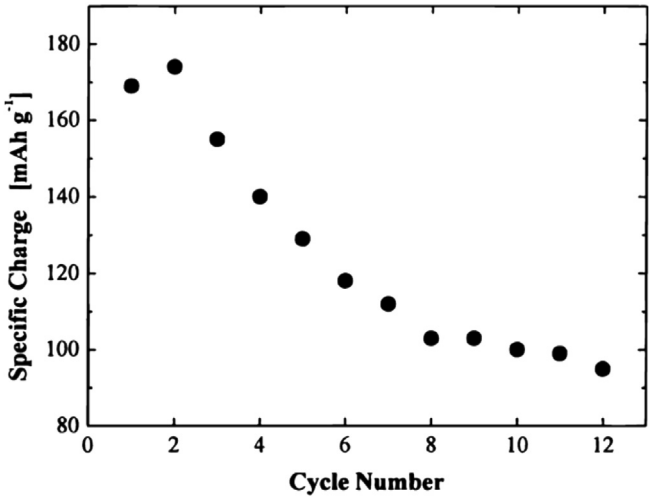


**Fig. 36.** Dependence of the specific charge on the cycle number obtained from potentiodynamic measurements at 50 $\mu V\ s^{-1}$ in the potential window from 1.5 to 4.0 V *vs.* $Li/Li^+$ [237].

**Table 4**
Annealing conditions for VONTs [207].

| Sample no. | $T_{ann}$ (°C) | Annealing time (h) | Annealing medium |
|---|---|---|---|
| #0 | 80 | – | Air |
| #1 | 200 | 1 | Air |
| #2 | 400 | 1 | Air |
| #3 | 200 | 1 | Ar |
| #4 | 400 | 1 | Ar |
| #5 | 200 | 6 | Ar |
| #6 | 200 | 10 | Ar |

thermally treating the VONTs leads to a partial removal of intercalated amines. In order to determine if longer annealing times would remove more amines and consequently further improve electrochemical performance, a series of VONT samples were thermally treated for different durations of time. Samples #3, #5 and #6 were annealed under flowing argon gas at a temperature of 200 °C for 1 h, 6 and 10 h respectively. The first 10 cycles for these samples are compared with the as-synthesised VONTs (sample #0) in Fig. 37(c). Sample #6 (10 h) performed better than sample #5 (6 h). It was proposed that this was due to the removal of a greater amount of amines for longer annealing times. However sample #3 (1 h) performed the best out of all four samples. It was suggested that the removal of the amines over longer annealing times decreases the basal spacing of the vanadium oxide layers and results in more compact structures, with worse electrochemical performance.

The effect of varying the potential window for discharging/charging on the electrochemical performance of as synthesised VONTs is shown in Fig. 37(d). The three potential windows chosen were 1.5–4 V, 2.0–4 V and 2.5–4 V. From Fig. 37(a) it was clear that the discharge capacity of the VONTs decreases rapidly with increasing cycle number between 1.5 V and 4.0 V. Increasing the cut-off voltage to 2.0 V shows less capacity fading, and there is even better stability for discharge to 2.5 V. However the capacity obtained with a cutoff voltage of 2.5 V is quite small at approximately 62.4 mAh $g^{-1}$. Li et al. concluded that post treatment of as synthesised VONTs can improve their electrochemical performance. VONTs heated to 200 and 400 °C in air no longer maintain their nanotube structure due to the removal of amines however VONTs heated to the same temperatures in argon gas did. The VONTs which were thermally annealed in Ar gas did show an improvement over the as-synthesised VONTs however they also suffered a rapid decay in specific capacity with increased cycling.

### 16.3. VONTs containing poly (ethylene oxide)

In an attempt to improve the cycling performance of as-synthesised VONTs Mohan et al. investigated the performance of VONTs containing poly (ethylene oxide) (PEO) [310]. VONTs were synthesised using the alkoxide route first reported by Spahr et al. [206] with one extra addition to the experimental method. PEO was added to the mixture of vanadium triisopropoxide and amines prior to hydrothermal treatment. XRD analysis revealed that structurally as synthesised VONTs and PEO-VONTs were very similar with {00*l*} reflections occurring at approximately the same angle for both samples. FTIR analysis indicated that the peaks associated with the stretching and bending modes of various C–H vibrations were not as intense for the PEO-VONTs as they were for the as synthesised VONTs. This implies that there is a smaller amount of intercalated amines for the PEO-VONTs than there are for the as-synthesised VONTs. From TEM images it was observed that as-synthesised VONTs are frequently grown separately with some being grown together whereas PEO-VONTs are frequently grown together and are formed as bundles. The fact that PEO-VONTs are more

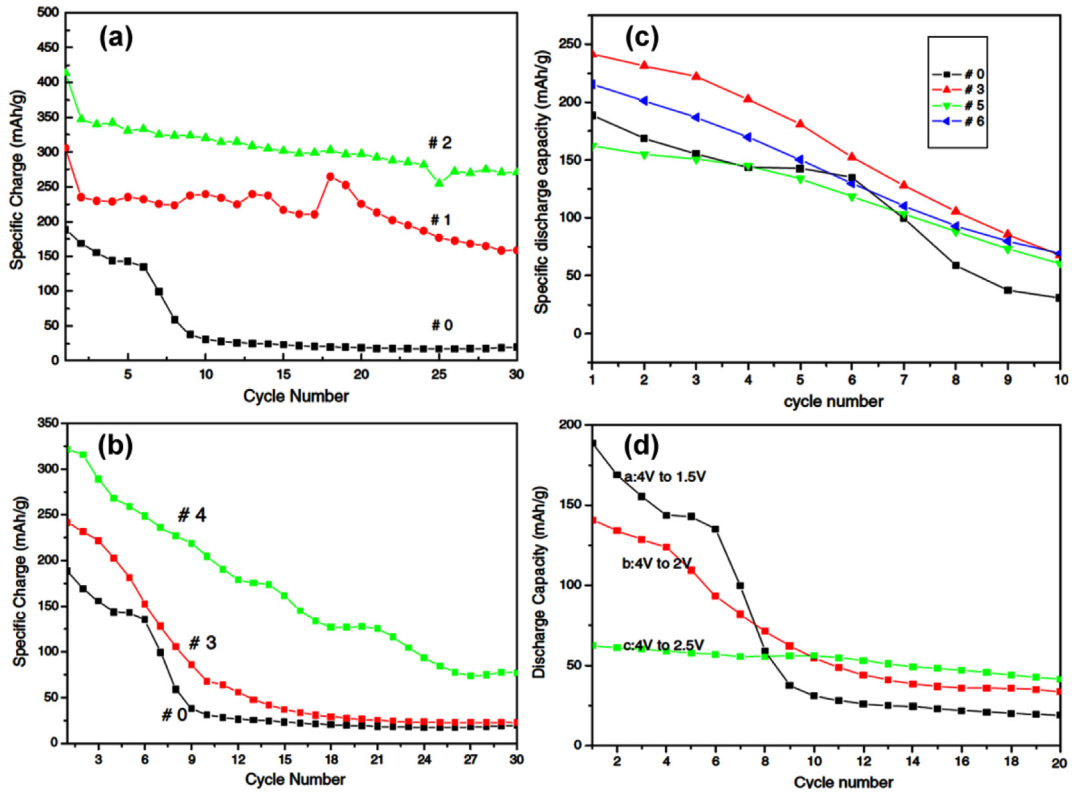


**Fig. 37.** Dependence of discharge capacity of VONTs treated at different temperatures under (a) static air and (b) flowing argon gas (c) for different annealing times. (d) Cycling behaviour for as-synthesised VONTs (sample #0) at different cut-off voltages [207].

frequently in bundles could result in an improved electrical connection between the VONTs, resulting in more of the VONTs actually participating in discharge and charge processes. As synthesised VONTs and PEO-VONTs were galvanostatically cycled for 50 cycles in a potential range of 2.0–4.0 V with a current density of 20 mA $g^{-1}$. The results of these tests are shown in Fig. 38.

The as-synthesised VONTs showed an initial specific capacity of 185 mAh $g^{-1}$, whereas the PEO-VONTs exhibited an initial specific capacity of 142 mAh $g^{-1}$. Hence initially the as-synthesised VONTs performed better than the PEO-VONTs. However the specific capacity for the PEO-VONTs decreased at a slower rate than the as-synthesised VONTs. The PEO-VONTs have a specific capacity of 95 mAh $g^{-1}$ after 15 cycles corresponding to 66.9% of its initial capacity. Mohan et al. proposed that the decreasing capacity in the PEO-VONTs might be due to decrease in average vanadium oxidation state. After 10 cycles the PEO-VONTs begin to outperform the as synthesised VONTs and continue this improved performance for the remainder of the 50 cycles. Mohan et al. suggested that the improved performance of the PEO-VONTs with increased cycling may be due to the increasing of $Li^+$ ion insertion/extraction into the PEO-VONTs. The PEO-VONTs contain less amines than the as-synthesised VONTs as was seen from TGA analysis. This reduced amount of amines within the vanadium oxide layers led to a slightly improved performance over as-synthesised VONTs. If there was a greater amount of amines removed there would be a more significant improvement.

### *16.4. Recent electrochemical characterisation of as-synthesised VONTs*

More recently, the electrochemical performance of as-synthesised VONTs was investigated again by Popa et al. in 2011 [311]. The VONTs were synthesised using the alkoxide route first reported by Spahr et al. [206]. The specific capacities and amounts of Li intercalated into the VONTs for the first 20 cycles are shown in Fig. 39. For these tests the potential of the electrochemical cell was maintained constant until the current reached a previously established limit (C/*t* rate). Subsequently, the potential was decreased (when discharging) or increased (when charging) using 5 mV steps. The rate used was C/100, that is, complete discharge in 100 h.

The discharge curves show slight changes of the slope at potential values of 2.4, 2.6, and 2.8 V. Popa et al. suggested that the absence of an obvious plateau in these curves is the clear indication of that there is no discrete phase formation during cycling. The shape of the first three cycles of the potentiostatic experiment is

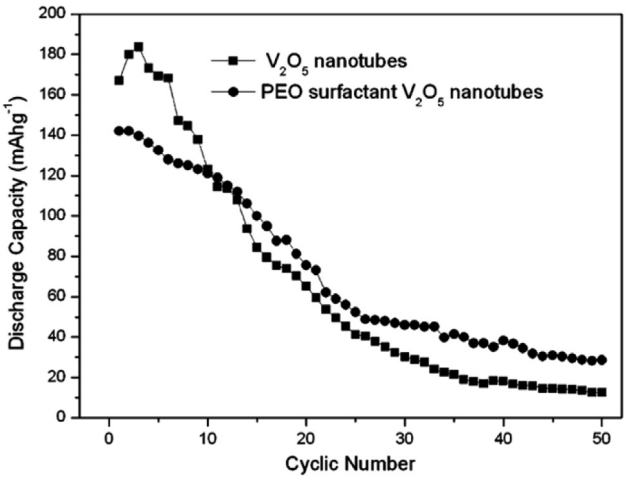


**Fig. 38.** Cycling property of VONTs and PEO-VONTs for the first 50 cycles [310].

different from the proceeding ones. It was proposed that this difference may arise from a slightly different intercalation processes occurring in the first three cycles compared to the later ones. One possibility is that initially, $Li^+$ ions inserted in a quite disordered way between the layers of vanadium oxide. With increased cycling the $Li^+$ ions might then diffuse to find favourable sites in the interlayer spaces of the structure, affecting the vanadium oxide structure. Fig. 39 shows the effect of cycling on the specific discharge capacity. After the first cycle, the specific capacity is $\approx$130 mAh $g^{-1}$, which corresponds to a Li-intercalation level of 0.66. The specific capacity rapidly decreases with increased cycling. This is in agreement with previously reported results for as-synthesised VONTs. After 20 cycles the specific capacity has dropped to $\approx$62 mAh $g^{-1}$. This corresponds to a 52% loss in specific capacity from the initial value after just 20 cycles. This decrease may be the result of side reactions, or may be due to Li ion intercalation sites blocked by amines. Once again from these results in can be concluded that as-synthesised amine containing VONTs do not retain a suitable fraction of their initial specific capacity with increased cycling. The specific capacity values decrease rapidly and this is most likely due to the amine molecules within the layers of vanadium oxide within the VONTs walls occupying $Li^+$ ion intercalation sites.

## 17. Ion exchange of amine molecules with diamine molecules

During discharge lithium ions are intercalated between the layers of vanadium oxide present in VONT walls. This is the same location that the structure maintaining amine templates are intercalated into prior to hydrothermal treatment. It is therefore conceivable that the initial poor performance of the VONTs was due to the presence of amines within the vanadium oxide layers. Initial attempts to remove the amines by refluxing the as synthesised VONTs in saturated solution of NaCl did little to improve their electrochemical performance. Initial reports that monoamines (primary amines) within synthesised VONTs could be exchanged with diamines (secondary amines) while still maintaining their tubular structure lead to the investigation of the exchange of amines by metal cations with the aim of improving electrochemical performance. The exchange of monoamines with diamines was first reported by Krumeich et al. [238]. VONTs were prepared using a vanadium triisopropoxide precursor with monoamines. The exchange reactions were performed by stirring a suspension of the as synthesised VONTs (about 100 mg) in 25 mL of ethanol with an excess of the exchanging diamine $H_2N[CH_2]_nNH_2$ with $2 \leq n \leq 20$ (about 1 mol equivalent with respect to the amount of monoamines in the tubes, i.e. two monoamine molecules are exchanged against one diamine molecule) for 12 h at room temperature. VONTs synthesised with a series of monoamines with varying molecular chain lengths underwent exchange reactions with diamines of various lengths. The interlayer spacing before and after the exchange reactions were measured from XRD data. The results of this work are summarised in Table 5 below.

It was proposed that the scroll like structure of the VONTs gives them a high structural flexibility as indicated by the readiness of exchange reactions as shown in Table 5. VONTs after the exchange reactions appear to have an interlayer spacing that is dependent on the exchanged diamine instead of the initially intercalated monoamine and most importantly the tubular structure is maintained. Krumeich et al. concluded that as the amines act as structure maintaining templates it was not possible to synthesise a pure, tubular vanadium oxide. With regard to electrochemical applications the functionalisation of the tube walls by substitution of the protonated organic template by alkali or alkaline-earth metal

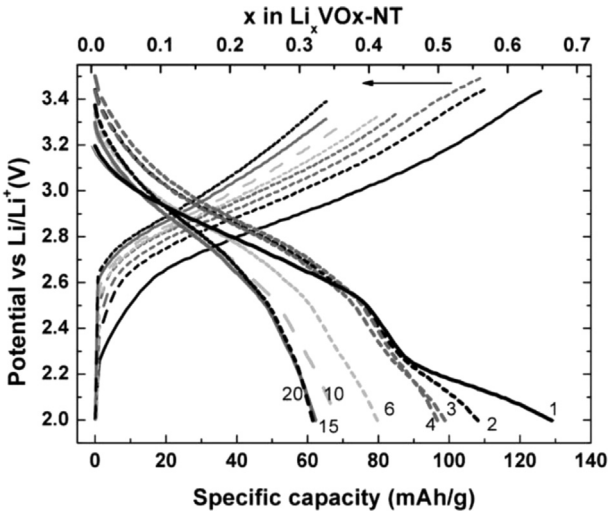


**Fig. 39.** Potential *vs.* specific capacity and the Li amount *x* in $Li_x$VONT obtained from potentiostatic studies on VONTs [311].

cations holds a more promising approach. This proposed theory would be further investigated by Reinoso.

## 18. Ion exchange of amine molecules with metal cations in VONTs

### 18.1. Structural characterisation

The controlled uptake and release of metal cations by VONTs was first reported by Reinoso et al. in 2000 [312]. Initially VONTs were synthesised by hydrothermal treatment of a solution of vanadium triisopropoxide and a primary amine as detailed above. The as synthesised VONTs were then mixed with a metal salt in a molar ratio of 1:4 respectively and stirred in a mixture of ethanol and water. EtOH and water were mixed in a 4:1 (v/v) ratio with 1 mL $mg^{-1}$ of VONTs. After stirring the resulting black powder was washed with ethanol and hexane and then allowed to dry in air. Reinoso et al. reported that the exchange behaviour of VONTs synthesised with dodecylamine was excellent with respect to the preservation of the tubular structure as well as the readiness of the intercalation. The full range of salts which were investigated is listed in Table 6. The wide range of salts which can be used in exchange reactions while still maintaining the nanotube morphology demonstrates the structural flexibility of the VONTs. As was the case when Krumeich et al. exchanged primary amines with diamines [238], VONTs before and after metal cation exchange reactions had different interlayer spacings, as shown in Table 6. The as synthesised VONTs were produced with dodecylamine and had an inter-layer distance of 2.8 nm.

**Table 6**
Interlayer spacings for VONTs after treatment with a variety of different salts [312].

| Salt | Inter-layer distance [nm] (XRD results) |
|---|---|
| NaCl | 1.1 |
| NaOH | 0.96 |
| NaI | 1.12 |
| KCl | 0.97 |
| $MgCl_2$ | 1.27 |
| $CaCl_2$ | 1.1 |
| $SrCl_2$ | 1.11 |
| $FeCl_2$ | 1.08 |
| $CoCl_2$ | 1.09 |
| $NiCl_2$ | 1.13 |
| $CuCl_2$ | 1.13 |
| $SmCl_3$ | 1.2 |
| $TbCl_3$ | 1.15 |
| NaCl + KCl | 0.96 |
| NaCl + $CaCl_2$ | 1.11 |

Reinoso et al. reported that the intercalation of various metal cations, i.e. alkaline, alkaline-earth and transition metals into VONTs synthesised with dodecylamine by exchange against the template is possible. Through TEM observations they noted that these reactions do not significantly affect the tubular morphology. As can be seen from Table 6 the removal of the intercalated amine by treatment with metal salts leads to a considerable reduction of the interlayer spacing. In the case of $Na^+$ the interlayer spacing varies from 2.8 nm to 1.1 nm. It was proposed that the decreased interlayer spacings indicate the successful (partial) removal of the primary amine template. For the incorporation of $Na^+$ cations several salts containing Na were used. It was found that the measured interlayer spacing values varied from 0.96 nm to 1.12 nm. Reinoso et al. proposed that the intercalation of alkaline metals other than $Na^+$ and $K^+$ is not possible. Attempts to treat as synthesised VONTs with diluted RbCl and CsCl lead a destruction of the VONTs and the formation of a lamellar product. It was found that several early transition metal cations such as $Fe^{2+}$, $Co^{2+}$, $Ni^{2+}$ and $Cu^{2+}$ can easily be exchanged with a reasonable preservation of the VONT structure. The most prominent structural change for all of these reactions is significant decrease of the distance between the vanadium oxide layers within the VONT walls. It was reported that the structure within the vanadium oxide layers remains unaltered as indicated by the unchanged {*hk*0} reflections seen in XRD patterns before and after exchange reactions. In spite of the unaltered atomic structure of the vanadium oxide layers, the arrangement of these layers was found to differ significantly from the layers present in amine-containing VONTs. These defects could be clearly seen

**Table 5**
Results of exchange reactions of intercalated monoamines with diamines [238].

| As-synthesised monoamine $VO_x$-NT | | Diamine exchanged $VO_x$-NT | | |
|---|---|---|---|---|
| Monoamine template | Layer distance [nm] (XRD data) | Diamine | Layer distance [nm] | |
| | | | XRD | ED |
| Hexylamine | 2.00 | 1,12-Diaminododecane | 1.84 | 1.5–1.6 |
| Undecylamine | 2.62 | 1,12-Diaminododecane | 1.83 | 1.8–2.0 |
| Hexadecylamine | 3.35 | 1,12-Diaminododecane | 1.86 | 1.60 |
| Butylamine | 1.66 | Ethylendiamine | 1.58 | |
| Hexylamine | 2.00 | Ethylendiamine | 1.30 | 1.0–1.1 |
| Undecylamine | 2.62 | Ethylendiamine | 1.60–1.70 | 1.3–1.4 |
| Hexadecylamine | 3.35 | Ethylendiamine | 1.50 | |
| Octylamine | 2.24 | 1,20-Eicosandiamine | 3.50 | |
| Hexadecylamine | 3.35 | 1,6-Diaminohexane | 1.52 | |

when cross-sectional TEM images of the VONTs after exchange reactions were taken, as shown in Fig. 40.

After exchange with $Na^+$ the vanadium oxide layers have become grouped into packs of three or more layers. As well as this nearly square arrays with larger inner diameters are sometimes observed. The partial removal of amine leads to a stiffening of the layers and to an increased attractive force between the layers of vanadium oxide and consequently a modified tubular morphology of the exchange product. Combustion test methods and inductively coupled plasma/optical emission spectroscopy were used to perform elemental analysis tests on VONTs before and after exchange reactions to determine the amount of amines which were being exchanged. VONTs synthesised with dodecylamine had 0.27 mol amine mol vanadium$^{-1}$ whereas VONTs in the $Na^+$ exchange product had 0.19 mol Na and 0.06 mol amine mol vanadium$^{-1}$. These values correspond to an amine exchange of 70%. The exchanges with $K^+$, $Mg^+$, $Ca^+$ and $Sr^+$ yielded very similar results. Reinoso et al. noted that it was not clear whether the remaining amount of template was essential for the preservation of the nanotube shape or not. Individual VONTs were found in the exchange product which measurably had different interlayer spacings within the same VONT. It was proposed that in these cases only a part of the amine had been removed.

### 18.2. The reversibility of ion exchange reactions

Reinoso et al. also went on to investigate the reactivity of Na-VONTs towards various metal salts [312]. Starting with the exchange product of VONTs treated with NaCl, it was reported that a part of the $Na^+$ cation can successfully be substituted with various other metal cations, including $K^+$, $Mg^+$, $Ca^+$ and $Sr^+$. It was proposed that the number of negative charges in the VONTs appears to be practically constant during the exchange reactions, since this number is always $\approx$0.25 mol of metal cation per mol of vanadium as mentioned above. This constant number of positive charges per vanadium atom indicates that the number of binding sites with the layers of vanadium oxide for guests appears to be constant and ionic. Also during exchange reactions there seems to be no change in the oxidation state of vanadium within the tube walls. It was also reported that the exchange reaction with $Na^+$ is partially reversible. It was found that the addition of crown ethers was necessary in order to replace the $Na^+$ cations in Na-VONTs to incorporate amines again. The resulting exchange product produces VONTs intercalated with dodecylamine again with their original interlayer spacing. However the elemental analysis indicated that approximately half of the $Na^+$ cations had been replaced by amines. It was concluded the removal of the amine template via exchange reactions with metal cations demonstrated the outstanding structural integrity of VONTs. The ability to essentially functionalise the layers of vanadium oxide within the walls of the VONTs could improve the electrochemical performance of VONTs leading to increased cycle life.

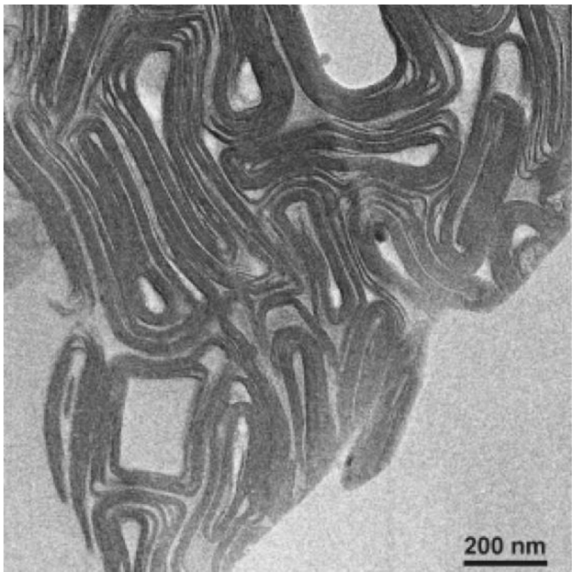


**Fig. 40.** Cross-sectional TEM image of Na-VONTs [312].

## 19. Electrochemical performance of VONTs exchanged with metal cations

### 19.1. Na-VONTs

The initial electrochemical characterisation of Na-VONTs was reported by Nordlinder et al. in 2001 [313]. In contrast with the earlier report by Spahr et al. [237] showing the poor performance of VONTs as a cathode material Nordlinder presented results showing stable and in some cases increasing capacity while cycling. In this study VONTs were synthesised with vanadium triisopropoxide and primary amines including dodecylamine and hexadecylamine. The as-synthesised VONTs were then subject to cation exchange reactions with NaCl salt using a method proposed by Krumeich et al. [238]. Working electrodes were fabricated using both as-synthesised VONTs and the exchange reaction product, i.e. the Na-VONTS. In both cases the VONT powder was mixed with carbon black and ethylene propylene diene terpolymer binder (5 wt % in cyclohexane) in the ratio of: 80:10:10 (by weight). The electrolytes consisted of 1 M solutions of salt dissolved in ethylene carbonate/dimethyl carbonate (EC/DMC) 2:1 by volume. Norlinder et al. used three different salts in this study to determine if different salts have any effect on the electrochemical behaviour of the VONT structures. The three salts which were used were lithium tetrafluoroborate ($LiBF_4$), lithium hexafluorophosphate ($LiPF_6$) and an imide salt lithium bistrifluoromethylsulfonylimide (LiTFSI). The cells were cycled between 1.8 and 3.5 V (*vs.* $Li/Li^+$) with a current loading ranging from 25 to 100 mA g$^{-1}$.

It was reported that VONTs containing intercalated amine molecules generally have lower capacities than $Na^+$ exchanged VONTs and proposed that this could be due to their higher molecular weight. Hence the results shown in Fig. 41 are for Na-VONTs. In contrast to the intercalation of Li ions into bulk crystalline $V_2O_5$, which shows the various phase transitions associated with increasing Li content, cycles with VONTs are absent of staging. This is common with amorphous and non-crystalline materials. This behaviour can be seen in the inset of Fig. 41. Also the discharge/charge curves have a tendency to plateau around 2.5 V. The cell performance is highly dependent on which salt was used when preparing the electrolyte. Cells containing $LiBF_4$ and $LiPF_6$ electrolytes show increasing capacities over time as can be seen in Fig. 41. The capacity increases for approximately the first 25 cycles after which it begins to decrease. The Na-VONT electrodes which were cycled with electrolyte containing LiTFSI showed a completely different behaviour. The initial capacity is $\approx$220 mAh g$^{-1}$ and is the highest value they achieve. This value slowly decreases with increasing number of cycles and after 100 cycles it has dropped to $\approx$170 mAh g$^{-1}$, corresponding to about a 30% decrease from the initial value. Although the best results were obtained for cells run in electrolyte containing LiTFSI, the practical use of LiTFSI is rather limited because at high potentials ($\approx$3.5 V) is has been shown to cause severe corrosion of the aluminium current collector [314].

Norlinder et al. performed *in situ* XRD measurements of Na-VONTs during the first cycle and observed that no large structural

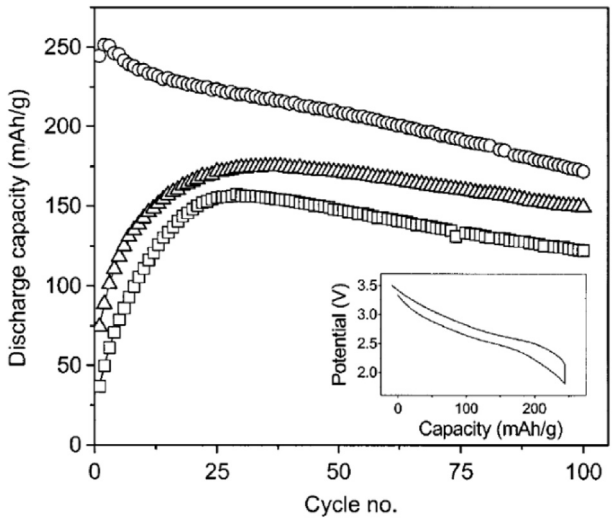


**Fig. 41.** Discharge capacities for cells cycled with three different salts in the electrolytes: LiTFSI (○), $LiBF_4$ (△), $LiPF_6$ (□). The inset displays the first discharge/charge cycle for the cell cycled with LiTFSI-electrolyte [313].

changes occurred during charge and discharge. The {003} reflection was carefully studied at different potentials as shown in Fig. 42(a). The peak position did not shift significantly, indicating that the interlayer distances do not change notably during cycling. VONT samples which had undergone 100 cycles were also examined *ex situ* by XRD. The XRD patterns of Na-VONTs before and after 100 cycles in electrolyte containing LiTFSI are shown in Fig. 42(b). The {003} reflection was clearly visible even after 100 cycles, indicating that the tubular structure remains largely intact. The {003} reflection is observed at an angle of $2\theta \approx 9.9^\circ$ for the uncycled Na-VONT. The same reflection for Na-VONTs after 100 cycles is seen at a higher angle of $2\theta \approx 10.3^\circ$. This shift in peak position corresponds to a decrease in the interlayer spacing of approximately 0.35 Å. It was proposed that this shifting of peak positions after considerable cycling may be an effect of small rearrangements in the interlayer structure during cycling. No additional peaks could be seen in the {*hk*0} XRD reflections indicating that no significant rearrangements of the vanadium oxide structure occur even after prolonged cycling.

Nordlinder et al. reported that Na-VONTs showed reversible charge and discharge cycles for at least 100 cycles. This was a significant improvement over initial electrochemical testing of as-synthesised VONTs containing amine templates. Spahr et al. reported a ≈40% decrease in capacity after just 10 cycles whereas Nordlinder reported a ≈30% decrease in 100 cycles. This was the first paper to show that VONTs are viable as a cathode material for lithium ion batteries. Similarly Dobley et al. initially reported on the electrochemical performance of VONTs which were the products of exchange reactions with $MnCl_2$ [300]. These Mn-VONTs were then galvanostatically discharged in a potential window of 2.0–4.0 V. After the first discharge the resulting capacity was calculated to be 140 mAh $g^{-1}$. It was reported that Mn-VONTs retain their morphology but observed that some cracking of the layered VONT walls can be seen on TEM.

*19.1.1. XPS study of Na-VONTs discharged to different potentials*

Continuing previous work, in 2003 Nordlinder et al. used X-ray photoelectron spectroscopy (XPS) to investigate the redox behaviour of Na-VONTs [315]. Once again $Na^+$ exchanged VONTs were used because of their superior properties over the as-synthesised material. The V 2p XPS results are shown in Fig. 43. Fig. 43(a) is for the pristine Na-VONTs and Fig. 43(b)–(e) are for Na-VONTs discharge to various potentials. A typical two-peak structure can be seen in the spectra, originating from the spin-orbit splitting of V $2p_{3/2}$ at 514–518 eV and V $2p_{1/2}$ at 522–526 eV. In Fig. 43 the solid lines represent the individual peaks and the total fit and the experimental data is represented by dots. When the electrodes are discharged, the shape of the V 2p peaks changes significantly. In fact the peak is shifted toward lower binding energies. To interpret the changing of peak shapes, the experimental spectra for samples discharged to 2.5 V were deconvoluted with two Voigt functions, one representing V(V) at ≈517.5 eV and the other representing V(IV) at ≈516.2 eV (Fig. 43(a–c)). For the samples which were discharged to 2.0 and 1.8 V, a third peak had to be included. This third peak can be attributed to the presence of a new oxidation state. Nordlinder et al. proposed that during discharge there is a partial reduction of V(IV) to V(III). Also the relation between the areas of the fitted peaks can then be seen as a measure of the different oxidation states of vanadium.

Nordlinder concluded that as lithium ions are intercalated into the Na-VONTs the V 2p peak weight shifts toward lower energies. XPS measurements show a coexistence of V(V), V(IV), and V(III) when the Na-VONTs are discharged to ≈2.0 V. This indicates that some of the vanadium may be inaccessible to reduction. It was proposed that this is partly responsible for the increase in the capacity seen over the first 20 charge/discharge cycles, which had previously been reported. This partial reduction of V(IV) to V(III) at potentials below 2.0 V and the presence of a mixture of three different oxidation states was supported by later work by Augustsson et al. [316].

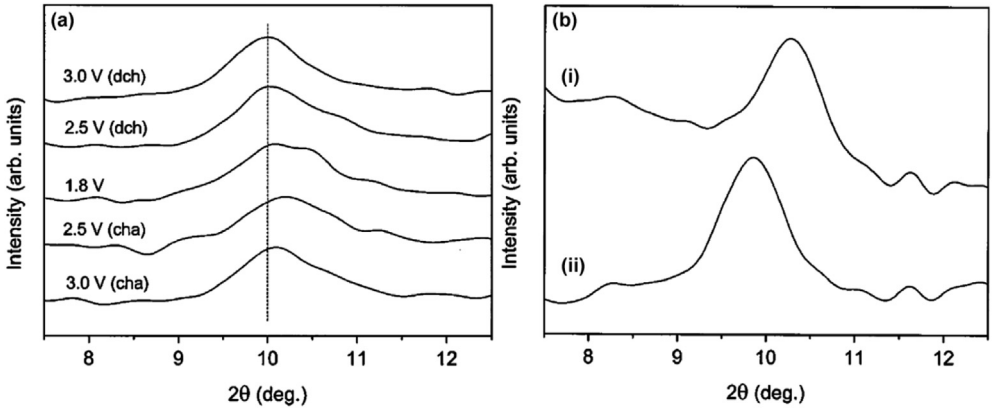


**Fig. 42.** (a) *In situ* XRD patterns recorded during the first discharge (dch) and charge (cha) of a cell using $LiBF_4$ salt in the electrolyte. (b) *Ex situ* XRD patterns for (i) Na-VONTs cycled 100 times with LiTFSI salt in the electrolyte (ii) uncycled Na–VONTs [313].

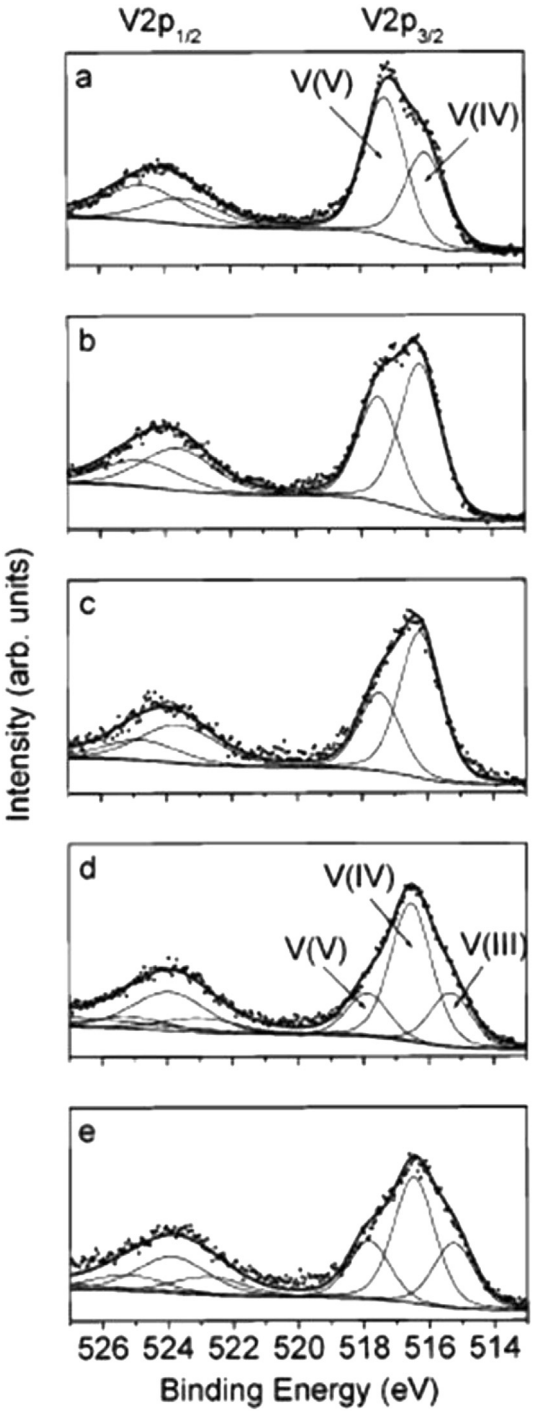


**Fig. 43.** XPS V 2p spectra for the pristine electrode (a) and electrodes discharged to 3.0 (b), 2.5 (c), 2.0 (d), and 1.8 V (e) [315].

### *19.2. Defect rich Na-VONTs*

Sun et al. reported that by varying the synthesis conditions it was possible to produce defect rich VONTs to compare electrochemically with pristine VONTs [305]. The VONTs were synthesised using traditional methods with vanadium triisopropoxide with one addition to the experimental method. Prior to hydrothermal treatment a volume of 2-propanol was added to the hydrolysed mixture of precursor and amines. It was reported that 2-propanol serves as a mild reducing agent. By increasing the amounts of precursor and decreasing the amounts of reducing agent Sun et al. found that defect rich VONTs with many cracks in the vanadium oxide walls can be synthesised. Both the pristine and defect rich VONTs were then subject to Na ion exchange reactions. In this work sodium hexafluorophosphate was used as a source of Na ions instead of the NaCl salts which were previously reported to be used by Nordlinder et al.

For cyclic voltammetric tests the voltage was swept at a rate of 1 mV $s^{-1}$ between 1.5 and 4.0 V *vs.* $Li^+$/Li. The resulting cyclic voltammograms (CVs) for the well-ordered and defect rich Na-VONTs are shown in Fig. 44(a) and (b). Sun et al. observed that the CVs for the well-ordered Na-VONTs contained several oxidation and reduction peaks and proposed that this behaviour is similar to crystalline orthorhombic $V_2O_5$ with multiple oxidation–reduction couples. The defect rich Na-VONTs however exhibit only one prominent reduction peak at ≈2.6 V. This behaviour is similar to results obtained from vanadium oxide materials derived from the sol–gel method. This reduction peak appears reversible as no change was observed after several cycles. In contrast to this however the CVs of the well-ordered Na-VONTs significantly change as cycling continues. Also the potential for the oxidation peak is more positive for the defect rich VONTs than for the well-ordered ones. Sun et al. noted that a more detailed study was required in order to explain this.

The responses of the well-ordered and defect rich Na-VONTs to galvanostatic testing were also presented. The electrodes were discharged/charged at a rate of ±60 mA $g^{-1}$ in a potential window of 1.5–4.0 V, *vs.* $Li^+$/Li. It was proposed that the specific capacity of VONTs can be affected by many factors. Initially the effect of ion exchange time on the specific capacity was investigated. Three samples of defect rich VONTs were treated for different ion exchange times. These times were 10 min, 30 min and 3 h. The effect that this had on their specific capacity values for the first 4 cycles is shown in Fig. 44(c). All three samples show an increase in specific capacity after the first cycle and then a small decrease as cycling continues. Out of the three samples the 30 min sodium exchanged sample exhibits the highest specific capacity values and the slowest rate of capacity decrease. The differences in specific capacity with ion exchange times are related to the amount of residual amine surfactant still embedded between the vanadium oxide layers after ion exchange. When the three samples were examined using thermogravimetric analysis it was found that the greatest mass loss occurred for the sample with the shortest ion exchange time, indicating that longer ion exchange times result in a more complete surfactant removal. The shortest exchange time leaves more organic amine molecules present within the vanadium oxide layers. It was proposed that the amine molecules block access to sites on the vanadium oxide layer that the lithium ions would occupy and as a result these VONTs have the lowest capacity out of the three samples tested. It was found that the sample treated for 3 h performs worse that the sample treated for 30 min. The sample treated for 3 h had the greatest amount of amine molecules exchanged as it was treated for the longest duration of time. The increased amount of removed amines resulted in this sample having the highest initial specific capacity value. However, looking at Fig. 44(c) it is clear that the 3 h sample has the steepest decrease in specific capacity after cycling. During charging, when the lithium ions are being removed, there is not enough surfactant molecules remaining between the layers of vanadium oxide to maintain its structure and consequently a fraction of the intercalated lithium ions remain within the structure. This reduces the number of Li ion occupation sites and lowers the specific capacity of additional cycles. Similar behaviour has been reported for other vanadium oxide nanostructures which do not contain organic templates such as nanorods and nanofibers [83,317–319]. During cycling, Li ions can become trapped between

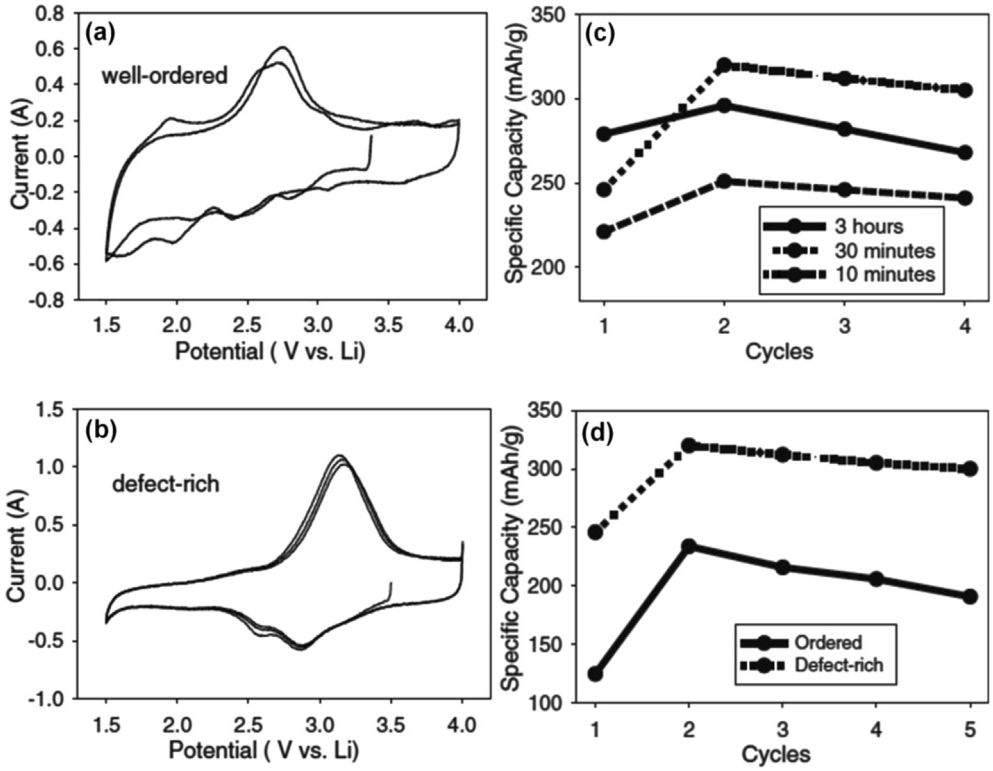


**Fig. 44.** (i) Cyclic voltammograms for Na-VONTs (30 min exchange time) (a) well-ordered VONTs (b) defect rich VONTs. (ii) Specific capacity values for various VONT samples (c) the effects of ion exchange time (d) comparison of well-ordered and defect rich VONTs prepared at the optimum ion exchange time [305].

layers of vanadium oxide within regions of the nanostructure due to a local collapsing of the layers, without any significant structural changes occurring to the nanostructure as a whole. This reduces the maximum amount of lithium which may be reversibly intercalated and consequently results in capacity fading.

Sun et al. also proposed that the atomic and nanometre-scale structure of the VONTs also have a significant effect on the resulting specific capacity values. Well-ordered and defect rich VONTs were treated for the optimum time of 30 min and their specific capacity values are compared in Fig. 44(d). It was found that the defect rich Na-VONTs had substantially higher specific capacity values than the well-ordered Na-VONTs. The values achieved for the well-ordered Na-VONTs were in agreement with previously reported values, in the range of 200 mAh $g^{-1}$ [313]. The defect rich Na-VONTs however achieved values above 300 mAh $g^{-1}$. This was a significant improvement over the well-ordered Na-VONTs and demonstrated the viability of defect rich Na-VONTs as a cathode material. A slower decrease in specific capacity for the defect rich Na-VONTs as compared to the well-ordered structures was observed. From elemental analysis it was reported that the amount of amines embedded within the layers of vanadium oxide of the well-ordered Na-VONTs after ion exchange for 30 min was about 10% higher than the defect rich Na-VONTs.

*19.2.1. The influence of amines on lithium insertion*

These results clearly show that the amount of amine molecules present within the layers of vanadium oxide within the tube walls dramatically affects the electrochemical performance of the VONTs. This supports the initial electrochemical characterisation of as-synthesised amine containing VONTs which demonstrated poor performance and rapidly decreasing specific capacity values [206]. Once again Sun et al. suggested that the poor performance of the well-ordered Na—VONTs was due to the presence of a larger amount of amines. The intercalated amine molecules reduce the specific capacity values in two ways: They reduce the available surface area for redox reactions, and they can also form aggregates which may block accessibility of the lithium ions to sites on the vanadium oxide layers. Within the layers of vanadium oxide present in the VONT walls, the only surface areas which are not accessible to lithium ions are the areas which are actively covered by surfactant molecules. The results of these ion exchange time experiments indicate that a certain amount of amine molecules are needed within the vanadium oxide layers to serve as spacers and prevent the collapse of the gallery spacing during electrochemical cycling. Also these results suggest that perfectly ordered structures, while aesthetically appealing, may not be the most optimal structures for many electrochemical applications.

O'Dwyer, et al. investigated how the structure of nanotubes and nanourchins of vanadium oxide was influenced by amine uptake as a structure-influencing template, and simultaneously tested its effect of lithium insertion and removal characteristics. By forming nano-urchin, it was demonstrated [320] that the reduced amine uptake during synthetic functionalisation when making nanotubes in radial arrays such as nano-urchin improves the Li ion insertion properties, resulting in higher specific capacities for the same phase of material. The primary difference is the degree of amine functionalisation, which is less for urchin structures synthesised from isopropoxide-based precursors. The differences in specific capacity are most probably related to the quantity of organic interlaminar surfactant. We know that the nanotubes of the nano-urchin possess a considerable volume of unreacted and pure $V_2O_5$ throughout its mostly scrolled laminar morphology, resulting in less residual surfactant between the $VO_x$ layers compared to xerogel-based nanotubes. This is a direct result of a lower degree of surfactant uptake/electrostatic binding and consequently provides a more

open pathway for $Li^+$ interlaminar intercalation/diffusion giving higher capacities.

High-resolution TEM studies revealed the unique observation of nanometre-scale nanocrystals of pristine unreacted $V_2O_5$ throughout the length of the nanotubes in the nano-urchin (Fig. 45 (right)). Electrochemical intercalation studies revealed that the well-ordered xerogel-based nanotubes exhibit similar specific capacities (235 mAh $g^{-1}$) to $Na^+$-exchanged nanorolls of $VO_x$ (200 mAh $g^{-1}$). The nanotubes of the nano-urchin 3-D assemblies, however, exhibit high charge capacities exceeding 437 mAh $g^{-1}$, which demonstrates the benefit of template removal and nanostructuring of the crystalline phases in $V_2O_5$ structures.

### 19.3. K-VONTs and Ca-VONTs

Following on from their initial electrochemical characterisation of Na-VONTs Nordlinder et al. investigated the electrochemical behaviour of $K^+$ and $Ca^{2+}$ VONTs and compared them with Na-VONTs [321]. The ion exchanged VONTs were tested electrochemically in electrolytes using two different kinds of lithium containing salts, one containing $LiBF_4$ and the other containing an ionic liquid LiTFSI. It was reported that the performance for these ion exchanged VONTs showed significant capacity even after 100 cycles as shown in Fig. 46. The average capacity for these VONTs was between 120 and 150 mAh $g^{-1}$. As was the case for the previously reported Na-VONTS there was an increase in the capacity of the initial 10–20 cycles, as shown in Fig. 46(a) and (b). While it is not yet clear what governs this behaviour some theories were proposed. One proposed explanation was that the insertion of Li ions into the VONTs is diffusion limited and consequently this might lead to an increase in the capacity as the lithium ions diffuse further into the host material. Another possibility was that the cations between the layers of vanadium oxide, i.e. the exchanged metal cations, may be electrochemically active and participate in the discharge/charge process. Nordlinder et al. reported that the as-synthesised VONTs, i.e. the VONTs still containing the amine template, have maximum capacities of ≈80 mAh $g^{-1}$, when cycled with both a $LiBF_4$ and LiTFSI based electrolytes. If the capacity is calculated with respect to the weight of vanadium instead of the total weight, the as-synthesised material is still not as good as the ion-exchanged material. It was proposed that VONTs with embedded dodecylamine may have less space for intercalated $Li^+$ ions because the amine molecules are bulkier than the metal cations. The amine molecules have a hydrocarbon chain attached to the positively charged $NH_3^{\pm}$ ion. This could explain the poor electrochemical performance of as-synthesised VONTs.

To investigate the materials' response to the applied current, a range of constant currents were used on each cell. In this manner the cells were cycled at different rates and the results are displayed in Fig. 46(c) and (d). The three different rates which were used were 5 mA $g^{-1}$ (C/30), 25 mA $g^{-1}$ (C/5) and 50 mA $g^{-1}$ (C/2). After each cell had been cycled at 50 mA $g^{-1}$, the current was then reduced to 5 mA $g^{-1}$ again. Once again this procedure was performed using both $LiBF_4$ and LiTFSI electrolytes. The cells were allowed to rest for at least 24 h before a new rate was applied. During the resting period the potential dropped to the equilibrium potential (around 3.4 V). At the initial C/30 rate all cells have an increasing capacity over the initial ten cycles with capacity values between 150 and 180 mAh $g^{-1}$. When the rate was decreased to C/5, stable capacities were achieved with values ranging between 120 and 160 mAh $g^{-1}$. The capacities at the C/2 rate were between 100 and 140 mAh $g^{-1}$ when the rate was then increased back to C/30 the capacity values increase back to values similar to their initial values. Hence all materials seem to regain most, or all, of their initial capacity when returned to the C/30 rate.

In a previous study on Na-VONTs Nordlinder et al. noticed a larger dependence of the type of electrolyte used on the electrochemical behaviour of the VONTs. An electrolyte with LiTFSI salt resulted in a more stable cycling behaviour than if $LiBF_4$ or $LiPF_6$ were used. However in this study Nordlinder reported that in this investigation the same distinct trend was not observed. It was proposed that the reason for this was that it is difficult to exactly reproduce the cycling behaviour for the VONTs noting that the composition of the electrode and the assembly of the two-electrode cell seem to have a large influence on the electrochemical performance. The working electrodes in the previous study consisted of a different type of current collector and they contained less active material. Both the type of current collector used and the mass loading of the VONTs could have affected the result because the lithium insertion into the nanotubes may be diffusion limited. It was concluded that how the electrodes are constituted is important and their effect on the performance must be further investigated.

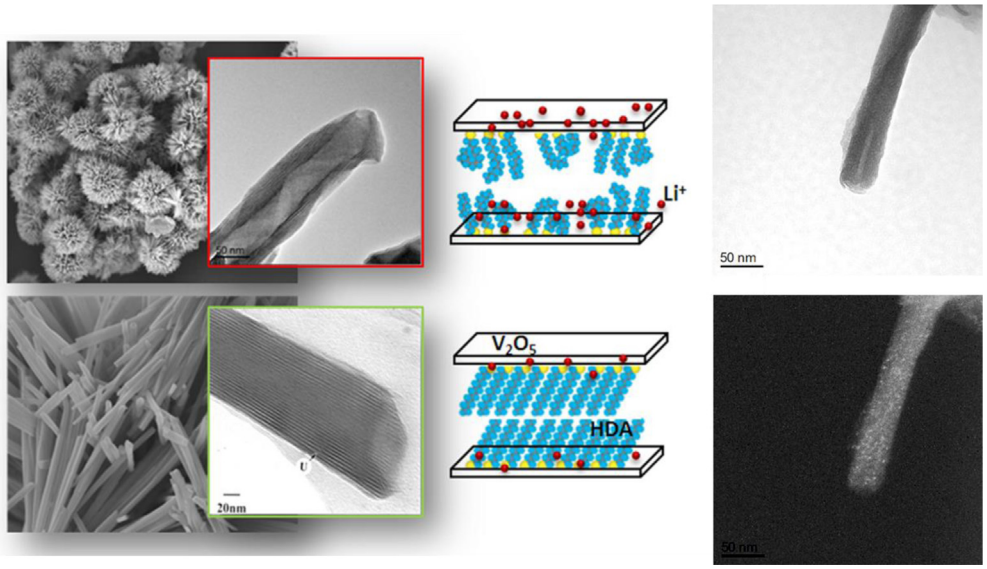


**Fig. 45.** Nano-urchin and nanotubes of $V_2O_5$ grown using a primary amine template. Minimising the density of amine between $V_2O_5$ lamina markedly improved the ability of the nanotube to intercalate a higher capacity of Li-ions.

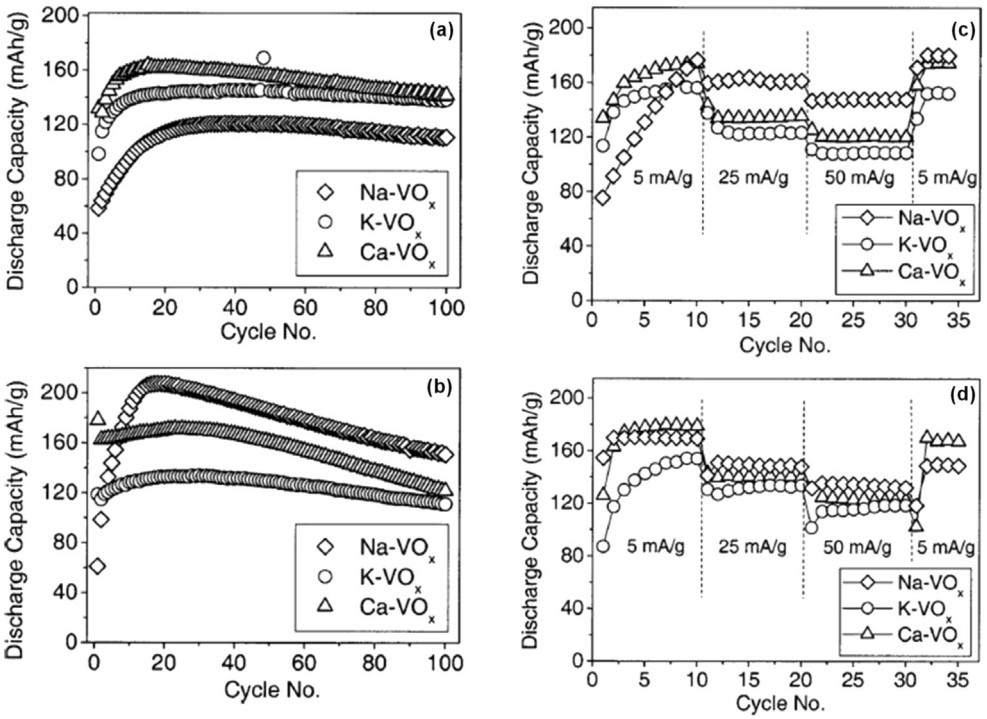


**Fig. 46.** (i) Discharge capacities for the ion-exchanged material cycled 100 times with (a) the $LiBF_4$ and (b) LiTFSI based electrolyte. (ii) Discharge capacity as a function of cycle number for different discharge rates for cells cycled with (a) the LiBF4 and (b) LiTFSI electrolyte. Applied currents of 5, 25, and 50 mA $g^{-1}$ correspond to C/30, C/5, and C/2 rates, respectively [321].

### *19.4. The effect of varying the potential window on Ca-VONTs*

Nordlinder et al. revisited calcium exchanged VONTs in 2006 and examined the effect of varying the potential window in which they are discharged and charged [322]. The first discharge and charge of a Ca-VONT in a potential window of 1.4–3.6 V with a current loading of 25 mA $g^{-1}$ is shown in Fig. 47(a). Weak plateaus in the discharge curve at 2.8 and 2.6 were observed indicating the absence of the formation of discrete phases. It was noted that there is an asymmetry in the shape of the discharge and charge curves indicating that both processes involve significantly different structural rearrangements. The Ca-VONTs were cycled galvanostatically, with a current loading of 25 mA $g^{-1}$, in a range of different potential windows including: 1.2–3.8 V, 1.4–3.6 V, 1.6–3.4 V and 1.8–3.2 V. The results of these tests are shown in Fig. 47(b). As expected, Nordlinder reported that the capacity increased if the potential window was extended. When a potential window between 1.2 and 3.8 V was used, the capacity was found to decrease rapidly with time. For this potential window the specific capacity decreased from ≈250 mAh $g^{-1}$ to ≈125 mAh $g^{-1}$ after just 30 cycles. This was most likely due to destructive side reactions and/or phase transitions. In a potential window of 1.6–3.4 V the specific capacity increases slightly over the first 30 cycles and in a potential window of 1.8–3.2 V the specific capacity remains constant for the first 30 cycles at about 130 mAh $g^{-1}$. The best performance was obtained in a potential window of 1.4–3.6 V. In this window the specific capacity obtained was reasonably stable at about 175 mAh $g^{-1}$. In summary, Nordlinder et al. reported that Ca-VONTs cells can be discharged to 1.5 V and charged to 3.5 V while still maintaining reversible battery operation without significant decreasing of the specific capacity. Choosing an appropriate potential window for discharging/charging VONTs is crucial to their performance.

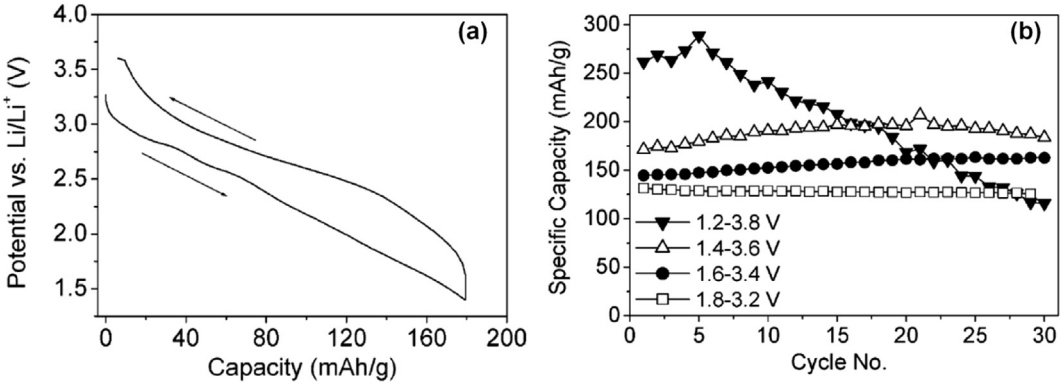


**Fig. 47.** (a) First cycle galvanostatic curves for a Ca-VONT electrode. (b) Charge capacity over 30 cycles for varying cutoff potentials [322].

## 20. Lithium vanadium oxide nanotubes

In 2010 Cui et al. reported the successful synthesis of lithium vanadium oxide nanotubes [323]. These were the first synthesised lithium containing VONTs to be reported. Inspired by the poor electrochemical performance of as synthesised VONTs which had been previously reported [237] Cui et al. investigated the synthesis of lithium VONTs with the primary aim of improving the performance of VONTs as a cathode material. The synthesis of these Li-VONTs was similar to a method previously used by Chandrappa et al. [243] with an additional step in the experimental procedure. $LiOH \cdot H_2O$ was dissolved in deionised water and added to the vanadium oxide precursor gel prior to the addition of amines. Traditional VONTs were also synthesised for electrochemical comparison with Li-VONTs. Their synthesis was the same except the $LiOH \cdot H_2O$ was not added to the mixture prior to thermal treatment. The as synthesised Li-VONTs appeared very similar to traditional VONTs in TEM images and from XRD measurements. The differences between the two types of VONTs could be seen from XPS measurements. XPS analysis revealed that the Li-VONTs are indeed composed of V, O, Li, C and N. C and N belong to the organic template indicating that the amine molecules and Li ions co-exist within the layers of vanadium oxide present in the walls of the tubes. From cyclic voltammetry it was found that the cathodic and anodic peaks for the two samples occur at approximately the same potentials. It is clear that the redox current of Li-VONTs is much higher than that of VONTs. Cui et al. proposed that these results indicated that Li-VONTs have higher capacity and faster kinetics towards $Li^+$ ions insertion/extraction compared to VONTs.

Galvanostatic tests were performed in the potential range of 1.0–4.0 V (*vs.* $Li/Li^+$) at a constant current density 30 mA $g^{-1}$. The first discharge for VONTs and Li-VONTs is shown in Fig. 48(b). The two samples show almost the same discharge behaviours, however there is a significant difference in their specific capacity values. For the mentioned potential range and current density, the initial specific capacity of Li-VONTs is about 457 mAh $g^{-1}$, which is considerably higher than that of VONTs (336 mAh $g^{-1}$). This result was in good agreement with the cyclic voltammetry result. The cycling performance for the two samples over the first 10 cycles is shown in the inset of Fig. 48(b). The significant improvement of the Li-VONTs over the VONTs is made evident when the specific capacities over the first 10 cycles are considered. The results show that the discharge capacity of Li-VONTs still retains a high capacity of 270 mAh $g^{-1}$ after 10 cycles, which is much higher than the capacity of VONTs (140 mAh $g^{-1}$). However Cui et al. observed that in both cases discharge capacity of the two samples degraded drastically. It was proposed that the improved electrochemical performance of Li-VONTs may be due to the incorporation of lithium-ions into the host lattice by strong ionic bonds, which had been previously shown to improve the structural stability and electronic conductivity of other vanadium oxide structures [324,325]. Cui et al. concluded that the resultant Li-VONTs exhibit high discharge capacity and good cycling performance compared to VONTs. While these results indicate a significant improvement on the electrochemical performance of VONTs compared with initial reports, the rapidly decreasing capacity values do not suggest that long term battery operation (500+ cycles) is viable with these structures.

## 21. Ferric ion exchanged vanadium oxide nanotubes

### 21.1. Preparation of Fe-VONTS

Initially as synthesised VONTs suffered from rapidly decaying capacities with increased number of cycles. The poor performance was attributed to the presence of amine molecules within the layers of vanadium oxide. Cation exchanged VONTs showed improved performance with stable values of ≈150 mAh $g^{-1}$ being reported for the first 10 cycles. The fabrication of ferric ion exchanged VONTs (Fe-VONTs) was reported in 2012 [326]. Zhou et al. were aware that amine templates have no contribution to electrochemical performance and impede the fast transport of lithium ion in VONTs and as such wished to remove as much of the amine molecules as possible while still maintaining the nanotubular morphology. Fe-VONTs were investigated with the principal aim of improving the electrochemical behaviour of the VONTs. Initially VONTs were synthesised using a technique first reported by Chandrappa et al. [243]. The as-synthesised VONTs were then subject to a ferric ion exchange process. $FeCl_3 \cdot 6H_2O$ was dissolved in water and added to a suspension of VONTs in water/ethanol. The mixture was stirred, washed and dried. The resulting precipitate consisted of Fe-VONTs. The interlayer spacings of VONTs and Fe-VONTs were measured from XRD analysis to determine the effects of the ion exchange reaction. It was found that after ferric ion exchange the distance between vanadium oxide layers within the VONTs decreased from 2.79 nm to 1.15 nm indicating the effective (partial) removal of the amines. This partial removal of amine templates was further verified by FTIR and XPS analysis. As seen with ion exchange reactions with metal cations, after the exchange reaction there is still a quantity of embedded amines within the vanadium oxide layers. It is believed that it is necessary to have some amines between the layers to maintain the nanotube structure.

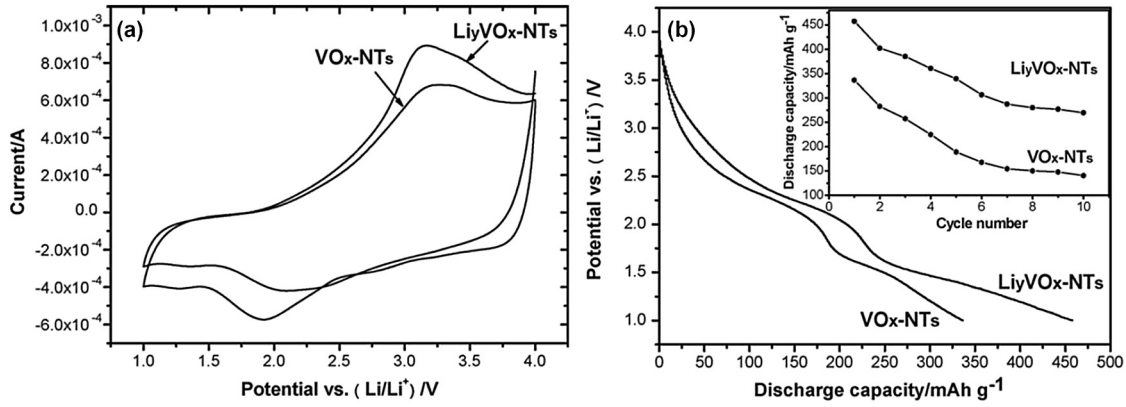


**Fig. 48.** (a) The first cyclic voltammogram curves for VONTs and Li-VONTs, (b) the initial discharge capacities of VONTs and Li-VONTs. The inset in (b) shows the cycling performance of the two samples [323].

*21.2. Electrochemical characterisation of Fe-VONTs*

In order to demonstrate the electrochemical properties of the samples, galvanostatic charge–discharge and cyclic voltammetry (CV) tests were performed on VONTs and Fe-VONTS. In both cases the VONTs and Fe-VONTs were cycled in a potential window of 1.5–4 V. The first charge and discharge curves for VONTs and Fe-VONTs at a series of different current densities are shown in Fig. 49(a) and (b). The chosen current densities for these tests were 50, 80, and 100 mA $g^{-1}$. The current density was varied to determine its effect on the electrochemical performance of the VONTs. The discharge and charge curves for both the VONTs and Fe-VONTs are smooth charge with the absence of any significant plateaus. There are 2 slight plateaus observed for the as-synthesised VONTs at about 1.6 and 2.2 V. There is however a significant difference between the specific capacity values obtained for VONTs and Fe-VONTs. The first discharge specific capacities of VONTs at 50, 80, and 100 mA $g^{-1}$ are 253, 242, and 225 mAh $g^{-1}$, respectively. In contrast to this Fe-VONTs deliver higher specific capacities of 311, 294, and 259 mAh $g^{-1}$ at the corresponding current densities. The values obtained for Fe-VONTs are in the order of ≈50 mAh $g^{-1}$ higher at each current density than those obtained for the as-synthesised VONTs.

The specific capacities for VONTs and Fe-VONTs for the first 50 cycles at the current densities mentioned above are shown in Fig. 49(c). The results over the first 50 cycles clearly demonstrate the superior performance of Fe-VONTs over the as-synthesised VONTs. In both cases, increasing the current density leads to a quicker loss of specific capacity. The rapid decrease in specific capacity of the as synthesised VONTs is clearly demonstrated once again. The initial specific capacity of the VONTs of ≈150 mAh $g^{-1}$ rapidly drops to below 50 mAh $g^{-1}$ after 25 cycles and after 50 cycles has a value of about 33 mAh $g^{-1}$. This is consistent for each of the current densities used. The corresponding capacity loss ratios at each current density are all over 85%. Losing 85% of their capacities over 50 cycles indicates once again that as-synthesised VONTs are not a viable cathode material for commercial lithium ion batteries. For Fe-VONTs, after 50 cycles at the current densities of 50, 80, and 100 mA $g^{-1}$, the specific capacities are slowly reduced to 178, 141, and 121 mAh $g^{-1}$ respectively. The corresponding capacity loss ratios for these values are 42.8%, 52%, and 53.3% respectively. The Fe-VONT sample cycled at the smallest current density showed the lowest % loss in capacity. All three Fe-VONT samples were still maintaining significant specific capacity values after the first 50 cycles and are in stark contrast to the as synthesised VONTs. The rapidly decreasing capacity values which plague the as-synthesised VONTs are not seen in the case of the Fe-VONTs.

The initial cyclic voltammetry curves of the VONT and Fe-VONT samples at a scan rate of 0.5 mV $s^{-1}$ are shown in Fig. 49(d). The downward cathodic peaks associated with Li ion insertion are located at 2.02 and 2.71 V for VONTs and at 2, 2.4, and 3.04 V for Fe-VONTs. The upward anodic peaks associated with Li ion extraction are located at 3.48 V for VONTs and at 3 and 3.28 V for Fe-VONTs. As observed from the curves, Fe-VONTs exhibit more pronounced redox peaks and larger peak areas than those of VONTs, and the potential positions of redox peaks are closer to each other for Fe-VONTs than for VONTs. These results demonstrate that Fe-VONTs possess faster kinetics toward lithium ion insertion/extraction and higher capacity than VONTs. Zhou et al. concluded that the improved electrochemical performance can be attributed to the effective removal of amine template without destroying the tubular morphology and the multi-walled structure. Furthermore, the ferric ion exchange process leads to the increase in the proportion of pentavalent vanadium, which also has contribution to the improvement of electrochemical capacity. The improved Fe-VONTs demonstrated dramatically higher capacity and significantly better cyclic capability than the as synthesised VONTs.

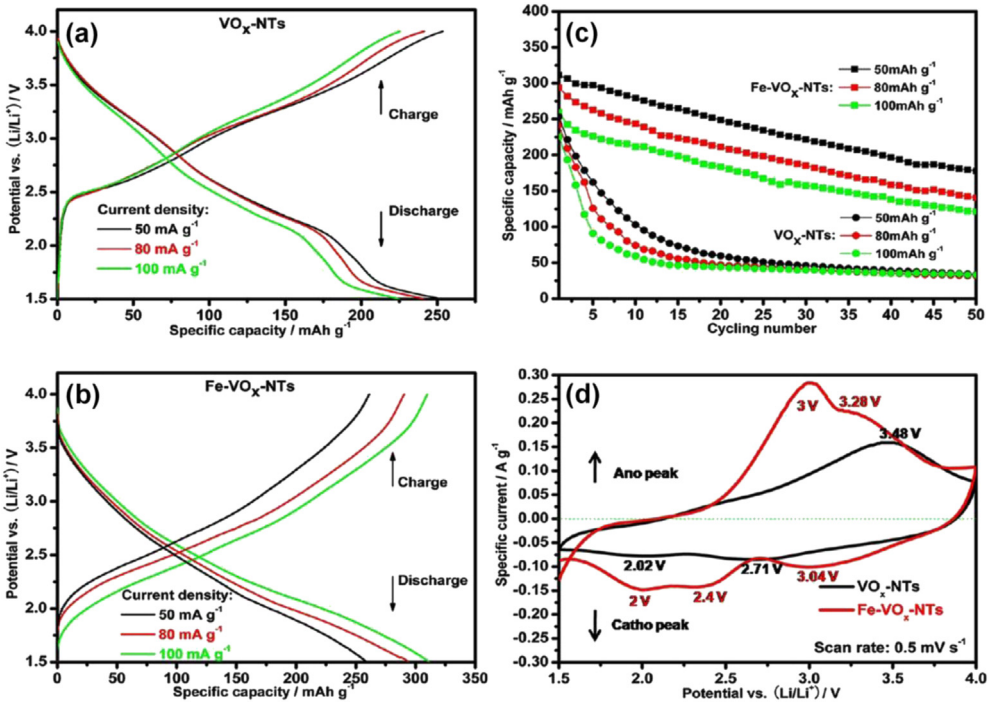


**Fig. 49.** First charge–discharge curves at different current densities for (a) VONTs and (b) Fe-VONTs. (c) Cycling performance of VONTs and Fe-VONTs under different discharge current densities. (d) The initial cyclic voltammogram curves for VONTs and Fe-VONTs [326].

## 22. Vanadium oxide nanostructures for lithium ion batteries

As previously mentioned many vanadium oxide nanostructures have been reported including nanobelts, nanorods, nanowires, nanourchins, nanospheres and flower like structures. As the electrochemical performance of $V_2O_5$ nanotubes has been reviewed in detail, the performance of the other nanostructures will now be summarised and compared. $V_2O_5$ nanobelts are synthesised by the hydrothermal treatment of a mixture of orthorhombic $V_2O_5$ and $H_2O_2$, as detailed by Li et al. [213]. The mixture was thermally treated for 2 days at 180 °C. The specific capacities for obtained for the first 6 discharges are demonstrated in Fig. 50(a). These cells were cycled in a potential window of 4.0–1.5 V with a constant current density of 0.2 mA $cm^{-2}$. The initial specific capacity of ≈288 mAh $g^{-1}$ quickly fades to ≈191 mAh $g^{-1}$ after the sixth discharge. This corresponds to a ≈34% loss in the initial specific capacity after just 6 cycles, indicating that capacity fading is a significant issue for $V_2O_5$ nanobelts cathodes for Li ion batteries. Centimetre long $V_2O_5$ nanowires were reported by Zhai et al. [327]. The synthesis of these nanowires was quite similar to the nanobelts reported by Li et al. $V_2O_5$ nanowires are also synthesised by the hydrothermal treatment of a mixture of orthorhombic $V_2O_5$ and $H_2O_2$ however the molar ratio of deionised water and $V_2O_5$ is different and the mixture is thermally treated at an increased temperature of 205 °C for 4 days. The cycling performance of $V_2O_5$ nanowires at a current density of 50 mA $g^{-1}$ in a potential window of 1.5 and 4.0 V is shown in Fig. 50(b). The initial discharge capacity of the $V_2O_5$ nanowires was reported to be as high as 351 mAh $g^{-1}$. The specific capacity quickly decreased with increased cycling. After 20 cycles the specific capacity had decreased to ≈175 mAh $g^{-1}$, this corresponds to a ≈50% decrease in the initial capacity value. Hence similar to $V_2O_5$ nanobelts, nanowires also suffer from significant capacity fading.

The template free hydrothermal synthesis of $V_2O_5$ nanorods was reported by Reddy et al. [328]. Initially a $V_2O_5$ xerogel was obtained through melt quenching of orthorhombic $V_2O_5$. The resulting xerogel was then thermally treated in an autoclave for 15 days at 180 °C, before being washed with deionised water and then dried at 300 °C for 10 h. Galvanostatic testing on the resulting nanorods was performed at a current density of 0.4 mA $cm^2$ in a potential window of 4.0–1.5 V. The first discharge capacity of the as-prepared vanadium oxide nanorods was reported to be 385 mAh $g^{-1}$. The specific capacity values obtained for 50 complete cycles are shown in Fig. 50(c). After the first discharge the specific capacity increased slightly to ≈411 mAh $g^{-1}$ after the fourth cycle. After this the specific capacity values began to fade, however the capacity fading observed for the nanorods was not as severe as reported for nanowires and nanobelts. After 20 cycles there was a ≈20% decrease in the initial specific capacity (≈50% decrease after 20 cycles for nanowires was reported) and after 50 cycles there was a ≈40% decrease in the initial specific capacity. This improvement in the cycling performance of $V_2O_5$ nanorods is most likely due to the long thermal treatment at high temperature (180 °C) and the 10 h of drying at an even higher temperature (300 °C). This thermal treatment removes the majority of physically and chemically bound water from the nanorods which has been shown to improve electrochemical performance [118]. The synthesis of $V_2O_5$ nanourchins was first reported by O'Dwyer et al. [183]. $V_2O_5$ nanourchins are high density radial arrays of $V_2O_5$ nanotubes which are synthesised by hydrothermal treatment of an ethanolic solution of vanadium triisopropoxide and hexadecylamine. The first discharge curve obtained for a $V_2O_5$ nanourchin sample is shown in Fig. 50(d). The discharge response obtained for the nanourchin sample is quite similar to that of orthorhombic $V_2O_5$, with each phase transition associated with increasing lithium content visible in the discharge curve. The specific capacity for the nanourchin sample after the first discharge has a value of 437 mAh $g^{-1}$, which is larger than the capacity values obtained for nanowires, nanorods and nanobelts samples. No data has been reported for the cycling performance of nanourchins so the degree of capacity fading for these samples is not known.

Recently the synthesis of dense and spherical nanostructured $V_2O_5$ particles was reported by Lin et al. [329] A one-step synthesis of the nanospheres was achieved via ultrasonic spray pyrolysis of an ammonium metavanadate precursor solution at various synthesis temperatures ranging from 500 to 700 °C. $V_2O_5$ nanosphere samples were galvanostatically cycled at a current density of 442 mA $g^{-1}$ in a range of different potential windows. The results of these tests are shown in Fig. 50(e). It was reported that the potential range significantly affects the cycle performance of the cathode. In a potential range of 4.0–1.5 V the initial specific capacity of ≈400 mAh $g^{-1}$ decreases to ≈200 mAh $g^{-1}$ after 30 cycles, corresponding to a ≈50% loss in the initial capacity. The cyclability significantly improves when the lower limit is increased from 1.5 V–2.5 V. In a potential window of 4.0–2.5 V, the cathode exhibits an initial discharge capacity of 135 mAh $g^{-1}$ and this value remains reasonably stable over the first thirty cycles. Also recently, the synthesis and electrochemical performance of copper doped $V_2O_5$ nanoflowers have been reported by Yu et al. [330] Their synthesis involves the hydrothermal treatment of a mixture of orthorhombic $V_2O_5$, $H_2O_2$, $NH_4H_2PO_4$ and $Cu(NO_3)_2{\cdot}4H_20$. The mixture is then thermally treated at 180 °C for 2 h, washed with distilled water and ethanol and then annealed again at 400 °C for 2 h. The specific capacity values obtained for the first fifty cycles at a current density of 58.8 mA $g^{-1}$, in a potential window of 4.0–2.01 V, are shown in Fig. 50(f). The initial specific capacity of ≈266 mAh $g^{-1}$ decreased to ≈226 mAh $g^{-1}$ after 50 cycles, this corresponded to just a 15% loss in the initial capacity. The Cu doped $V_2O_5$ samples exhibit improved electrochemical performance compared to other $V_2O_5$ nanostructures. Recently doped $V_2O_5$ nanostructures have been attracting a lot of attention in hopes of overcoming the capacity fading inherent with un-doped nanostructures. $V_2O_5$ samples doped with metals such as silver [331,332], niobium [333,334], titanium [216,333], tantalum [335,336] and manganese [230,300] offer the possibility of further improving the electrochemical performance of various $V_2O_5$ structures and will be the subject of further research in the years to come.

## 23. Conclusions and outlook

Our dependency on Li-ion and emerging alternatives in the next decade will likely require enhancements in the performance and stability of Li-ion battery chemistries, and those of alternatives such as Li–S and Li–air approaches. Cathode material development is critical for battery performance advances. Knowledge of cathode materials structure, accommodation of various cations such as Li, but also $Mn^{2+}$, $Mg^{2+}$ and $Al^{3+}$ for example, will likely drive further development at the juncture of materials chemistry, solid state chemistry and battery electrochemistry. The development of large-scale Li-ion batteries, particularly for EV/HEVs requires materials that can deliver higher power density, excellent rate capability and cycle life and importantly, improved safety characteristics that are critical for safe usage.

Reducing the active dimensions of cathode materials has gone a long way toward improving the rate and cycling performance, and the reader is referred to other review articles that summarise materials and Li-ion battery performance aspects that are outside the scope of this review [337–341]. In these cases, the nanostructuring of materials is likely to help filter chemistries, structures and

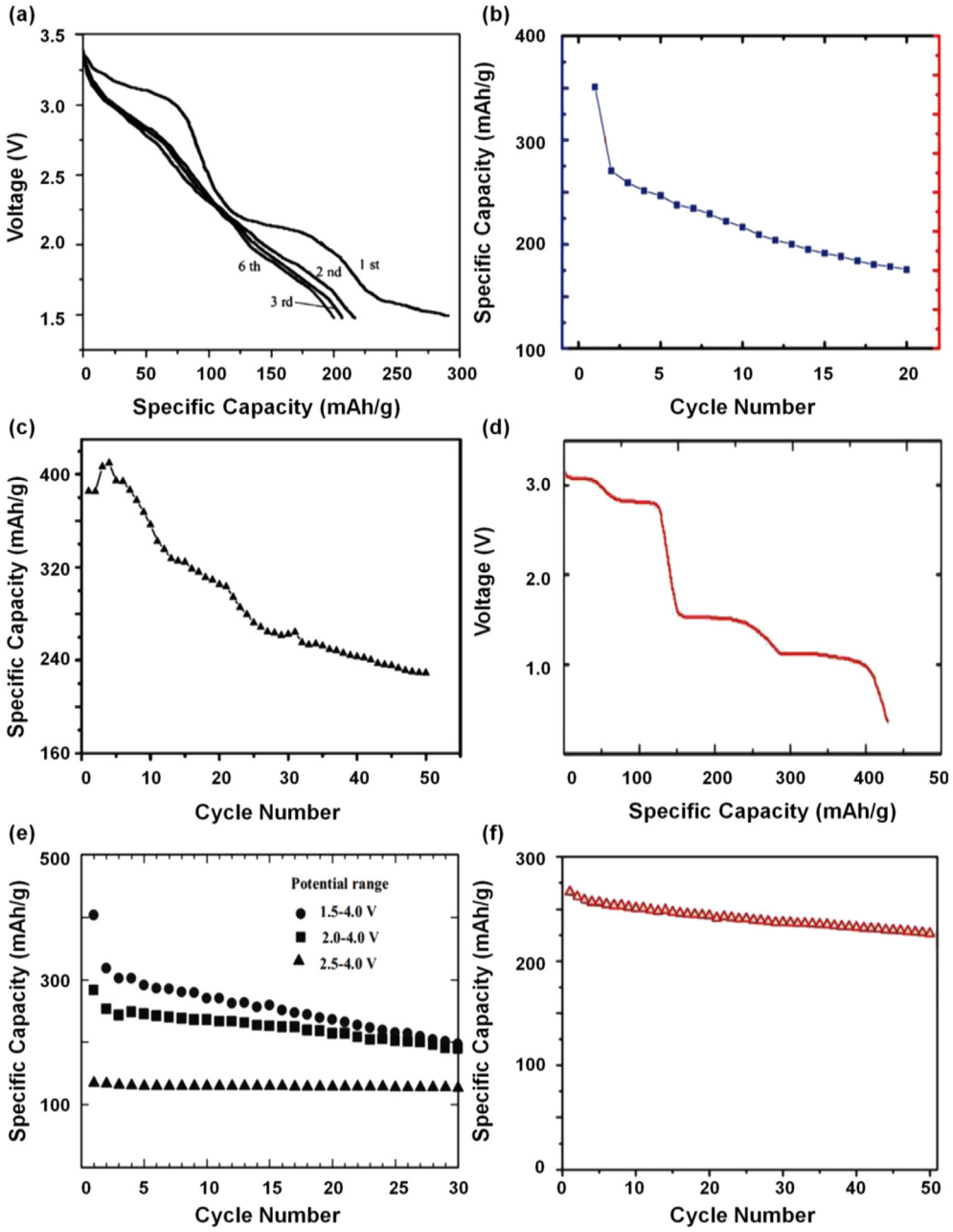


**Fig. 50.** Electrochemical performance of various $V_2O_5$ nanostructures (a) nanobelts [213], (b) nanowires [327], (c) nanorods [328], (d) nanourchins [183], (e) nanospheres [329], (f) nanoflowers [330].

electrode composition that are tuned for batteries with defined power and energy density requirements. The ability to scale electrode materials size can confer enormous benefits in charge rate enhancement for increased power and storage capacity for greater energy density, once the increased surface area does not facilitate unwanted chemical side reactions with the electrolyte.

Layered materials were some of the first materials used in Li and Li-ion battery tests and today, nanoscale analogues of some of these materials are being reinvestigated. The redux of layered materials has been driven by advances in the synthesis of 2D crystalline materials such as graphene and transition metal dichalcogenides such as $MoS_2$, $Ta_2S$ and many other materials [342]. The many structural, chemical and electrochemical aspects of $V_2O_5$ outlined in this review highlight the influence of layered materials structure and morphology on intercalation mechanisms. The ability to controllably alter the morphology and the crystal structure of layered materials and other cation-accommodating phases might prove insightful for the development of alternative bronzes of 2D layered materials currently being synthesised. The somewhat negative influence of organic templates on electrochemical performance highlighted here is also worth considering in cases where such moieties are needed to control nanomaterial size and assembly on electrodes.

$V_2O_5$ is still receiving considerable interest as a positive electrode material [343–351]. Even in xerogel or thin film form, it serves as a model material for morphology-related effects in cation insertion and removal characteristics that influence the cycling stability, and its chemistry in certain anionic electrolytes is very well understood. The presence of defects and vacancies strongly influences the properties of transition metal oxides [352] such as

electrochemical capacity and reactivity, ambipolar conductivity and transport, and electrode potential.

Atypical insertion capacities are now well known in $V_2O_5$. When the stoichiometries of $Li_xV_2O_5$, with $x > 3$ are found that the process is not described by non-faradaic intercalation [353,354]. Scrosati and Garche [355] demonstrated that proton-stabilised cation vacancies, as formed by roasting the polycrystalline powder in an $O_2$/$H_2O$ atmosphere, allowed capacities beyond theoretical maximum based on intercalation into a pristine crystal. This observation has now been observed in $MnO_2$ and other materials and it is feasible that it may be obtained in bronzes or variants of $V_2O_5$ and other layered materials where solid state ionic protocols can rationally control the number of useful vacancies or defects in this regard. With the resurgence in Li-ion batteries research and promising developments in 2D layered materials, intercalation (non-faradaic, into the lattice), pseudocapacitance (faradaic, charge transfer due to 'intercalation' of Li within the van der Waals gaps in some layered materials) and defect-mediated higher storage capacities may offer some routes towards better performance in battery and supercapacitor materials.

## References


[1] J.M. Tarascon, M. Armand, Nature 414 (2001) 359–367.
[2] C.A. Vincent, Solid State Ionics 134 (2000) 159–167.
[3] N. Marinčić, J. Appl. Electrochem. 5 (1975) 313–318.
[4] N. Marinčić, J. Appl. Electrochem. 6 (1976) 51–58.
[5] M.S. Whittingham, J. Electrochem. Soc. 122 (1975) 526–527.
[6] M.S. Whittingham, Science 192 (1976) 1126–1127.
[7] M.S. Whittingham, Mater. Res. Bull. 9 (1974) 1681–1689.
[8] J. Cessna, Corrosion 27 (1971) 244–254.
[9] E. Heitz, in: Advances in Corrosion Science and Technology, Springer, 1974, pp. 149–243.
[10] K. Abraham, Electrochim. Acta 38 (1993) 1233–1248.
[11] Y. Nishi, J. Power Sources 100 (2001) 101–106.
[12] D. Fauteux, R. Koksbang, J. Appl. Electrochem. 23 (1993) 1–10.
[13] A. Dey, J. Electrochem. Soc. 118 (1971) 1547–1549.
[14] J. Besenhard, Carbon 14 (1976) 111–115.
[15] R. Yazami, P. Touzain, J. Power Sources 9 (1983) 365–371.
[16] M. Lazzari, B. Scrosati, J. Electrochem. Soc. 127 (1980) 773–774.
[17] M. Armand, Materials for Advanced Batteries, Plenum Press, New York, 1980, p. 145.
[18] K. Sawai, Y. Iwakoshi, T. Ohzuku, Solid State Ionics 69 (1994) 273–283.
[19] R. Bittihn, R. Herr, D. Hoge, J. Power Sources 43 (1993) 223–231.
[20] K. Ozawa, Solid State Ionics 69 (1994) 212–221.
[21] T. Nagura, Prog. Batt. Solar Cells 9 (1990) 209.
[22] M.S. Whittingham, Preparation of Intercalated Chalcogenides, US Patent No. 4,040,917, August 9, 1977.
[23] J. Akridge, H. Vourlis, Solid State Ionics 28 (1988) 841–846.
[24] Z. Tomczuk, K. Anderson, D. Vissers, M. Roche, J. Electrochem. Soc. 127 (1980) 1881–1885.
[25] M. Broussely, P. Biensan, B. Simon, Electrochim. Acta 45 (1999) 3–22.
[26] P. Cignini, M. Icovi, S. Panero, G. Pistoia, C. Temperoni, J. Electroanal. Chem. Interfacial Electrochem. 102 (1979) 333–341.
[27] G. Pistoia, C. Temperoni, P. Cignini, M. Icovi, S. Panero, J. Electroanal. Chem. Interfacial Electrochem. 108 (1980) 169–180.
[28] M.A. Habib, D. Glueck, Sol. Energy Mater. 18 (1989) 127–141.
[29] M.S. Whittingham, J. Electrochem. Soc. 123 (1976) 315–320.
[30] J. Besenhard, R. Schöllhorn, J. Electrochem. Soc. 124 (1977) 968–971.
[31] T. Ohzuku, M. Kitagawa, T. Hirai, J. Electrochem. Soc. 137 (1990) 769–775.
[32] K. Mizushima, P. Jones, P. Wiseman, J. Goodenough, Mater. Res. Bull. 15 (1980) 783–789.
[33] K. Mizushima, P.C. Jones, P.J. Wiseman, J.B. Goodenough, Solid State Ionics 3–4 (1981) 171–174.
[34] R. Koksbang, J. Barker, H. Shi, M. Saidi, Solid State Ionics 84 (1996) 1–21.
[35] K. Takada, N. Aotani, K. Iwamoto, S. Kondo, Solid State Ionics 79 (1995) 284–287.
[36] G.T.K. Fey, M.C. Hsieh, H.K. Jaw, T.J. Lee, J. Power Sources 44 (1993) 673–680.
[37] T. Sasaki, T. Nonaka, H. Oka, C. Okuda, Y. Itou, Y. Kondo, Y. Takeuchi, Y. Ukyo, K. Tatsumi, S. Muto, J. Electrochem. Soc. 156 (2009) A289–A293.
[38] G. Amatucci, C. Schmutz, A. Blyr, C. Sigala, A. Gozdz, D. Larcher, J. Tarascon, J. Power Sources 69 (1997) 11–25.
[39] J. Cho, H. Jung, Y. Park, G. Kim, H.S. Lim, J. Electrochem. Soc. 147 (2000) 15–20.
[40] J. Dahn, E. Fuller, M. Obrovac, U. von Sacken, Solid State Ionics 69 (1994) 265–270.
[41] S. Yamada, M. Fujiwara, M. Kanda, J. Power Sources 54 (1995) 209–213.
[42] J. Dahn, U. von Sacken, C. Michal, Solid State Ionics 44 (1990) 87–97.
[43] M. Thackeray, J. Electrochem. Soc. 142 (1995) 2558–2563.
[44] H. Huang, P.G. Bruce, J. Power Sources 54 (1995) 52–57.
[45] M. Rossouw, A. De Kock, L. De Picciotto, M. Thackeray, W. David, R. Ibberson, Mater. Res. Bull. 25 (1990) 173–182.
[46] L. Guohua, H. Ikuta, T. Uchida, M. Wakihara, J. Electrochem. Soc. 143 (1996) 178–182.
[47] J. Cho, G. Kim, Electrochem. Solid-State Lett. 2 (1999) 253–255.
[48] V. Manev, B. Banov, A. Momchilov, A. Nassalevska, J. Power Sources 57 (1995) 99–103.
[49] R. Gummow, A. De Kock, M. Thackeray, Solid State Ionics 69 (1994) 59–67.
[50] I.J. Davidson, R.S. McMillan, J.J. Murray, J.E. Greedan, J. Power Sources 54 (1995) 232–235.
[51] G. Vitins, K. West, J. Electrochem. Soc. 144 (1997) 2587–2592.
[52] M. Osiak, H. Geaney, E. Armstrong, C. O'Dwyer, J. Mater. Chem. A 2 (2014) 9433–9460.
[53] B. Scrosati, Electrochim. Acta 45 (2000) 2461–2466.
[54] M. Broussely, F. Perton, J. Labat, R.J. Staniewicz, A. Romero, J. Power Sources 43 (1993) 209–216.
[55] T. Ohzuku, A. Ueda, J. Electrochem. Soc. 141 (1994) 2972–2977.
[56] J.N. Reimers, J.R. Dahn, J. Electrochem. Soc. 139 (1992) 2091–2097.
[57] R. Gummow, M. Thackeray, W. David, S. Hull, Mater. Res. Bull. 27 (1992) 327–337.
[58] B. Wang, J.B. Bates, F.X. Hart, B.C. Sales, R.A. Zuhr, J.D. Robertson, J. Electrochem. Soc. 143 (1996) 3203–3213.
[59] L. Montoro, M. Abbate, J. Rosolen, Electrochem. Solid-State Lett. 3 (2000) 410–412.
[60] Y.M. Chiang, Y.I. Jang, H. Wang, B. Huang, D.R. Sadoway, P. Ye, J. Electrochem. Soc. 145 (1998) 887–891.
[61] T.J. Boyle, D. Ingersoll, T.M. Alam, C.J. Tafoya, M.A. Rodriguez, K. Vanheusden, D.H. Doughty, Chem. Mater. 10 (1998) 2270–2276.
[62] J. Cho, Y.J. Kim, B. Park, Chem. Mater. 12 (2000) 3788–3791.
[63] C. Delmas, I. Saadoune, Solid State Ionics 53–56 (Part 1) (1992) 370–375.
[64] R.J. Gummow, M.M. Thackeray, Solid State Ionics 53–56 (Part 1) (1992) 681–687.
[65] R. Alcántara, P. Lavela, J.L. Tirado, R. Stoyanova, E. Zhecheva, J. Electrochem. Soc. 145 (1998) 730–736.
[66] Z. Liu, A. Yu, J.Y. Lee, J. Power Sources 81 (1999) 416–419.
[67] A. Ritchie, J. Power Sources 96 (2001) 1–4.
[68] I.E. Wachs, Dalt. Trans. 42 (2013) 11762–11769.
[69] G.C. Bond, S.F. Tahir, Appl. Catal. 71 (1991) 1–31.
[70] G.C. Bond, P. König, J. Catal. 77 (1982) 309–322.
[71] A. Erdöhelyi, F. Solymosi, J. Catal. 123 (1990) 31–42.
[72] N. Ozer, C.M. Lampert, Thin Solid Films 349 (1999) 205–211.
[73] K. Nagase, Y. Shimizu, N. Miura, N. Yamazoe, Appl. Phys. Lett. 60 (1992) 802–804.
[74] M. Benmoussa, A. Outzourhit, A. Bennouna, E.L. Ameziane, Thin Solid Films 405 (2002) 11–16.
[75] A. Talledo, C.G. Granqvist, J. Appl. Phys. 77 (1995) 4655–4666.
[76] Y.L. Cheah, V. Aravindan, S. Madhavi, J. Electrochem. Soc. 160 (2013) A1016–A1024.
[77] J. Liu, H. Xia, D. Xue, L. Lu, J. Am. Chem. Soc. 131 (2009) 12086–12087.
[78] M. Lira-Cantú, P. Gómez-Romero, J. Electrochem. Soc. 146 (1999) 2029–2033.
[79] E.J. Jeon, Y.W. Shin, S.C. Nam, W.I. Cho, Y.S. Yoon, J. Electrochem. Soc. 148 (2001) A318–A322.
[80] A. Bystrom, K. Wilhelmi, O. Brotzen, Acta Chem. Scand. 4 (1950).
[81] Y. Wang, G. Cao, Chem. Mater. 18 (2006) 2787–2804.
[82] M.J. Armstrong, C. O'Dwyer, W.J. Macklin, J.D. Holmes, Nano Res. 7 (2014) 1–62.
[83] N.A. Chernova, M. Roppolo, A.C. Dillon, M.S. Whittingham, J. Mater. Chem. 19 (2009) 2526–2552.
[84] D.W. Murphy, P.A. Christian, F.J. DiSalvo, J.N. Carides, J. Electrochem. Soc. 126 (1979) 497–499.
[85] D.W. Murphy, P.A. Christian, F.J. DiSalvo, J.V. Waszczak, Inorg. Chem. 18 (1979) 2800–2803.
[86] R.J. Cava, A. Santoro, D.W. Murphy, S.M. Zahurak, R.M. Fleming, P. Marsh, R.S. Roth, J. Solid State Chem. 65 (1986) 63–71.
[87] B. Zachau-Christiansen, K. West, T. Jacobsen, Solid State Ionics 9–10 (Part 1) (1983) 399–404.
[88] J. Galy, J. Solid State Chem. 100 (1992) 229–245.
[89] C. Delmas, H. Cognac-Auradou, J.M. Cocciantelli, M. Ménétrier, J.P. Doumerc, Solid State Ionics 69 (1994) 257–264.
[90] B. Pecquenard, D. Gourier, N. Baffier, Solid State Ionics 78 (1995) 287–303.
[91] K. West, B. Zachau-Christiansen, T. Jacobsen, S. Skaarup, Solid State Ionics 76 (1995) 15–21.
[92] C. Julien, I. Ivanov, A. Gorenstein, Mater. Sci. Eng. B 33 (1995) 168–172.
[93] N.M. Asl, J.-H. Kim, W.C. Lee, Z. Liu, P. Lu, Y. Kim, Electrochim. Acta 105 (2013) 403–411.
[94] P.L. Moss, R. Fu, G. Au, E.J. Plichta, Y. Xin, J.P. Zheng, J. Power Sources 124 (2003) 261–265.
[95] P. Rozier, J.M. Savariault, J. Galy, Solid State Ionics 98 (1997) 133–144.
[96] X. Zhang, R. Frech, Electrochim. Acta 42 (1997) 475–482.
[97] M. Isobe, Y. Ueda, Mater. Res. Bull. 34 (1999) 1719–1728.
[98] C. Delmas, H. Cognac-Auradou, J. Cocciantelli, M. Menetrier, J. Doumerc, Solid State Ionics 69 (1994) 257–264.
[99] C.R. Walk, N. Margalit, J. Power Sources 68 (1997) 723–725.

[100] C. Delmas, S. Brèthes, M. Ménétrier, J. Power Sources 34 (1991) 113–118.
[101] J.M. Cocciantelli, M. Ménétrier, C. Delmas, J.P. Doumerc, M. Pouchard, M. Broussely, J. Labat, Solid State Ionics 78 (1995) 143–150.
[102] B. Garcia, M. Millet, J.P. Pereira-Ramos, N. Baffier, D. Bloch, J. Power Sources 81–82 (1999) 670–674.
[103] J.M. Cocciantelli, J.P. Doumerc, M. Pouchard, M. Broussely, J. Labat, J. Power Sources 34 (1991) 103–111.
[104] J.M. Coccíantelli, M. Ménétrier, C. Delmas, J.P. Doumerc, M. Pouchard, P. Hagenmuller, Solid State Ionics 50 (1992) 99–105.
[105] C. Leger, S. Bach, P. Soudan, J.-P. Pereira-Ramos, J. Electrochem. Soc. 152 (2005) A236–A241.
[106] A. Ditte, C. R. Acad. Sci. Paris 101 (1885) 698.
[107] W. Biltz, Ber. Dtsch. Chem. Ges. 37 (1904) 1098.
[108] G.Z. Wegelin, Chem. Ind. Kolloide 11 (1912) 25.
[109] E.Z. Müller, Chem. Ind. Kolloide 8 (1911) 302.
[110] Z. El Mandouh, M. Selim, Thin Solid Films 371 (2000) 259–263.
[111] W. Ostermann, Wiss. Ind. Hamburg 1 (1922) 17.
[112] N. Gharbi, C. R'Kha, D. Ballutaud, M. Michaud, J. Livage, J.P. Audiere, G. Schiffmacher, J. Non Cryst. Solids 46 (1981) 247–257.
[113] C. Sanchez, J. Livage, J.P. Audiere, A. Madi, J. Non Cryst. Solids 65 (1984) 285–300.
[114] S. Kittaka, S. Sasaki, N. Ogawa, N. Uchida, J. Solid State Chem. 76 (1988) 40–51.
[115] P. Aldebert, N. Baffier, N. Gharbi, J. Livage, Mater. Res. Bull. 16 (1981) 669–676.
[116] J.-J. Legendre, J. Livage, J. Colloid Interface Sci. 94 (1983) 75–83.
[117] L. Rivoalen, A. Revcolevschi, J. Livage, R. Collongues, J. Non Cryst. Solids 21 (1976) 171–179.
[118] J. Livage, Chem. Mater. 3 (1991) 578–593.
[119] W. Prandtl, L. Hess, Z. Anorg. Chem. 82 (1913) 103–129.
[120] F. Chaput, B. Dunn, P. Fuqua, K. Salloux, J. Non Cryst. Solids 188 (1995) 11–18.
[121] J. Livage, Solid State Ionics 86 (1996) 935–942.
[122] N. Özer, Thin Solid Films 305 (1997) 80–87.
[123] F.J. Anaissi, G.J. Demets, H.E. Toma, Electrochem. Commun. 1 (1999) 332–335.
[124] B. Araki, C. Mailhé, N. Baffier, J. Livage, J. Vedel, Solid State Ionics 9–10 (Part 1) (1983) 439–444.
[125] K. West, B. Zachau-Christiansen, M.J.L. Østergård, T. Jacobsen, J. Power Sources 20 (1987) 165–172.
[126] K. West, B. Zachau-Christiansen, T. Jacobsen, S. Skaarup, Electrochim. Acta 38 (1993) 1215–1220.
[127] K. West, B. Zachau-Christiansen, T. Jacobsen, S. Skaarup, J. Power Sources 43 (1993) 127–134.
[128] H.K. Park, W.H. Smyrl, M.D. Ward, J. Electrochem. Soc. 142 (1995) 1068–1073.
[129] V. Vivier, J. Farcy, J.-P. Pereira-Ramos, Electrochim. Acta 44 (1998) 831–839.
[130] E. Potiron, A. Le Gal La Salle, A. Verbaere, Y. Piffard, D. Guyomard, Electrochim. Acta 45 (1999) 197–214.
[131] A.L. Tipton, S. Passerini, B.B. Owens, W.H. Smyrl, J. Electrochem. Soc. 143 (1996) 3473–3477.
[132] H. Hirashima, K. Sudoh, J. Non Cryst. Solids 145 (1992) 51–54.
[133] K. Sudoh, H. Hirashima, J. Non Cryst. Solids 147–148 (1992) 386–388.
[134] D.B. Le, S. Passerini, A.L. Tipton, B.B. Owens, W.H. Smyrl, J. Electrochem. Soc. 142 (1995) L102–L103.
[135] D.B. Le, S. Passerini, J. Guo, J. Ressler, B.B. Owens, W.H. Smyrl, J. Electrochem. Soc. 143 (1996) 2099–2104.
[136] W. Dong, J.S. Sakamoto, B. Dunn, Sci. Technol. Adv. Mater. 4 (2003) 3–11.
[137] A. Mansour, S. Dallek, P. Smith, W. Baker, J. Electrochem. Soc. 149 (2002) A1589–A1597.
[138] J.H. Harreld, W. Dong, B. Dunn, Mater. Res. Bull. 33 (1998) 561–567.
[139] D.R. Rolison, B. Dunn, J. Mater. Chem. 11 (2001) 963–980.
[140] K. Salloux, F. Chaput, H.P. Wong, B. Dunn, M.W. Breiter, J. Electrochem. Soc. 142 (1995) L191–L192.
[141] W. Dong, D.R. Rolison, B. Dunna, Electrochem. Solid-State Lett. 3 (2000) 457–459.
[142] S. Passerini, D. Ba Le, W.H. Smyrl, M. Berrettoni, R. Tossici, R. Marassi, M. Giorgetti, Solid State Ionics 104 (1997) 195–204.
[143] G. Sudant, E. Baudrin, B. Dunn, J.-M. Tarascon, J. Electrochem. Soc. 151 (2004) A666–A671.
[144] A. Mansour, P. Smith, W. Baker, M. Balasubramanian, J. McBreen, J. Electrochem. Soc. 150 (2003) A403–A413.
[145] A. Mansour, P. Smith, M. Balasubramanian, J. McBreen, J. Electrochem. Soc. 152 (2005) A1312–A1319.
[146] F. Coustier, J.-M. Lee, S. Passerini, W.H. Smyrl, Solid State Ionics 116 (1999) 279–291.
[147] A.N. Mansour, P.H. Smith, W.M. Baker, M. Balasubramanian, J. McBreen, Electrochim. Acta 47 (2002) 3151–3161.
[148] J. Livage, Materials 3 (2010) 4175–4195.
[149] F. Cheng, Z. Tao, J. Liang, J. Chen, Chem. Mater. 20 (2007) 667–681.
[150] L.B. Kish, Phys. Lett. A 305 (2002) 144–149.
[151] M.S. Gudiksen, L.J. Lauhon, J. Wang, D.C. Smith, C.M. Lieber, Nature 415 (2002) 617–620.
[152] C. Berger, Z. Song, T. Li, X. Li, A.Y. Ogbazghi, R. Feng, Z. Dai, A.N. Marchenkov, E.H. Conrad, P.N. First, J. Phys. Chem. B 108 (2004) 19912–19916.
[153] W. Lu, C.M. Lieber, Nat. Mater. 6 (2007) 841–850.
[154] P. Poizot, S. Laruelle, S. Grugeon, L. Dupont, J. Tarascon, Nature 407 (2000) 496–499.
[155] U. Kasavajjula, C. Wang, A.J. Appleby, J. Power Sources 163 (2007) 1003–1039.
[156] C.K. Chan, H. Peng, G. Liu, K. McIlwrath, X.F. Zhang, R.A. Huggins, Y. Cui, Nat. Nano. 3 (2008) 31–35.
[157] A.N. Shipway, E. Katz, I. Willner, ChemPhysChem 1 (2000) 18–52.
[158] X. Wang, C.J. Summers, Z.L. Wang, Nano Lett. 4 (2004) 423–426.
[159] S. He, B. Song, D. Li, C. Zhu, W. Qi, Y. Wen, L. Wang, S. Song, H. Fang, C. Fan, Adv. Funct. Mater. 20 (2010) 453–459.
[160] O. Veiseh, C. Sun, J. Gunn, N. Kohler, P. Gabikian, D. Lee, N. Bhattarai, R. Ellenbogen, R. Sze, A. Hallahan, Nano Lett. 5 (2005) 1003–1008.
[161] D.A. Giljohann, D.S. Seferos, W.L. Daniel, M.D. Massich, P.C. Patel, C.A. Mirkin, Angew. Chem. Int. Ed. 49 (2010) 3280–3294.
[162] F. Patolsky, B.P. Timko, G. Yu, Y. Fang, A.B. Greytak, G. Zheng, C.M. Lieber, Science 313 (2006) 1100–1104.
[163] R.S. Friedman, M.C. McAlpine, D.S. Ricketts, D. Ham, C.M. Lieber, Nature 434 (2005) 1085.
[164] Y. Cui, L.J. Lauhon, M.S. Gudiksen, J. Wang, C.M. Lieber, Appl. Phys. Lett. 78 (2001) 2214.
[165] J. Hu, T.W. Odom, C.M. Lieber, Acc. Chem. Res. 32 (1999) 435–445.
[166] Y. Cui, C.M. Lieber, Science 291 (2001) 851–853.
[167] H. Dai, E.W. Wong, Y.Z. Lu, S. Fan, C.M. Lieber, Nature 375 (1995) 769–772.
[168] W. Han, S. Fan, Q. Li, Y. Hu, Science 277 (1997) 1287–1289.
[169] W.U. Huynh, J.J. Dittmer, A.P. Alivisatos, Science 295 (2002) 2425–2427.
[170] S. Iijima, Nature 354 (1991) 56–58.
[171] R. Tenne, L. Margulis, M. Genut, G. Hodes, Nature 360 (1992) 444–446.
[172] M.C. Hersam, Nat. Nano. 3 (2008) 387–394.
[173] C.N.R. Rao, B.C. Satishkumar, A. Govindaraj, M. Nath, ChemPhysChem 2 (2001) 78–105.
[174] Z.W. Pan, Z.L. Wang, Science 291 (2001) 1947–1949.
[175] M.S. Arnold, P. Avouris, Z.W. Pan, Z.L. Wang, J. Phys. Chem. B 107 (2003) 659–663.
[176] Y. Sun, B. Mayers, Y. Xia, Nano Lett. 3 (2003) 675–679.
[177] Y. Geng, S.J. Wang, J.-K. Kim, J. Colloid Interface Sci. 336 (2009) 592–598.
[178] G. Zou, H. Li, D. Zhang, K. Xiong, C. Dong, Y. Qian, J. Phys. Chem. B 110 (2006) 1632–1637.
[179] C. Ye, Y. Bando, G. Shen, D. Golberg, J. Phys. Chem. B 110 (2006) 15146–15151.
[180] N. Kröger, R. Deutzmann, M. Sumper, Science 286 (1999) 1129–1132.
[181] S.-J. Park, S. Kim, S. Lee, Z.G. Khim, K. Char, T. Hyeon, J. Am. Chem. Soc. 122 (2000) 8581–8582.
[182] W. Gerberich, W. Mook, C. Perrey, C. Carter, M. Baskes, R. Mukherjee, A. Gidwani, J. Heberlein, P. McMurry, S. Girshick, J. Mech. Phys. Solids 51 (2003) 979–992.
[183] C. O'Dwyer, D. Navas, V. Lavayen, E. Benavente, M.A. Santa Ana, G. Gonzalez, S.B. Newcomb, C.M.S. Torres, Chem. Mater. 18 (2006) 3016–3022.
[184] Y. Fang, S. Guo, C. Zhu, S. Dong, E. Wang, Langmuir 26 (2010) 17816–17820.
[185] M. Terrones, J.-C. Charlier, A. Gloter, E. Cruz-Silva, E. Terres, Y. Li, A. Vinu, Z. Zanolli, J. Dominguez, H. Terrones, Nano Lett. 8 (2008) 1026–1032.
[186] P.G. Bruce, B. Scrosati, J.-M. Tarascon, Angew. Chem. Int. Ed. 47 (2008) 2930–2946.
[187] Z. Lu, D. MacNeil, J. Dahn, Electrochem. Solid-State Lett. 4 (2001) A191–A194.
[188] J.W. Fergus, J. Power Sources 195 (2010) 939–954.
[189] M. Wakihara, Mater. Sci. Eng. R Rep. 33 (2001) 109–134.
[190] X. Li, F. Cheng, B. Guo, J. Chen, J. Phys. Chem. B 109 (2005) 14017–14024.
[191] J. Schoiswohl, S. Surnev, F. Netzer, G. Kresse, J. Phys. Condens. Matter 18 (2006) R1.
[192] C. Ban, N.A. Chernova, M.S. Whittingham, Electrochem. Commun. 11 (2009) 522–525.
[193] R. Lopez, L.C. Feldman, R.F. Haglund Jr., Phys. Rev. Lett. 93 (2004) 177403.
[194] J. Schoiswohl, M. Sock, S. Eck, S. Surnev, M. Ramsey, F. Netzer, G. Kresse, Phys. Rev. B 69 (2004) 155403.
[195] W. Avansi Jr., C. Ribeiro, E.R. Leite, V.R. Mastelaro, Cryst. Growth Des. 9 (2009) 3626–3631.
[196] G. Li, K. Chao, H. Peng, K. Chen, Z. Zhang, Inorg. Chem. 46 (2007) 5787–5790.
[197] C. Wu, Y. Xie, Energy Environ. Sci. 3 (2010) 1191–1206.
[198] C.K. Chan, H. Peng, R.D. Twesten, K. Jarausch, X.F. Zhang, Y. Cui, Nano Lett. 7 (2007) 490–495.
[199] T. Allersma, R. Hakim, T. Kennedy, J. Mackenzie, J. Chem. Phys. 46 (1967) 154.
[200] A.M. Cao, J.S. Hu, H.P. Liang, L.J. Wan, Angew. Chem. Int. Ed. 44 (2005) 4391–4395.
[201] J. Haber, M. Witko, R. Tokarz, Appl. Catal. A Gen. 157 (1997) 3–22.
[202] E. Mamedov, V. Cortés Corberán, Appl. Catal. A Gen. 127 (1995) 1–40.
[203] F.D. Hardcastle, I.E. Wachs, J. Phys. Chem. 95 (1991) 5031–5041.
[204] C.N.R. Rao, Annu. Rev. Phys. Chem. 40 (1989) 291–326.
[205] J. Meyer, S. Hamwi, M. Kröger, W. Kowalsky, T. Riedl, A. Kahn, Adv. Mater. 24 (2012) 5408–5427.
[206] M.E. Spahr, P. Bitterli, R. Nesper, M. Müller, F. Krumeich, H.U. Nissen, Angew. Chem. Int. Ed. 37 (1998) 1263–1265.
[207] H.X. Li, L.F. Jiao, H.T. Yuan, M. Zhang, J. Guo, L.Q. Wang, M. Zhao, Y.M. Wang, Electrochem. Commun. 8 (2006) 1693–1698.
[208] J.S. Sakamoto, B. Dunn, J. Electrochem. Soc. 149 (2002) A26–A30.

[209] F. Cheng, J. Chen, J. Mater. Res. 21 (2006) 2744–2757.
[210] A.S. Arico, P. Bruce, B. Scrosati, J.-M. Tarascon, W. van Schalkwijk, Nat. Mater. 4 (2005) 366–377.
[211] Y. Wang, K. Takahashi, H. Shang, G. Cao, J. Phys. Chem. B 109 (2005) 3085–3088.
[212] J. Liu, X. Wang, Q. Peng, Y. Li, Adv. Mater. 17 (2005) 764–767.
[213] G. Li, S. Pang, L. Jiang, Z. Guo, Z. Zhang, J. Phys. Chem. B 110 (2006) 9383–9386.
[214] Z. Chen, Y. Qin, D. Weng, Q. Xiao, Y. Peng, X. Wang, H. Li, F. Wei, Y. Lu, Adv. Funct. Mater. 19 (2009) 3420–3426.
[215] A. Holsteen, I.S. Kim, L.J. Lauhon, Nano Lett. 14 (2014) 1898–1902.
[216] R. Ostermann, D. Li, Y. Yin, J.T. McCann, Y. Xia, Nano Lett. 6 (2006) 1297–1302.
[217] K. Takahashi, S.J. Limmer, Y. Wang, G. Cao, J. Phys. Chem. B 108 (2004) 9795–9800.
[218] C. O'Dwyer, V. Lavayen, M.A. Santa Ana, S.B. Newcomb, E. Benavente, G. Gonzalez, C.M.S. Torres, Phys. Status Solidi B Basic Solid State Phys. 243 (2006) 3285–3289.
[219] G. Li, K. Chao, C. Zhang, Q. Zhang, H. Peng, K. Chen, Inorg. Chem. 48 (2009) 1168–1172.
[220] Z.-S. Wu, W. Ren, L. Wen, L. Gao, J. Zhao, Z. Chen, G. Zhou, F. Li, H.-M. Cheng, ACS Nano 4 (2010) 3187–3194.
[221] M.R. Parida, C. Vijayan, C.S. Rout, C.S. Sandeep, R. Philip, P. Deshmukh, J. Phys. Chem. C 115 (2010) 112–117.
[222] C. Wu, Y. Xie, L. Lei, S. Hu, C. OuYang, Adv. Mater. 18 (2006) 1727–1732.
[223] P.J. Hagrman, R.C. Finn, J. Zubieta, Solid State Sci. 3 (2001) 745–774.
[224] J. Livage, Coord. Chem. Rev. 178 (1998) 999–1018.
[225] C. O'Dwyer, V. Lavayen, S.B. Newcomb, M.A.S. Ana, E. Benavente, G. Gonzalez, C.M.S. Torres, J. Electrochem. Soc. 154 (2007) K29–K35.
[226] C. O'Dwyer, V. Lavayen, S.B. Newcomb, E. Benavente, M.A. Santa Ana, G. Gonzalez, C.M.S. Torres, Electrochem. Solid-State Lett. 10 (2007) A111–A114.
[227] J. Muster, G.T. Kim, V. Krstić, J.G. Park, Y.W. Park, S. Roth, M. Burghard, Adv. Mater. 12 (2000) 420–424.
[228] S. Myung, M. Lee, G.T. Kim, J.S. Ha, S. Hong, Adv. Mater. 17 (2005) 2361–2364.
[229] P. Liu, S.-H. Lee, H.M. Cheong, C. Tracy, J. Pitts, R. Smith, J. Electrochem. Soc. 149 (2002) H76–H80.
[230] L. Krusin-Elbaum, D.M. Newns, H. Zeng, V. Derycke, J.Z. Sun, R. Sandstrom, Nature 431 (2004) 672–676.
[231] M. Ancona, S. Kooi, W. Kruppa, A. Snow, E. Foos, L. Whitman, D. Park, L. Shirey, Nano Lett. 3 (2003) 135–138.
[232] R. Sordan, M. Burghard, K. Kern, Appl. Phys. Lett. 79 (2001) 2073–2075.
[233] G.R. Patzke, F. Krumeich, R. Nesper, Angew. Chem. Int. Ed. 41 (2002) 2446–2461.
[234] R. Tenne, Nat. Nano. 1 (2006) 103–111.
[235] S.W. Lee, N. Yabuuchi, B.M. Gallant, S. Chen, B.-S. Kim, P.T. Hammond, Y. Shao-Horn, Nat. Nano. 5 (2010) 531–537.
[236] X. Jia, C. Yan, Z. Chen, R. Wang, Q. Zhang, L. Guo, F. Wei, Y. Lu, Chem. Commun. 47 (2011) 9669–9671.
[237] M.E. Spahr, P. Stoschitzki-Bitterli, R. Nesper, O. Haas, P. Novák, J. Electrochem. Soc. 146 (1999) 2780–2783.
[238] F. Krumeich, H.J. Muhr, M. Niederberger, F. Bieri, B. Schnyder, R. Nesper, J. Am. Chem. Soc. 121 (1999) 8324–8331.
[239] H.J. Muhr, F. Krumeich, U.P. Schönholzer, F. Bieri, M. Niederberger, L.J. Gauckler, R. Nesper, Adv. Mater. 12 (2000) 231–234.
[240] M. Niederberger, H.-J. Muhr, F. Krumeich, F. Bieri, D. Günther, R. Nesper, Chem. Mater. 12 (2000) 1995–2000.
[241] F. Sediri, F. Touati, N. Gharbi, Mater. Lett. 61 (2007) 1946–1950.
[242] B. Alonso, J. Livage, J. Solid State Chem. 148 (1999) 16–19.
[243] G.T. Chandrappa, N. Steunou, S. Cassaignon, C. Bauvais, J. Livage, Catal. Today 78 (2003) 85–89.
[244] G. Chandrappa, N. Steunou, J. Livage, Nature 416 (2002) 702.
[245] H. Kweon, K.W. Lee, E.M. Lee, J. Park, I. Kim, C.E. Lee, G. Jung, A. Gedanken, Y. Koltypin, Phys. Rev. B 76 (2007) 045434.
[246] J. Cao, J. Choi, J. Musfeldt, S. Lutta, M. Whittingham, Chem. Mater. 16 (2004) 731–736.
[247] W. Chen, J. Peng, L. Mai, Q. Zhu, Q. Xu, Mater. Lett. 58 (2004) 2275–2278.
[248] X. Chen, X. Sun, Y. Li, Inorg. Chem. 41 (2002) 4524–4530.
[249] V. Lavayen, C. O'Dwyer, G. Cárdenas, G. González, C. Sotomayor Torres, Mater. Res. Bull. 42 (2007) 674–685.
[250] M. Wörle, F. Krumeich, F. Bieri, H.-J. Muhr, R. Nesper, Z. Anorg. Allg. Chem. 628 (2002) 2778–2784.
[251] L.I. Vera-Robles, A. Campero, J. Phys. Chem. C 112 (2008) 19930–19933.
[252] B. Choudary, M. Lakshmi Kantam, V. Neeraja, T. Bandyopadhyay, P. Narsi Reddy, J. Mol. Catal. A Chem. 140 (1999) 25–29.
[253] E. Baudrin, G. Sudant, D. Larcher, B. Dunn, J.-M. Tarascon, Chem. Mater. 18 (2006) 4369–4374.
[254] S.-H. Lee, H.M. Cheong, M. Je Seong, P. Liu, C.E. Tracy, A. Mascarenhas, J.R. Pitts, S.K. Deb, J. Appl. Phys. 92 (2002) 1893–1897.
[255] G. Chandrappa, N. Steunou, S. Cassaignon, C. Bauvais, P.K. Biswas, J. Livage, J. Solgel Sci. Technol. 26 (2003) 593–596.
[256] F. Krumeich, H.J. Muhr, M. Niederberger, F. Bieri, R. Nesper, Z. Anorg. Allg. Chem. 626 (2000) 2208–2216.
[257] F. Krumeich, H.-J. Muhr, M. Niederberger, F. Bieri, M. Reinoso, R. Nesper, MRS Online Proc. Libr. 581 (1999).
[258] F. Bieri, F. Krumeich, H.-J. Muhr, R. Nesper, Helv. Chim. Acta 84 (2001) 3015–3022.
[259] J. Wei, Y. Zhu, J. Zhang, Chin. Sci. Bull. 52 (2007) 1920–1924.
[260] D. McNulty, D.N. Buckley, C. O'Dwyer, ECS Trans. 35 (2011) 237–245.
[261] A. Bouhaouss, P. Aldebert, Mater. Res. Bull. 18 (1983) 1247–1256.
[262] S. Iijima, T. Ichihashi, Nature 363 (1993) 603–605.
[263] S.J. Tans, A.R. Verschueren, C. Dekker, Nature 393 (1998) 49–52.
[264] W.A. De Heer, A. Chatelain, D. Ugarte, Science 270 (1995) 1179–1180.
[265] A. Bachtold, P. Hadley, T. Nakanishi, C. Dekker, Science 294 (2001) 1317–1320.
[266] Z. Yao, H.W.C. Postma, L. Balents, C. Dekker, Nature 402 (1999) 273–276.
[267] A.C. Dillon, K. Jones, T. Bekkedahl, C. Kiang, D. Bethune, M. Heben, Nature 386 (1997) 377–379.
[268] W. Liang, M. Bockrath, D. Bozovic, J.H. Hafner, M. Tinkham, H. Park, Nature 411 (2001) 665–669.
[269] S. Park, M. Vosguerichian, Z. Bao, Nanoscale 5 (2013) 1727–1752.
[270] J. Wang, Electroanalysis 17 (2005) 7–14.
[271] M.M. Shulaker, G. Hills, N. Patil, H. Wei, H.-Y. Chen, H.-S.P. Wong, S. Mitra, Nature 501 (2013) 526–530.
[272] M. Remškar, Adv. Mater. 16 (2004) 1497–1504.
[273] E.T. Thostenson, Z. Ren, T.-W. Chou, Compos. Sci. Technol. 61 (2001) 1899–1912.
[274] P. Serp, M. Corrias, P. Kalck, Appl. Catal. A Gen. 253 (2003) 337–358.
[275] Q. Zhang, J.Q. Huang, W.Z. Qian, Y.Y. Zhang, F. Wei, Small 9 (2013) 1237–1265.
[276] I. Valitova, M. Amato, F.M. Mohammadi, G. Cantele, A. Maffucci, C. Santato, R. Martel, F. Cicoira, Nanoscale 5 (2013) 4638–4646.
[277] R. Tenne, in: Advanced Sensors for Safety and Security, Springer, 2013, pp. 299–302.
[278] M. Nath, A. Govindaraj, C. Rao, Adv. Mater. 13 (2001) 283–286.
[279] Y.D. Li, X.L. Li, R.R. He, J. Zhu, Z.X. Deng, J. Am. Chem. Soc. 124 (2002) 1411–1416.
[280] A. Rothschild, J. Sloan, R. Tenne, J. Am. Chem. Soc. 122 (2000) 5169–5179.
[281] G. Surnamelalwani, G. Surnamehenslee, G. Surnamefarshid, G. Surnameparmar, G. Surnamelin, G. Surnameqin, G. Surnamemikos, G. Surnamesitharaman, Acta Biomater. 9 (2013) 8365–8373.
[282] Y. Feldman, E. Wasserman, D. Srolovitz, R. Tenne, Science 267 (1995) 222–225.
[283] W.K. Hsu, B.H. Chang, Y.Q. Zhu, W.Q. Han, H. Terrones, M. Terrones, N. Grobert, A.K. Cheetham, H.W. Kroto, D.R. Walton, J. Am. Chem. Soc. 122 (2000) 10155–10158.
[284] M. Remskar, A. Mrzel, Z. Skraba, A. Jesih, M. Ceh, J. Demšar, P. Stadelmann, F. Lévy, D. Mihailovic, Science 292 (2001) 479–481.
[285] J. Jelenc, M. Remskar, Nanoscale Res. Lett. 7 (2012) 1–9.
[286] N.G. Chopra, R. Luyken, K. Cherrey, V.H. Crespi, M.L. Cohen, S.G. Louie, A. Zettl, Science 269 (1995) 966–967.
[287] X. Blase, A. Rubio, S. Louie, M. Cohen, Europhys. Lett. 28 (1994) 335.
[288] A. Rubio, J.L. Corkill, M.L. Cohen, Phys. Rev. B 49 (1994) 5081.
[289] C.H. Lee, S. Qin, M.A. Savaikar, J. Wang, B. Hao, D. Zhang, D. Banyai, J.A. Jaszczak, K.W. Clark, J.C. Idrobo, Adv. Mater. 25 (2013) 4544–4548.
[290] G.K. Mor, O.K. Varghese, M. Paulose, K. Shankar, C.A. Grimes, Sol. Energy Mater. Sol. Cells 90 (2006) 2011–2075.
[291] M. Shao, X. Xu, J. Huang, Q. Zhang, L. Ma, Sci. Adv. Mater. 5 (2013) 962–981.
[292] J.-Y. Huang, K.-Q. Zhang, Y.-K. Lai, Int. J. Photoenergy 2013 (2013).
[293] A. Pozio, M. Carewska, F. Mura, R. D'Amato, M. Falconieri, M. De Francesco, G. Appetecchi, J. Power Sources 247 (2014) 883–889.
[294] G. Radovsky, R. Popovitz-Biro, D.G. Stroppa, L. Houben, R. Tenne, Acc. Chem. Res. 47 (2013) 406–416.
[295] M.N. Tahir, A. Yella, J.K. Sahoo, H. Annal-Therese, N. Zink, W. Tremel, Phys. Status Solidi B 247 (2010) 2338–2363.
[296] A. Yella, E. Mugnaioli, M. Panthöfer, H.A. Therese, U. Kolb, W. Tremel, Angew. Chem. Int. Ed. 48 (2009) 6426–6430.
[297] R.D. Heidenreich, W. Hess, L. Ban, J. Appl. Crystallogr. 1 (1968) 1–19.
[298] D. Ugarte, Nature 359 (1992) 707–709.
[299] X. Wang, L. Liu, A.J. Jacobson, Chem. Commun. (1998) 1009–1010.
[300] A. Dobley, K. Ngala, S. Yang, P.Y. Zavalij, M.S. Whittingham, Chem. Mater. 13 (2001) 4382–4386.
[301] V. Petkov, P. Zavalij, S. Lutta, M. Whittingham, V. Parvanov, S. Shastri, Phys. Rev. B 69 (2004) 085410.
[302] I. Hellmann, C. Täschner, R. Klingeler, A. Leonhardt, B. Büchner, M. Knupfer, J. Chem. Phys. 128 (2008) 224701.
[303] G. Gannon, C. O'Dwyer, J.A. Larsson, D. Thompson, J. Phys. Chem. B 115 (2011) 14518–14525.
[304] C. O'Dwyer, G. Gannon, D. McNulty, D.N. Buckley, D. Thompson, Chem. Mater. 24 (2012) 3981–3992.
[305] D. Sun, C.W. Kwon, G. Baure, E. Richman, J. MacLean, B. Dunn, S.H. Tolbert, Adv. Funct. Mater. 14 (2004) 1197–1204.
[306] M. Yu, X. Liu, Y. Wang, Y. Zheng, J. Zhang, M. Li, W. Lan, Q. Su, Appl. Surf. Sci. 258 (2012) 9554–9558.
[307] M. Bhuvaneswari, S. Selvasekarapandian, S. Fujihara, S. Koji, Solid State Ionics 177 (2006) 121–127.
[308] X. Chen, X. Wang, Z. Wang, J. Wan, J. Liu, Y. Qian, Nanotechnology 15 (2004) 1685.

[309] B. Azambre, M. Hudson, O. Heintz, J. Mater. Chem. 13 (2003) 385–393.
[310] V.M. Mohan, B. Hu, W. Qiu, W. Chen, J. Appl. Electrochem. 39 (2009) 2001–2006.
[311] A.I. Popa, E. Vavilova, C. Täschner, V. Kataev, B. Büchner, R.D. Klingeler, J. Phys. Chem. C 115 (2011) 5265–5270.
[312] J.M. Reinoso, H.J. Muhr, F. Krumeich, F. Bieri, R. Nesper, Helv. Chim. Acta 83 (2000) 1724–1733.
[313] S. Nordlinder, K. Edström, T. Gustafsson, Electrochem. Solid-State Lett. 4 (2001) A129–A131.
[314] L.J. Krause, W. Lamanna, J. Summerfield, M. Engle, G. Korba, R. Loch, R. Atanasoski, J. Power Sources 68 (1997) 320–325.
[315] S. Nordlinder, A. Augustsson, T. Schmitt, J. Guo, L.C. Duda, J. Nordgren, T. Gustafsson, K. Edström, Chem. Mater. 15 (2003) 3227–3232.
[316] A. Augustsson, T. Schmitt, L.-C. Duda, J. Nordgren, S. Nordlinder, K. Edstrom, T. Gustafsson, J.-H. Guo, J. Appl. Phys. 94 (2003) 5083–5087.
[317] A. Pan, J.-G. Zhang, Z. Nie, G. Cao, B.W. Arey, G. Li, S.-Q. Liang, J. Liu, J. Mater. Chem. 20 (2010) 9193–9199.
[318] L. Mai, L. Xu, C. Han, X. Xu, Y. Luo, S. Zhao, Y. Zhao, Nano Lett. 10 (2010) 4750–4755.
[319] G. Gu, M. Schmid, P.-W. Chiu, A. Minett, J. Fraysse, G.-T. Kim, S. Roth, M. Kozlov, E. Muñoz, R.H. Baughman, Nat. Mater. 2 (2003) 316–319.
[320] C. O'Dwyer, V. Lavayen, D.A. Tanner, S.B. Newcomb, E. Benavente, G. Gonzalez, C.M.S. Torres, Adv. Funct. Mater. 19 (2009) 1736–1745.
[321] S. Nordlinder, J. Lindgren, T. Gustafsson, K. Edström, J. Electrochem. Soc. 150 (2003) E280–E284.
[322] S. Nordlinder, L. Nyholm, T. Gustafsson, K. Edström, Chem. Mater. 18 (2005) 495–503.
[323] C.-J. Cui, G.-M. Wu, J. Shen, B. Zhou, Z.-H. Zhang, H.-Y. Yang, S.-F. She, Electrochim. Acta 55 (2010) 2536–2541.
[324] L. Liu, L. Jiao, J. Sun, Y. Zhang, M. Zhao, H. Yuan, Y. Wang, J. Alloys Compd. 471 (2009) 352–356.
[325] L. Liu, L. Jiao, J. Sun, M. Zhao, Y. Zhang, H. Yuan, Y. Wang, Solid State Ionics 178 (2008) 1756–1761.
[326] X. Zhou, G. Wu, G. Gao, J. Wang, H. Yang, J. Wu, J. Shen, B. Zhou, Z. Zhang, J. Phys. Chem. C 116 (2012) 21685–21692.
[327] T. Zhai, H. Liu, H. Li, X. Fang, M. Liao, L. Li, H. Zhou, Y. Koide, Y. Bando, D. Golberg, Adv. Mater. 22 (2010) 2547–2552.
[328] C.V.S. Reddy, S.A. Wicker, E.H. Walker, Q.L. Williams, R.R. Kalluru, J. Electrochem. Soc. 155 (2008) A599–A602.
[329] S. Lin, B. Shao, I. Taniguchi, Mater. Res. Bull. 49 (2014) 291–296.
[330] H. Yu, X. Rui, H. Tan, J. Chen, X. Huang, C. Xu, W. Liu, D.Y.W. Yu, H.H. Hng, H.E. Hoster, Q. Yan, Nanoscale 5 (2013) 4937–4943.
[331] M. Tousley, A. Wren, M. Towler, N. Mellott, Mater. Chem. Phys. 137 (2012) 596–603.
[332] U. Schlecht, B. Guse, I. Raible, T. Vossmeyer, M. Burghard, Chem. Commun. (2004) 2184–2185.
[333] A. Sakunthala, M. Reddy, S. Selvasekarapandian, B. Chowdari, P.C. Selvin, Energy Environ. Sci. 4 (2011) 1712–1725.
[334] D.H. Kang, K.C. Nam, H.J. Cha, J. Eur. Ceram. Soc. 26 (2006) 2117–2121.
[335] C.O. Avellaneda, L.O. Bulhões, Sol. Energy Mater. Sol. Cells 90 (2006) 444–451.
[336] Y. Chen, I.E. Wachs, J. Catal. 217 (2003) 468–477.
[337] H. Kim, J. Cho, Nano Lett. 8 (2008) 3688–3691.
[338] H. Wang, L.-F. Cui, Y. Yang, H. Sanchez Casalongue, J.T. Robinson, Y. Liang, Y. Cui, H. Dai, J. Am. Chem. Soc. 132 (2010) 13978–13980.
[339] M. Hu, X. Pang, Z. Zhou, J. Power Sources 237 (2013) 229–242.
[340] L. Lu, X. Han, J. Li, J. Hua, M. Ouyang, J. Power Sources 226 (2013) 272–288.
[341] B. Xu, D. Qian, Z. Wang, Y.S. Meng, Mater. Sci. Eng. R Rep. 73 (2012) 51–65.
[342] H. Fei, Y. Lin, M. Wei, J. Colloid Interface Sci. 425 (2014) 1–4.
[343] S. Tepavcevic, H. Xiong, V.R. Stamenkovic, X. Zuo, M. Balasubramanian, V.B. Prakapenka, C.S. Johnson, T. Rajh, ACS Nano 6 (2011) 530–538.
[344] C.-J. Cheng, S.-J. Bao, C.M. Li, Mater. Lett. 120 (2014) 283–286.
[345] M. Sathiya, A. Prakash, K. Ramesha, J.M. Tarascon, A. Shukla, J. Am. Chem. Soc. 133 (2011) 16291–16299.
[346] Y. Liu, M. Clark, Q. Zhang, D. Yu, D. Liu, J. Liu, G. Cao, Adv. Energy Mater. 1 (2011) 194–202.
[347] J. Zhu, L. Cao, Y. Wu, Y. Gong, Z. Liu, H.E. Hoster, Y. Zhang, S. Zhang, S. Yang, Q. Yan, P.M. Ajayan, R. Vajtai, Nano Lett. 13 (2013) 5408–5413.
[348] A. Pan, H.B. Wu, L. Yu, T. Zhu, X.W. Lou, ACS Appl. Mater. Interfaces 4 (2012) 3874–3879.
[349] K. Kang, Y.S. Meng, J. Bréger, C.P. Grey, G. Ceder, Science 311 (2006) 977–980.
[350] Y.-K. Sun, S.-T. Myung, B.-C. Park, J. Prakash, I. Belharouak, K. Amine, Nat. Mater. 8 (2009) 320–324.
[351] M.J. Armstrong, D.M. Burke, T. Gabriel, C. O'Regan, C. O'Dwyer, N. Petkov, J.D. Holmes, J. Mater. Chem. A 1 (2013) 12568–12578.
[352] B. Kang, G. Ceder, Nature 458 (2009) 190–193.
[353] F. Cheng, J. Liang, Z. Tao, J. Chen, Adv. Mater. 23 (2011) 1695–1715.
[354] J. Cho, J. Mater. Chem. 20 (2010) 4009–4014.
[355] B. Scrosati, J. Garche, J. Power Sources 195 (2010) 2419–2430.